Influence of aerosols on polarization of skylight in gaseous absorption bands

Dissertation
zur Erlangung des akademischen Grades des
Doktors der Naturwissenschaften
am Fachbereich Geowissenschaften
der Freien Universität Berlin

vorgelegt von

Eyk Bösche

Berlin, 2008

1. Gutachter: Prof. Dr. Jürgen Fischer

2. Gutachter: Ass. Prof. Ralf Bennartz

Supervisor: Prof. Dr. Jürgen Fischer

Co-Supervisor: Dr. Piet Stammes

Tag der Disputation: 10.06.2008

Selbstständigkeitserklärung

Hiermit erkläre ich, Eyk Bösche, die vorliegende Arbeit selbstständig verfasst und nur die angegebene Literatur und die angegebenen Hilfsmittel verwendet zu haben.

Contents

Chapter 1

Introduction

1.1 The atmospheric constituents

Compared to the diameter of the Earth, the atmosphere is very thin (about 100 km). It is mainly composed of molecular nitrogen (N_2, 78%), molecular oxygen (O_2, 21%) and argon (Ar, 0.9%). The remaining 0.1% are so-called trace gases, such as carbon dioxide (CO_2), ozone (O_3) and nitrogen dioxide (NO_2). Also water vapor (H_2O) occurs in the atmosphere with highly variable abundance (moist air can contain up to 4% water vapor). In addition to these gases suspended tiny particles, called aerosols and clouds, are situated within the atmosphere. Naturally or anthropogenically induced changes in the composition of Earth's atmosphere can cause regional and global changes in climate, air quality, and the protective layer of stratospheric ozone. The atmospheric concentrations of greenhouse gases such CO_2 play an important role in determining the global climate [Forster et al., 2007]. Atmospheric aerosols also play an important role in the radiative energy budget of the atmosphere. Aerosols can perturb atmospheric radiation through their direct effects of scattering and absorption of radiation. Moreover, aerosols can also have an indirect effect via their interaction with clouds, by acting as Cloud Condensation Nuclei (CCN). This is discussed in Section 1.4.

1.2 Atmospheric aerosols

Aerosols are small particles, in the range of sub-micron to several microns, suspended in the atmosphere, which can be in the solid or in the liquid phase. They originate both from natural and man-made (anthropogenic) sources [Seinfeld and Pandis, 1998]. Aerosols can be categorized amongst others in primary and secondary aerosols (see Table 1.1). Primary aerosols are directly emitted as particles into the atmosphere e.g. by volcanoes, by biomass burning, from evaporation of sea spray, from wind lifting dust particles into suspension, etc.. Secondary aerosols originate from chemical reactions (gas-to-particle conversion). Contrary to the long lived and well mixed greenhouse gases, aerosols have a shorter residence time in the atmosphere. They remain suspended in the atmosphere for periods between hours to days and are eventually removed from the atmosphere by precipitation (wet deposition) or by deposition at the surface (dry deposition). The geographical distribution (horizontally and vertically) of aerosols is non-uniform and varies strongly in concentration, composition and with time.

When aerosols interact with radiation, two different processes can occur. First, the aerosol can re-radiate the received energy without changing the wavelength (scattering). Second, the received energy can be re-emitted at a different wavelength or transformed into heat energy (absorption). The sum of theses two processes is called extinction. The direction of scattered light can be described by the asymmetry factor g, which is the fraction of the incident light scattered in forward direction. If all light is scattered forward the asymmetry factor is 1 and if it tends towards -1, more light is scattered backwards (reflected). The ratio between the fraction of light lost to scatting (scattering coefficient) and to extinction (extinction coefficient) is called the single scatting albedo ω and ranges from 0 to 1. The larger the single scattering albedo, the more light attenuation is caused by scattering. When integrating the extinction coefficient over a vertical column the optical thickness τ is obtained. The aerosol optical thickness describes the degree to which aerosols attenuate light on its way through the atmosphere.

Table 1.1: Main sources of aerosols [Seinfeld and Pandis, 1998]. Note: Volatile Organic Compound (VOC).

Primary Aerosols	Secondary Aerosols
Natural	**Natural**
Mineral aerosol	Sulfates from biogenic gases
Sea salt	Sulfates from volcanic SO_2
Volcanic dust	Organic aerosols from VOCs
Organic aerosols	Nitrates from NO_x
Anthropogenic	**Anthropogenic**
Industrial dust	Sulfates from SO_2
Soot	Organic aerosols from VOCs
Biomass burning	Nitrates from NO_x

1.3 Radiative effects of aerosols

Changes in the amount of radiatively active atmospheric constituents can perturb the balance between solar radiation coming into the atmosphere and radiation going out (radiative forcing). A positive radiative forcing tends to warm the atmosphere, and negative forcing tends to cool the atmosphere. A more specific definition is given by [Ramaswamy et al., 2001].

Table 1.1 shows the anthropogenic and natural radiative forcings of the Erath system between 1750 and 2005 [Forster et al., 2007]. Increasing concentrations of the long-lived, and globally distributed greenhouse gases, such as carbon dioxide (CO_2), methane (CH_4), nitrous oxide (N_2O), and halocarbons, have led to a positive radiative forcing of +2.63 W m^{-2}, with an uncertainty of ±0.26 W m^{-2}. Aerosols can influence the radiation balance of the atmosphere in different ways, directly, semi-directly, or indirectly. The total direct radiative forcing by aerosols is estimated to be –0.5 W m^{-2} with an uncertainty of ±0.4 W m^{-2}. The radiative forcing due to indirect aerosol effects is estimated to be –0.7 W m^{-2}, with an uncertainty between -1.1 to +0.4 W m^{-2}. In contrast to the scientific understanding of the effects of long-lived greenhouse gases, the scientific understanding of the aerosol effects is medium to low. The combined anthropogenic radiative forcing is estimated to be +1.6 [–1.0, +0.8] W m^{-2}.

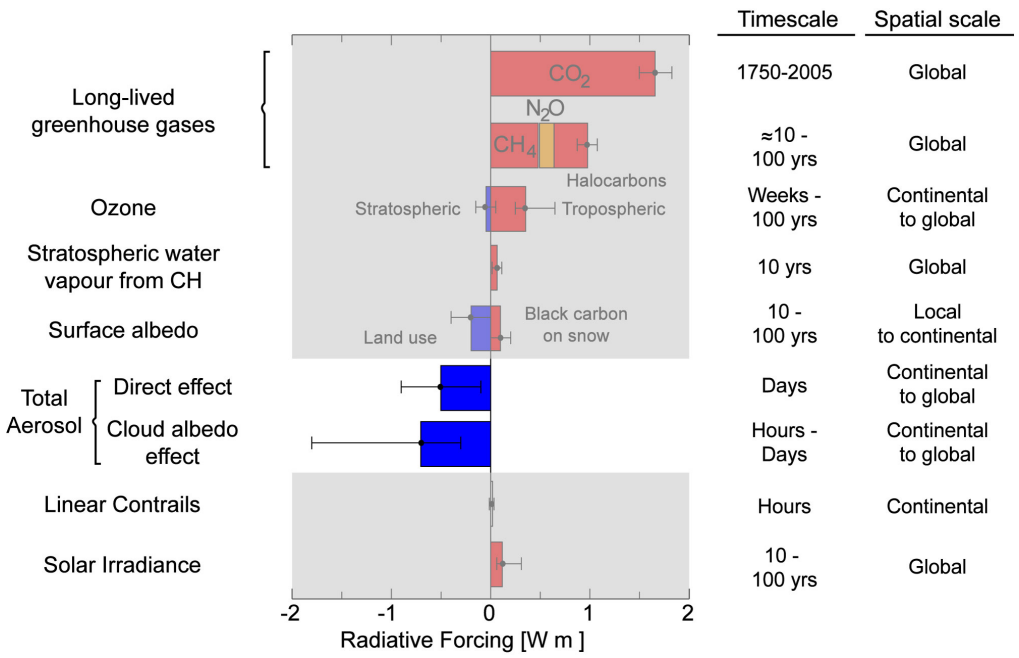

Figure 1.1: Global mean radiative forcing of atmospheric constituents, surface albedo effect and solar irradiance between 1750 and 2005 [Forster et al., 2007]. Each radiative forcing term has an error bar attached, indicating the uncertainties of the global mean radiative forcing. The timescale represent the length of time that a given radiative forcing term would persist in the atmosphere after the associated emissions and changes ceased.

1.3.1 Direct aerosol effects

The radiative forcing of climate by the direct aerosol effect relates to changes in the net radiative fluxes in the atmosphere. This is caused by the modulation of atmospheric scattering properties and absorption properties, attributable to anthropogenic changes in the concentration, and optical properties of aerosols [Charlson et al., 1992], [Seinfeld and Pandis, 1998], [Haywood and Ramaswamy, 1998], [Haywood and Boucher, 2000], [Abel et al., 2005], [Bellouin et al., 2005], [Bates et al., 2006]. Increasing the amount of aerosols (aerosol optical thickness) leads to net cooling effects of the atmosphere, by attenuating sunlight on its way through the atmosphere. Sulphate, fossil fuel organic carbon, fossil fuel black carbon, biomass burning and mineral dust aerosols are all identified as having a large anthropogenic component and exerting a significant direct radiative forcing [Haywood and Ramaswamy, 1998], [Abel et al., 2005], [Bates et al., 2006]. Aerosol scattering and optical properties, such as the scattering asymmetry factor g, the single scattering albedo ω, or the optical thickness τ, are important parameters for determining the direct radiative forcing effect [Haywood et al., 2000], [Penner et al., 2001].

1.3.2 Semi-direct aerosol effects

The semi-direct aerosol effect describes the absorption of solar radiation by aerosols, which can result either in a local reduction of cloud cover, or can inhibit cloud formation [Hansen, et al., 1997], [Ackerman et al., 2000], [Johnson et al., 2004]. By reducing the cloud cover, the surface energy budget can alter significantly. In polluted conditions, such as the south Asian haze, with a sufficient level of e.g. absorbing soot, the warming of the aerosol layer can desiccate stratocumulus cloud layers, alter the properties of the trade-wind cumulus layer and thus influence the hydrological cycle [Ramanathan et al., 2001a], [Ramanathan et al., 2001b], [Lohman and Feichter, 2005]. However, the impact of the semi-direct aerosol effect on the climate and its mechanisms are up to now little understood [Johnson et al., 2004], [Forster et al., 2007].

1.3.3 Indirect aerosol effects

The indirect effect is the mechanism by which aerosols modify the microphysical properties of clouds and thereby the radiative properties, amount and lifetime of clouds. To determine the indirect aerosol effect it is important to understand how effective aerosols act as condensation nuclei, which depends on their size, chemical composition, mixing state and ambient environment [Haywood and Boucher, 2000], [Penner et al., 2001]. The enhancement of cloud albedo due to an increased concentration of cloud droplets, associated with an increased number of CCN (modification of cloud droplet size), is known as the *"first indirect effect"* [Twomey, 1977]. Furthermore aerosols affect the microphysical properties of clouds by shifting the droplet distribution toward smaller sizes. This affects the liquid water content, cloud height, and lifetime of clouds (less precipitation) and is known as the *"second indirect effect"* [Albrecht, 1989], [Lohman and Feichter, 2005].

However, long-lived greenhouse gases exert their effects globally, whereas aerosols exert their effects regionally and locally. It is important to bear in mind that the direct and indirect aerosol effects (mainly cooling the atmosphere), as well as the greenhouse gas warming are partly coupled [Ramanathan et al., 2001], [Forster et al., 2007]. For instance, the radiative forcing caused by the direct and indirect aerosol effects (cooling) can reduce surface latent and sensible heat transfer, and in turn reduce surface evaporation. This can cause a reduction in atmospheric water vapor (a greenhouse gas), which can counteract greenhouse gas warming. On the other hand the second indirect aerosol effect can lead to a longer lifetime of clouds and reduce precipitation, thus more water vapor remains in the

atmosphere. An exact estimation of the influence of aerosols on the climate, the consequences of coupled greenhouse gas warming and aerosol cooling is difficult. This is caused by uncertainties in the estimation of future pollution emissions, greenhouse gas releases into the atmosphere and the insufficient knowledge of aerosol/cloud microphysics interactions.

1.4 Remote sensing of aerosols

1.4.1 Ground-based remote sensing

Solar radiation, reflected or transmitted by the Earth's atmosphere, contains information about the atmospheric constituents through their absorption and scattering signatures. Aerosol remote sensing using active or passive ground-based instruments, such as LIDAR (Light Detection and Ranging) instruments, or sunphotometers (measuring direct and scattered sunlight), enable one to derive aerosol optical and microphysical properties, e.g. the aerosol optical thickness, single scattering albedo, the aerosol size distribution, aerosol shape, and the aerosol refractive index. Ground-based remote sensing measurements are taken at a number of sites, either at long-term monitoring sites, or at field campaigns. Sunphotometer networks, such as the Aerosol Robotic Network program (AERONET), enable one to derive aerosol optical properties, provide information about multi-annual trend changes in aerosol loading and optical properties [Holben et al., 1998], [Dubovik et al., 2000a], [Dubovik et al., 2001]. Theses sites include most aerosol types, such as sulfate, biogenic, marine and desert dust aerosols, as well as various combinations of aerosol types. Ground-based remote sensing observations provide accurate information on aerosol properties and are essential for the validation of satellite measurements and the validation of atmospheric model simulations. Moreover the combination of satellite and ground-based remote sensing observations provides near-global retrievals of aerosol properties.

1.4.2 Satellite remote sensing

Accurate estimates of the direct and indirect effects of tropospheric aerosols on climate require precise global information on aerosol. Compared to local ground-based measurements, satellites offer the potential to collect aerosol information on a global scale [King et al., 1999], [Kaufman et al., 2002].

Active remote sensing satellites such as the Cloud-Aerosol Lidar & Infrared Pathfinder Satellite (CALIPSO) [Berthier et al., 2006], as well as passive remote sensing satellite instruments, such as the Medium resolution imaging spectrometer (MERIS) [Rast and Bezy, 1999], the sea-viewing wide field-of-view sensor (SeaWiFS) [Schollaert et al., 2003], the Global Ozone Monitoring Experiment (GOME) [Burrows et al., 1999], the Scanning Imaging Absorption Spectrometer for Atmospheric Cartography (SCIAMACHY) [Bovensmann et al., 1999], [Schutgens and Stammes, 2002], Ozone Monitoring Instrument (OMI) [Levelt et al., 2006], the Multiangle Imaging SpectroRadiometer (MISR) [Diner, et al., 1989], the Advanced Very High Resolution Radiometer (AVHRR) [Rao et al., 1989], the Moderate Resolution Imaging Spectroradiometer (MODIS) [King and Kaufman, 1992], the Polarization and directionality of the Earth's reflectance (POLDER) [Deschamps et al., 1994], [Deuzé et al., 2000], [Duforet et al., 2007], or the upcoming Aerosol Polarimetry Sensor (APS) [Mishchenko et al., 2007] and the Orbiting Carbon Observatory (OCO) [Crisp et al., 2004], [Haring et al., 2005], provide global information about aerosols, clouds and trace gases in the troposphere and their complex interactions. Despite recent developments in space technology, satellite measurements have some limitations. Most satellite aerosol retrievals are limited to daytime and clear sky conditions, and it is difficult to detect aerosols over land due to surface reflection. Moreover, some satellites need several days of observations to obtain global coverage and thus strong local variations of e.g. aerosols are difficult to detect. Polar orbiting satellites only measure once a day, thus diurnal variations cannot be detected. Future geostationary satellites like Meteosat Second Generation (MSG) [Thieuleux, 2005] will be used to obtain diurnal variations of aerosol properties.

Most satellite remote sensing techniques of tropospheric aerosols rely upon radiance measurements, which are interpreted using algorithms that determine best fits to precalculated radiances. Some of the retrievals ignore polarization effects of the reflected radiation. This often is a reasonable approximation, but taking polarization into account can offer additional information and improve retrievals [Deschamps et al., 1994], [Deuzé et al., 2000], [Duforet et al., 2007], [Natraj et al., 2007].

1.5 Polarization of diffusely transmitted skylight

Polarization is a property of transverse waves such as light. Polarized light is light in which the electric field of the light wave exhibits a preferential direction. In case of unpolarized light, the electric and magnetic field oscillates in random directions perpendicular to the direction of propagation (the wave's direction of travel). There are several ways unpolarized light, such as sunlight incident on the Earth's atmosphere, can be polarized. Polarization can be caused for instance by reflection, by absorption or by scattering.

In 1871 Lord Rayleigh [Rayleigh, 1871] explained the polarization of clear-sky daylight in terms of dipole radiation, singly scattered by air molecules. Rayleigh's theoretical explanation predicts that light is completely polarized at a scattering angle of Θ = 90° and that it is unpolarized in the direction of the sun, or anti-sun. The sky's polarization pattern can be a little more complicated than the single scattering theory predicts. Brewster (1781-1868), Babinet (1793-1872) and Arago (1786-1853) for instance had already discovered that the sky opposite to the sun, or in the direction of the sun, is not completely unpolarized. Instead it is parallel polarized [Coulson, 1988]. The intersection from perpendicular to parallel polarization is called the neutral point. The Arago neutral point is located at about 20° above the antisolar point. Two other neutral points are around 15° to 20° above and below the sun (the Babinet and Brewster neutral points). The deviation of the neutral points from the sun and anti-sun can by explained by means of multiple-scattering effects [van de Hulst, 1948], [Chandrasekar and Elbert, 1951], [Chandrasekar and Elbert, 1954]. In 1852, Sir George Gabriel Stokes showed that any state of polarized light could be described completely by reference to four physically observable characteristics, known as the Stokes parameters [Stokes, 1852]. The first parameter I describes the total intensity, Q and U the linear polarization, and V the circular polarization of a light beam [van de Hulst, 1981]. Stokes also proved that these parameters could not only describe unpolarized light, but also partially polarized and completely polarized light. Extensive studies have been carried out which explain and show the sky's polarization pattern [Sekera, 1957], [Coulson, 1988], [Lee, 1998], [Gal et al., 2001], [Horvath et al., 2002].

1.5.1 Polarization in gaseous absorption bands

A gaseous absorption band is a series of very closely spaced absorption lines, characteristic of the gas. The strength and width of these lines depend on the vertical profile of temperature and pressure. Measurements of atmospherically transmitted or reflected sunlight in absorption bands show a detailed spectral fine-structure, depending on the spectral resolution of the instrument. The spectral fine-structure can also be found for polarization. Up to now, only few high-spectral resolution measurements of the polarization of diffusely transmitted skylight, within absorption bands, have been carried out (see Fig. 1.3) [Stammes et al., 1994], [Preusker et al., 1995], [Aben et al., 1997]. These observations showed that on cloudless days the degree of linear polarization within the O_2A absorption band can be significantly higher or lower than the absorption-free continuum polarization. Stammes et al. (1994) proposed that the strong oxygen absorption is shielding lower layers of the atmosphere from incident sunlight. Therefore most of the light has been scattered at high altitudes, whereas in the continuum no such shielding occurs. So, if the polarization properties of the lower atmospheric layers differ from those of the upper layers, a change of polarization can occur. This shows that measurements inside absorption bands potentially offer additional information about the aerosol altitude.

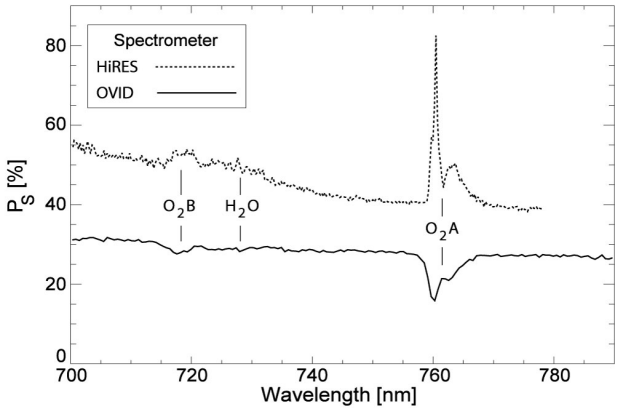

Figure 1.2: Ground-based measurements of the degree of linear polarization P_s of the cloud free sky as a function of wavelength. As measured at the Institute for Space Sciences, in Berlin, Germany, with the spectrometer OVID (solid line), with a spectral resolution of 2.0 nm, and as measured with the spectrometer HiRES (dotted line), with a spectral resolution of 0.3 nm. Geometry at both days: solar zenith angle $\theta_0 \approx 40^\circ$, viewing zenith angle $\theta = 60^\circ$, azimuth angle $\phi - \phi_0 = 180^\circ$, and scattering angle $\Theta = 100^\circ$.

1.6 Radiative transfer simulations including polarization

To simulate ground- and satellite-based measurements, a radiative transfer model is needed. The model has to solve the radiative transfer equation in a multi-layered atmosphere, including multiple scattering, absorption, as well as polarization. The atmosphere is illuminated at the top by the sun and bounded below by a reflecting surface. For monochromatic multiple scattering simulations of the degree of linear polarization in the absorption-free continuum, we use the doubling–adding method (DAK – Doubling-Adding KNMI) [de Haan et al., 1987], [Stammes et al., 1989], [Stammes, 2001]. DAK is designed for line-by-line calculations of radiance, polarization and irradiance at the top of the atmosphere (TOA), and inside the atmosphere. As the name doubling-adding indicates, the technique can be split into two parts. First, the doubling part starts with an optically very thin plane-parallel homogeneous layer. In this layer one or two scattering events may occur. Therefore the radiative transfer equation can be solved analytically with high accuracy. An identical layer is then added. The reflection and transmission from this combined layer are calculated including successive reflections back and forth between the layers. The doubling of layers is repeated until the layer reaches the desired optical thickness. In this manner, multiple scattering of light is taken into account. Second, the adding part is very similar to the doubling procedure, but the adding mechanism combines two layers with different optical properties. These two layers are combined to a single one. This combined layer is then added to a third layer and so forth, until the Stokes vectors at the boundaries of all model layers are known.

Very accurate monochromatic doubling-adding multiple scattering calculations (line-by-line) inside gaseous absorption bands, including polarization, require a multitude of calculations. For the O_2A band for instance we use around 2.000 calculations. This is necessary because absorption spectra of oxygen are highly irregular and strongly dependent on temperature and pressure. These line-by-line calculations are very time consuming, especially if taking polarization into account. Therefore this method is not very suitable for detailed studies of the influence of aerosols on polarization of skylight in gaseous absorption bands.

Various approximation methods are available to reduce the computational effort [Bennartz and Fischer, 2000], [Stam et al., 2000a]. Most of these methods are based on the k-distribution method [Lacis and Oinas, 1991]. The idea of a conventional k-distribution method

is to put absorption lines, within a certain wavelength interval, in increasing order of absorption strength rather than of wavelength. This results in a smooth dependence of the absorption coefficient. This, in turn, makes spectral integration much easier and less time consuming. In this thesis we use the k-binning method, which is based on the modified k-distribution approach [Bennartz and Fischer, 2000], [Bennartz and Preusker, 2007]. Integrating the k-binning method in monochromatic multiple scattering calculations (DAK) for vertically inhomogeneous atmospheres, including polarization, can improve the calculation time, while maintaining a high accuracy compared to line-by-line simulations.

1.7 Outline of this thesis

The theme of this thesis is *"Influence of aerosols on polarization of skylight in gaseous absorption bands"*. Measurements of the spectral and angular polarization signature of solar radiation reflected or transmitted by the Earth's atmosphere provide superior results in the retrieval of aerosol properties such as refractive index, multimodal particle size distribution and particle type, compared to those obtained using only intensity [Mishchenko and Travis, 1997]. The reason is that polarization features are very sensitive to particle size, shape, and refractive index. Intensity measurements alone often lead to ambiguous solutions of e.g. aerosol size distribution, aerosol type, or refractive index [Tanre et al., 1996]. Another advantage of polarimetric measurements is that the calibration accuracy that can be achieved is much higher than for intensity measurements and thus the error in the retrieval can be reduced [Mishchenko and Travis, 1997]. Therefore long term observations of the spectral and angular polarization signatures of atmospheric light are important to increase our state of knowledge regarding aerosol properties.

The research questions pursued in this thesis are:

1.) What are the characteristic aerosol properties in Cabauw, The Netherlands? The measurement site is characterized by urban/industrial and moderate maritime influences.
2.) How do aerosols affect polarization observations of the zenith skylight in the spectral region of the O_2A band and which aerosol information do these observations contain?
3.) How do aerosols affect polarization and intensity observations at top-of-atmosphere in the spectral regions of the O_2 and CO_2 absorption bands, and which aerosol information do these observations contain?
4.) What is the effect of uncertainties of the vertical distribution of aerosol and the neglect of polarization on the estimate of trace gases such as CO_2?

To address the above questions the work performed in this thesis is: (a) Performing observations of the degree of linear polarization of the cloud free zenith sky in Cabauw, the Netherlands. (b) Studying the sensitivity of the degree of linear polarization of the continuum radiation in the Sun's principal plane (the plane defined by the Sun and the zenith direction) as a function of aerosol microphysical parameters. (c) Retrieving aerosol microphysical parameters such as the real and imaginary part of the refractive index, the median radius and geometric standard deviation of the bimodal size distribution (both fine and coarse modes), and the relative number weight of the fine mode by finding the best fit between model and observation data. (d) Studying the influence of aerosol altitude, microphysics and optical thickness on the degree of linear polarization of the zenith skylight in the spectral region of the O_2A band. (e) Studying the sensitivity of the degree of linear polarization and intensity at top-of-atmosphere in the spectral regions of O_2 and CO_2 absorption bands to changes of aerosol altitude, microphysics and surface albedo.

In Chapter 2 we analyze the sensitivity of the degree of linear polarization in the Sun's principal plane as a function of aerosol microphysical parameters. A classification of the importance of the aerosol microphysical and optical parameters is given. This sensitivity study is applied to an analysis of ground-based polarization measurements. We compare polarization measurements with radiative transfer simulations under both clear-and hazy-sky conditions in an urban area (Cabauw, The Netherlands, 51.58° N, 4.56° E). Conclusions about the microphysical properties of aerosol are drawn from the comparison.

In Chapter 3 we analyse the influence of aerosol altitude, microphysics and optical thickness on simulations of the degree of linear polarization of the zenith skylight in the spectral region of the O_2A band, between 755 to 775 nm. The analysis is motivated by several observations of the degree of linear polarization of skylight in the O_2A band which do not yet have a quantitative explanation. To be able to perform these simulations we developed a fast method for multiple scattering calculations in gaseous absorption bands, including polarization. The method is a combination of doubling-adding and k-binning methods. We present an error estimation of this method by comparing with accurate line-by-line radiative transfer simulations.

In Chapter 4 we study the sensitivity of the degree of linear polarization and intensity at top-of-atmosphere in the spectral regions of O_2 and CO_2 absorption bands to changes of scattering layer altitude and surface albedo. For the simulations we use spectral response functions which are representative for the Orbiting Carbon Observatory (OCO) instrument. For the CO_2 band at 1.610 nm we study the scattering layer altitude influence on the column CO_2 estimate and also the errors from neglecting polarization.

In Chapter 5 we conclude with a summary of this thesis and an outlook.

Chapter 2

Effect of aerosol microphysical properties on polarization of skylight: sensitivity study and measurements

E. Boesche, P. Stammes, R. Preusker, T. Ruhtz and J. Fischer, *Applied Optics* **45**, 8790-8805 (2006).

Abstract

We analyze the sensitivity of the degree of linear polarization in the Sun's principal plane as a function of aerosol microphysical parameters: the real and imaginary parts of the refractive index, the median radius and geometric standard deviation of the bimodal size distribution (both fine and coarse modes), and the relative number weight of the fine mode at a wavelength of 675 nm. We use Mie theory for single-scattering simulations and the doubling–adding method with the inclusion of polarization for multiple scattering. It is shown that the behavior of the degree of linear polarization is highly sensitive to both the small mode of the bimodal size distribution and the real part of the refractive index of aerosols, as well as to the aerosol optical thickness; whereas not all parameters influence the polarization equally. A classification of the importance of the input parameters is given. This sensitivity study is applied to an analysis of ground-based polarization measurements. For the passive remote sensing of microphysical and optical properties of aerosols, a ground-based spectral polarization measuring system was built, which aims to measure the Stokes parameters I, Q, and U in the visible (from 410 to 789 nm) and near-infrared (from 674 to 995 nm) spectral range with a spectral resolution of 7 nm in the visible and 2.4 nm in the near infrared. We compare polarization measurements with radiative transfer simulations under both clear-and hazy-sky conditions in an urban area (Cabauw, The Netherlands, 51.58° N, 4.56° E). Conclusions about the microphysical properties of aerosol are drawn from the comparison.

2.1 Introduction

The impact of tropospheric aerosols on the climate system is difficult to determine quantitatively. This difficulty is caused, on the one hand, by the high temporal and spatial variability of the amount, chemical composition and size of aerosols, which are difficult to determine on a global scale [Houghton et al., 1995], [Kaufman et al., 2002]. On the other hand, it is attributable to the fact that aerosol effects are taken into account rather rudimentarily in climate models [Ledley et al., 1999], [Houghton et al. 2001], [Lohman and Lesins, 2002]. First, the radiative forcing of climate by aerosols relates to changes in the net radiative fluxes in the atmosphere. The latter are caused by the modulation of atmospheric scattering and absorption properties attributable to anthropogenic changes in the concentration and optical properties of aerosols (the direct aerosol effect) [Charlson et al., 1992]. Second, cloud reflectivity is enhanced because of the increased concentration of cloud droplets associated with the increased number of condensation nuclei in polluted air (the first indirect aerosol effect) [Brenguier et al., 2000], [Brenguier et al., 2003]. Third, aerosols affect the microphysical properties of clouds by shifting the droplet distribution toward smaller sizes. Therefore polluted clouds are less likely to produce drizzle and less likely to rain out (the second indirect aerosol effect) [Twomey et al., 1984], [Brenguier et al., 2000], [Rosenfeld and Feingold, 2003]. Fourth, aerosols change the concentration of radiatively effective and chemically reactive trace gases because of the heterogeneous processes that take place on their surfaces. It is already clear that the radiative forcing of aerosol particles is similar or can even exceed (with a negative sign) the radiative forcing of the anthropogenic greenhouse gases, if indirect effects are included [Houghton et al., 2001].

Microphysical parameters, such as refractive index, size distribution, and shape, are necessary as input for the calculation of optical properties, but thus far they are inadequately known for most types of aerosol. Therefore further development of adequate optical measurement methods for the determination of microphysical properties of aerosol is needed [Lacis and Mishchenko, 1995].

Remote sensing with ground-based passive radiation instruments can make an important contribution to fundamental studies of atmospheric aerosols. The influence of aerosols on the radiation budget at the surface can be quantified by diffuse and direct irradiance measurements with broadband pyranometers and pyrheliometers. The aerosol optical

thickness can be derived from extinction measurements of direct sunlight, the aerosol size distribution from the spectral behavior of the optical thickness, and the single-scattering albedo from diffuse sky radiance measurements. Generally, this can be done only under the assumption that the other aerosol characteristics are known [Dubovik and King, 2000]. Sunphotometer and sky photometer are common instruments for these measurements. They are in operational use for the remote sensing of aerosols, for example, in the aerosol robotic network (AERONET) [Holben et al., 1998].

The measurements of the degree of polarization of diffuse skylight offer an additional source of information about aerosols. The consideration of polarization complements the spectral and angular radiance measurements and produces a significantly higher sensitivity to microphysical properties of aerosols than do radiance measurements [Mukai et al., 1996], [Cairns et al., 1997], [Mishchenko and Travis, 1997]. Therefore a polarization spectrometer can be regarded as an optimal instrument for aerosol remote sensing measurements in the solar spectral range since it uses all the available information: the directional and spectral dependence of the Stokes parameters (radiance and polarization). The measurements of the angular and spectral dependence of the polarization of skylight can be used principally to estimate the refractive index, the single-scattering albedo, the columnar (or altitude-integrated) size distribution, and the aspect ratio of aerosols [Deuzè et al., 1993], [Zhao et el., 1997], [Breon et al., 1997], [Schulz et al., 1998], [Cairns et al., 1999], [Vermeulen et al., 2000]. Thus far measurements and interpretations of ground-based skylight polarization are rather scarce.

Our aim is to show the sensitivity of the degree of linear polarization of skylight in the Sun's principal plane (the plane defined by the Sun and the zenith direction) to changes of the microphysical and optical properties of aerosols. This sensitivity study is applied to an interpretation of ground-based measurements of the degree of linear polarization. Ground-based measurements show that aerosol polarization comes mainly from the small spherical aerosol particles [Vermeulen et al., 2000]. Aerosols are often assumed to be spherical. Recent studies of nonspherical tropospheric aerosols are devoted mainly to dustlike and sea saltlike tropospheric aerosols [Mishchenko et al., 1995], [Kahn et al., 1998], [Barnaba and Gobbi, 2001], [Chamaillard et al, 2003]. Considering the measurement location (Cabauw, The Netherlands) and the meteorological conditions in this area, we assume spherical aerosols for this study, thus allowing the application of Mie theory. The sensitivity study is

limited to a single wavelength outside of the absorption bands. We first show the measurement results of the spectral dependence of skylight polarization, but a further investigation of the spectral information content will be part of future studies. In Section 2.2 the definition of relevant polarization parameters, such as the Stokes parameters and the scattering matrix, are briefly discussed. Then the sensitivity of the degree of linear polarization of skylight in the principal plane to changes in the microphysical properties of aerosols is shown for Mie single-scattering calculations (Subsections 2.3.1 and 2.3.2) and multiple-scattering simulations (Subsections 2.3.3 and 2.3.4). In Section 2.4 we outline a new ground-based measurement system of the Freie Universität Berlin integrated spectrographic system–polarization (FUBISS–POLAR). It was developed at the Institute for Space Sciences (Freie Universität Berlin) to investigate the optical properties of aerosols [Ruhtz et al, 2002]. FUBISS–POLAR was designed to provide multiangle measurements of the polarization of diffuse skylight and measurements of the atmospheric transmission in a wide spectral range. In Section 2.5 we compare the FUBISS–POLAR measurements in the principal plane with the radiative transfer simulations. The comparison of radiative transfer simulations with in situ measurements allows us to draw conclusions regarding the aerosol refractive index, the aerosol size distribution, and the fine mode fraction of the aerosol optical thickness.

2.2 Definition of polarization parameters and observation geometry

2.2.1 Stokes parameters and polarization

The state of polarization of a light beam can be defined through the components of the Stokes vector. The state of polarization of a light beam can be defined through the components of Stokes vector $\mathbf{I}$ [Chandrasekhar, 1960], [van de Hulst, 1981], by measuring the relative intensities I of the light beam after it has passed through polarization devices at different orientations of their transmission axes [Shurcliff, 1962]:

$$\mathbf{I} = \begin{pmatrix} I \\ Q \\ U \\ V \end{pmatrix} = \begin{pmatrix} I_{0^\circ} + I_{90^\circ} \\ I_{0^\circ} - I_{90^\circ} \\ I_{45^\circ} - I_{135^\circ} \\ I_{+} - I_{-} \end{pmatrix} \tag{2.1}$$

where 0°, 45°, 90°, and 135° denote the orientations of the polarization transmission axes with respect to a reference plane, and + and – are the right- and left-handed circular polarization components. Here the reference plane can be arbitrarily chosen through the direction of propagation of the light beam. Throughout this paper we use the principal plane as the reference plane. Stokes parameter I describes the total intensity, Q and U the linear polarization, and V the circular polarization of the light beam. From the Stokes parameters the following polarization parameters can be derived [Hovenier et al., 2004]:

$$P = \frac{(Q^2 + U^2 + V^2)^{1/2}}{I}, \tag{2.2}$$

$$P_l = \frac{(Q^2 + U^2)^{1/2}}{I}, \tag{2.3}$$

$$P_c = -\frac{V}{I}, \tag{2.4}$$

where P is the total degree of polarization, P_l is the degree of linear polarization, and P_c is the degree of circular polarization. Symmetry demands that U = 0 for skylight measurements within the principal plane. To preserve the sign of Q, the degree of linear polarization in the principal plane can be written as

$$P_s = -\frac{Q}{I}. \tag{2.5}$$

In the following discussion the circular component V of the Stokes vector is neglected, because numerous experiments and simulations show that V has a marginal influence on the total degree of polarization in the atmosphere [Egan, 1992], [Stammes, 1989].

2.2.2 Scattering matrix

We consider independent light scattering by an ensemble of randomly oriented particles, which has a plane of symmetry. The scattering plane contains the direction of propagation of the incident and scattered light and will serve as the reference plane. The Stokes parameters of the scattered beam for scattering angle can be written as a linear transformation of the Stokes parameters of the incident beam [Chandrasekhar, 1960], [Shurcliff, 1962], [Hovenier et al., 2004]:

$$\begin{pmatrix} I_{sca} \\ Q_{sca} \\ U_{sca} \\ V_{sca} \end{pmatrix} = \begin{bmatrix} F_{11} & F_{12} & 0 & 0 \\ F_{12} & F_{22} & 0 & 0 \\ 0 & 0 & F_{33} & F_{34} \\ 0 & 0 & -F_{34} & F_{44} \end{bmatrix} \begin{pmatrix} I_{in} \\ Q_{in} \\ U_{in} \\ V_{in} \end{pmatrix} \tag{2.6}$$

where the subscripts “sca” and “in” stand for scattered and incoming beams. The matrix $\mathbf{F}$, with elements F_{ij}, is called the scattering matrix, and its elements are functions of the scattering angle. Owing to the constraints on the ensemble of particles, the scattering matrix has only six independent elements. The scattering matrix depends on the refractive index, the size distribution, and the shape of the scattering particles and contains all the polarizing properties of the ensemble of randomly oriented particles.

For spherical particles, the scattering matrix can be calculated using Mie theory. If the incident light is nonpolarized, the first column of the scattering matrix suffices to determine the intensity and state of polarization of the light scattered once. For accurate multiple-scattering calculations, however, the complete scattering matrix is necessary because nonpolarized light becomes polarized after being scattered. Function F_{11} is called the phase function and is normalized such that

$$\frac{1}{2}\int_0^1 F_{11}(\Theta)\sin\Theta \mathrm{d}\Theta = 1 \tag{2.7}$$

For nonpolarized incident light, F_{11} is proportional to the scattered intensity as a function of the scattering angle. The ratio $-F_{12}/F_{11}$ represents the degree of linear polarization if the incoming light is nonpolarized [see Eq. (2.5)]. Furthermore, we must have $\left|F_{ij}/F_{11}\right| \le 1$, and for spheres the relations $F_{11} = F_{22}$ and $F_{22} = F_{44}$ hold [Liou, 2002].

2.2.3 Geometric characteristics for the atmosphere

The direction of radiation at an arbitrary point within the atmosphere is specified by zenith angle θ and azimuth angle ϕ (see Fig. 2.1). The direction of incident sunlight is specified by θ_0 and ϕ_0. Zenith angle θ is measured from the positive *z* direction, i.e., the local vertical. Azimuth angle ϕ is measured clockwise when looking in the positive *z* direction. The zero direction of the azimuth is arbitrary; thus only differences in azimuth $\phi - \phi_0$ are important. In the principal plane the scattering angle Θ between the incident light and the scattered light (see Fig. 2.1) is given as follows: for $\phi - \phi_0 = 0°$, the scattering angle $\Theta = |\theta_0 - \theta|$; for $\phi - \phi_0 = 180°$, $\Theta = \theta_0 + \theta$. The angular ranges are as follows: $0° \le \theta$, $\theta_0 \le 90°$, $0° \le \phi \le 360°$, and $0° \le \Theta \le 180°$.

2.3 Simulations of the degree of linear polarization of skylight

Here we discuss the sensitivity of the degree of linear polarization to changes of aerosol microphysical and optical properties. This sensitivity is studied here using Mie calculations (Subsections 2.3.1 and 2.3.2) and multiple-scattering simulations (Subsections 2.3.3 and 2.3.4). From the Mie single-scattering calculations of the degree of linear polarization as a function of scattering angle $P_s(\Theta)$ we further derive the single-scattering albedo ω and the scattering matrix $\mathbf{F}(\Theta)$. These values, taken from selected Mie calculations, serve as input for the multiple-scattering simulations of the degree of linear polarization as a function of the viewing zenith angle $P_s(\theta)$. For the simulations we use a standard set of aerosol input parameters (see Tables 2.1 and 2.2) and change one of the parameters in a given range, and the others remain unchanged.

2.3.1 Mie calculation input parameters

The degree of linear polarization of single scattering by spherical particles is computed by using Mie scattering theory [de Rooij and van der Stap, 1984]. The input parameters required for Mie calculations include (see also Table 2.1): wavelength of the incident light, the real and imaginary parts of aerosol refractive index m, and the aerosol size distribution. The wave-

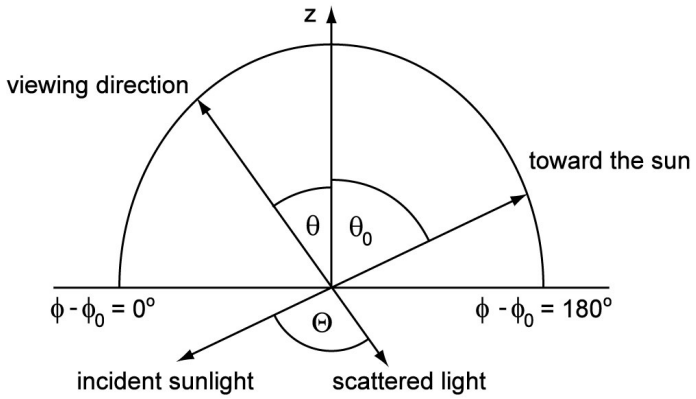

Figure 2.1: Scattering Scattering geometry in the principal plane. The viewing direction and the solar direction are, together with the local vertical, in one plane. Θ is the scattering angle.

length was chosen to be 675 nm, where only ozone absorption in the Chappuis band has to be taken into account, and remains constant throughout the sensitivity study. As size distribution, a bimodal lognormal distribution was chosen, given by

$$n_N(r) = \frac{dN}{dr} = w\frac{N_f}{\sqrt{2\pi}\ln(\sigma_f)}\frac{1}{r}\exp\left\{-\frac{1}{2}\left[\frac{\ln(r)-\ln(r_f)}{\ln(\sigma_f)}\right]^2\right\} + (1-w)\frac{N_c}{\sqrt{2\pi}\ln(\sigma_c)}\frac{1}{r}\exp\left\{-\frac{1}{2}\left[\frac{\ln(r)-\ln(r_c)}{\ln(\sigma_c)}\right]^2\right\}, \quad (2.8)$$

where $n_N(r)$ is the number distribution ($\mu m^{-1}\,cm^{-3}$), $N_{f,c}$ are the total aerosol number concentrations for the fine and coarse modes, $r_{f,c}$ are the fine and coarse mode number median radii, $\sigma_{f,c}$ are the fine and coarse mode geometric standard deviations of the distribution [Seinfeld and Pandis, 1997], and w is the weighting factor of the fine mode. The typical values for weighting factor w are in the range of 0.9992– 0.9998 [Torres et al., 2002]. It is sometimes convenient for comparison between size distributions to express the size parameters of different distributions in terms of two common parameters, the effective radius and the effective variance. For each mode the effective radius r_{eff}, or area weighted mean radius, can be used as larger particles tend to be more efficient scatterers:

$$r_{\text{eff},i} = r_i(1+v_{\text{eff},i})^{2.5}, \qquad i = f, c, \quad (2.9)$$

where i represents fine and coarse mode values [see also Eq. (2.8)]. Similarly for the standard deviation of a distribution, the effective variance v_{eff} can be used:

$$v_{\text{eff},i} = \exp\left[\ln(\sigma_i)^2\right] - 1, \qquad i = f, c. \tag{2.10}$$

An advantage of the lognormal distribution is that the standard deviations for the number, surface, and volume distributions are identical, and therefore the surface median radius r_S and the volume median radius r_V can be written in terms of the number median radius r_N and standard deviation σ_N as follows [Seinfeld and Pandis, 1997]:

$$\ln(r_{S,i}) = \ln(r_{N,i}) + 2\ln^2(\sigma_{N,i}), \qquad i = f, c, \tag{2.11}$$

$$\ln(r_{V,i}) = \ln(r_{N,i}) + 3\ln^2(\sigma_{N,i}), \qquad i = f, c. \tag{2.12}$$

To have realistic standard aerosol input parameters for the single- and multiple-scattering calculations, we constructed a precalculated lookup table, which was based on AERONET climatology data including the variability for several sites [Dubovik et al., 2001]. We compared measurements of the degree of linear polarization in the principal plane, taken on 11 October 2004 in Cabauw, The Netherlands (see Section 2.5) and the lookup table results. The parameters of the best fit, subsequently referred to as the Cabauw case (see Table 2.1), were taken as the standard input for the Mie sensitivity study. The range of the real and imaginary parts of refractive index m, as well as the number median radii $r_{f,c}$ and the geometric standard deviations $\sigma_{f,c}$ of the aerosol size distribution chosen for the sensitivity study, comprise a wide range of tropospheric aerosol properties [Dubovik et al., 2001], [d'Almeida et al., 1991]. The same refractive index has been assumed for the fine and coarse mode particles of the aerosol size distribution.

Table 2.1: Mie simulation input parameters. The Cabauw values are used as standard input for the Mie simulations. The fourth column gives the range in which the values are varied for the sensitivity study. For comparison purposes the fifth and sixth columns give the average values as measured by AERONET in urban locations (Greenbelt and Paris) [Dubovik et al., 2001].

Parameter	Symbol	Standard Value (Cabauw, The Netherlands)	Range	Greenbelt (USA)	Paris (France)
Wavelength	$\lambda\,(\mu\mathrm{m})$	0.675	constant	0.675	0.675
Real part of the refractive index	m_r	1.400	1.330-1.600	1.410	1.400
Imaginary part of the refractive index	m_i	0.007	0.000-0.020	0.003	0.009
Median radius of the fine mode	$r_f\,(\mu\mathrm{m})$	0.080	0.010-0.110	0.081	0.067
Median radius of the coarse mode	$r_c\,(\mu\mathrm{m})$	0.425	0.150-0.650	0.565	0.428
Standard deviation of the fine mode	σ_f	1.400	1.200-2.200	1.460	1.537
Standard deviation of the coarse mode	σ_c	2.100	1.500-2.500	2.120	2.203
Weighting factor of the fine mode	w	0.9995	0.998-1.000	0.9995	0.9995

2.3.2 Mie Single-scattering polarization results

The focus of the single-scattering sensitivity study of the degree of linear polarization as a function of scattering angle $P_s(\Theta)$ turns on the following four criteria: the sensitivity of the polarization in the forward-scattering direction ($0° < \Theta < 90°$), the sensitivity of the polarization in the backscattering direction ($90° < \Theta < 180°$), the sensitivity of the maximum degree of linear polarization, and the sensitivity of its position.

The color contour diagrams in the left panels of Figures 2.2–2.4 present the complete picture of the behavior of $P_s(\Theta)$ as a function of each aerosol microphysical parameter. The corresponding xy plots in the right panels show the slice planes of $P_s(\Theta)$ for certain values of the varied input parameters. The values are indicated in the contour diagrams by dashed horizontal lines. For comparison of the $P_s(\Theta)$ curves, the standard Cabauw case is indicated by solid black curves in the right panels.

For $P_s(\Theta)$ in the forward-scattering direction, the strongest influence is found for changes of the median radius, the standard deviation, and the weighting factor of the fine mode [see Figs. 2.3(a), 2.3(b), 2.4(a), 2.4(b), 2.4(e), and 2.4(f)]. The variations of the real part of the refractive index and median radius of the coarse mode have a minor influence [see Figs. 2.2(c), 2.2(d), 2.3(c), and 2.3(d)], while variations of the imaginary part of the refractive index

and the standard deviation of the coarse mode have an insignificant influence [see Figs. 2.2(a), 2.2(b), 2.4(c), and 2.4(d)]. For the maximum degree of linear polarization, the influence is strongest for the fine modes of the median radius, the standard deviation, and the weighting factor [see Figs.2. 3(a), 2.3(b), 2.4(a), 2.4(b), 2.4(e), and 2.4(f)]. The real part of the refractive index and the median radius of the coarse mode have a weaker influence

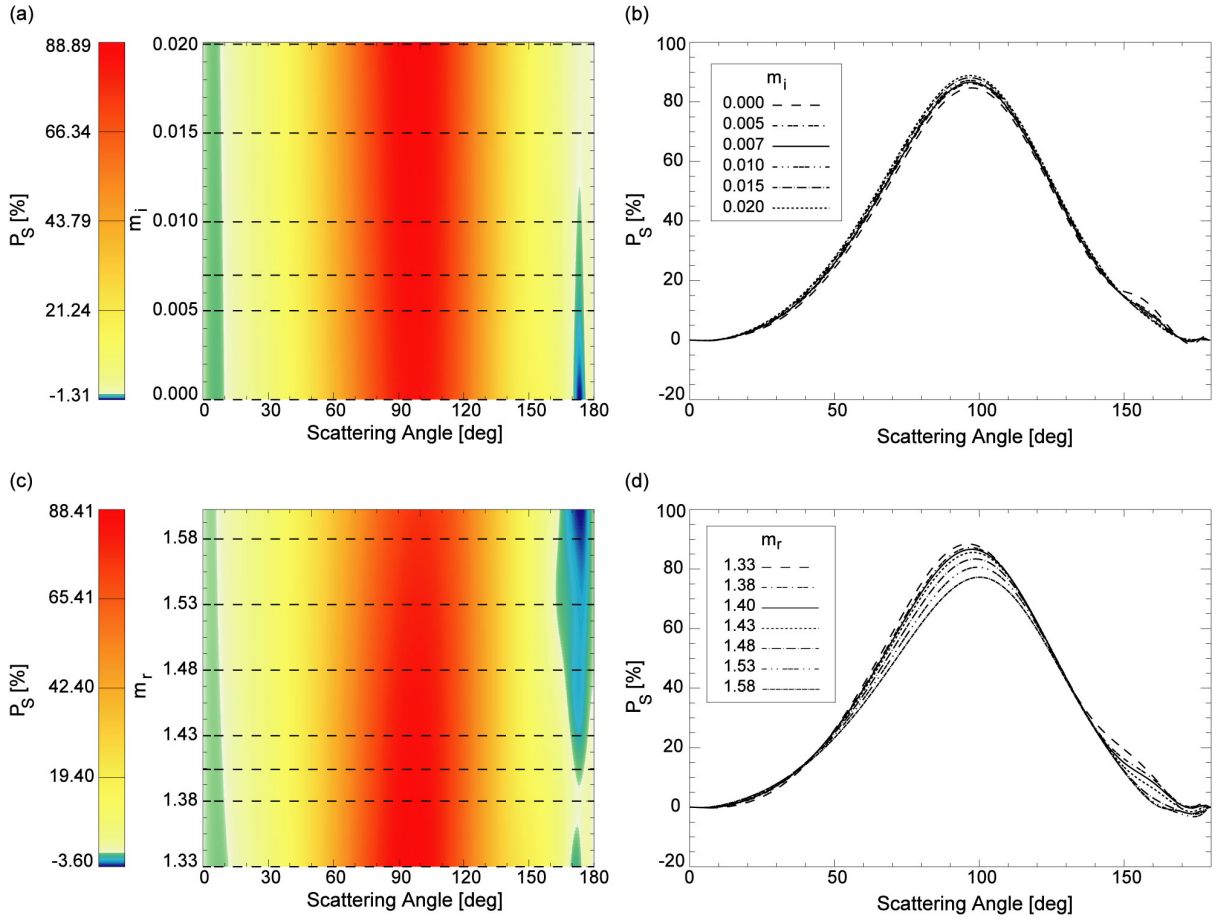

Figure 2.2: Mie simulations of the degree of linear polarization P_s at $\lambda = 675$ nm as a function of the scattering angle and varied aerosol parameter. The Cabauw case was used as standard input and one parameter was varied, and the others remain unchanged (see Table 2.1). The varied parameters are (a), (b), the imaginary part of the refractive index and (c), (d), the real part of the refractive index. The left column shows the degree of linear polarization versus the varied input parameter and scattering angle. The color bar goes from red to yellow (P_s > 0) to white (P_s = 0) and from green to blue (P_s < 0). In the right column, the corresponding xy plots show slice planes of the degree of linear polarization versus the scattering angle. The slice planes are indicated in the colored figures by dashed lines. For comparison, the Cabauw case is indicated by a solid black curve in the slice plane figures.

[see Figs. 2.2(c), 2.2(d), 2.3(c), and 2.3(d)], while the imaginary part of the refractive index and the standard deviation of the coarse mode have an insignificant influence on the maximum [see Figs. 2.2(a), 2.2(b), 2.4(c), 2.4(d)]. For the position of the maximum degree of linear polarization, the strongest influence can be found by varying the real part of the refractive index [see Figs. 2.2(c) and 2.2(d)]. For $P_s(\Theta)$ in the backscattering direction, the strongest influence is found for changes in the fine modes of the median radius, the standard deviation, and the weighting factor [see Figs. 2.3(a), 2.3(b), 2.4(a), 2.4(b), 2.4(e), and 2.4(f)]. Changes in the other Mie input parameters have a minor or insignificant influence on the degree of polarization in the backscattering direction.

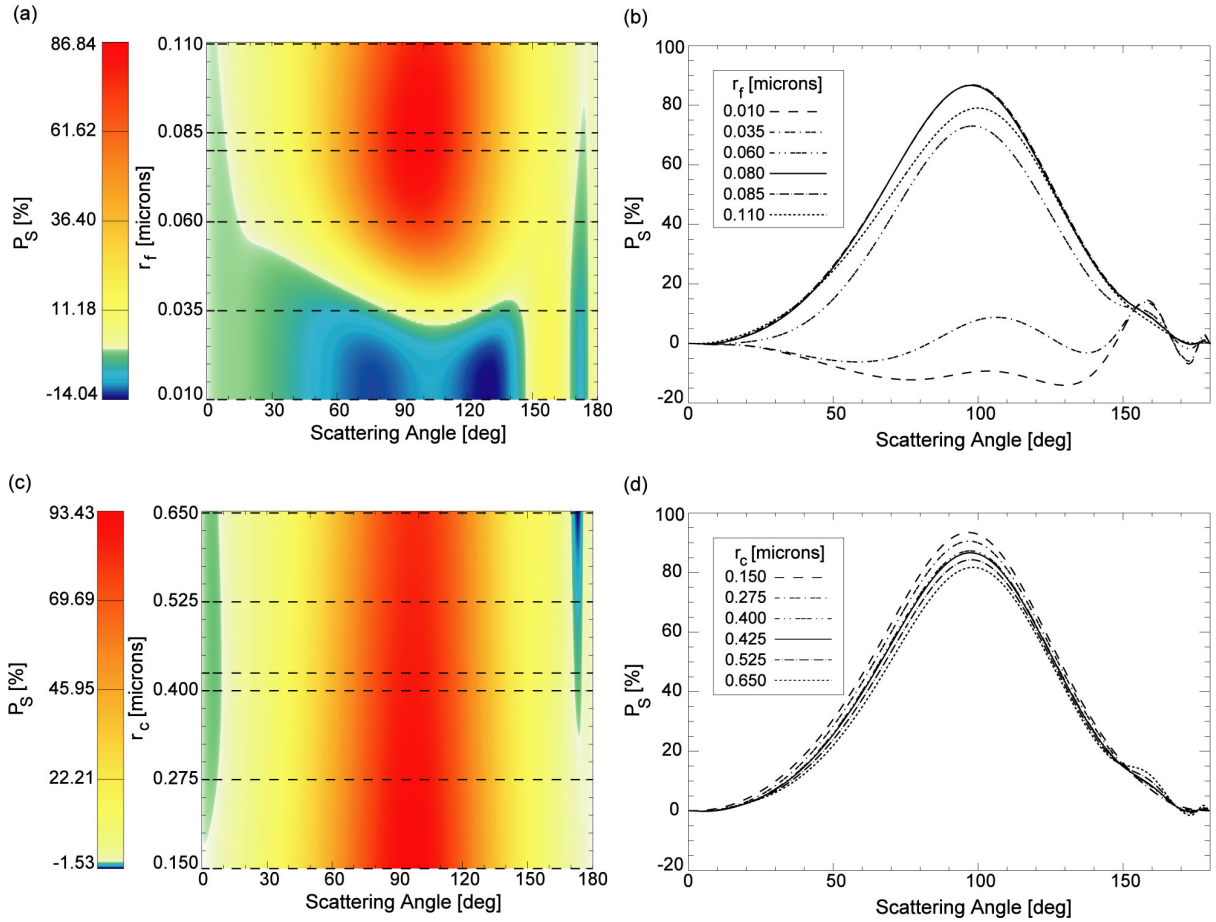

Figure 2.3: Same as in Figure 2.2, but for the median radius of (a), (b), the fine mode and (c), (d), the coarse mode.

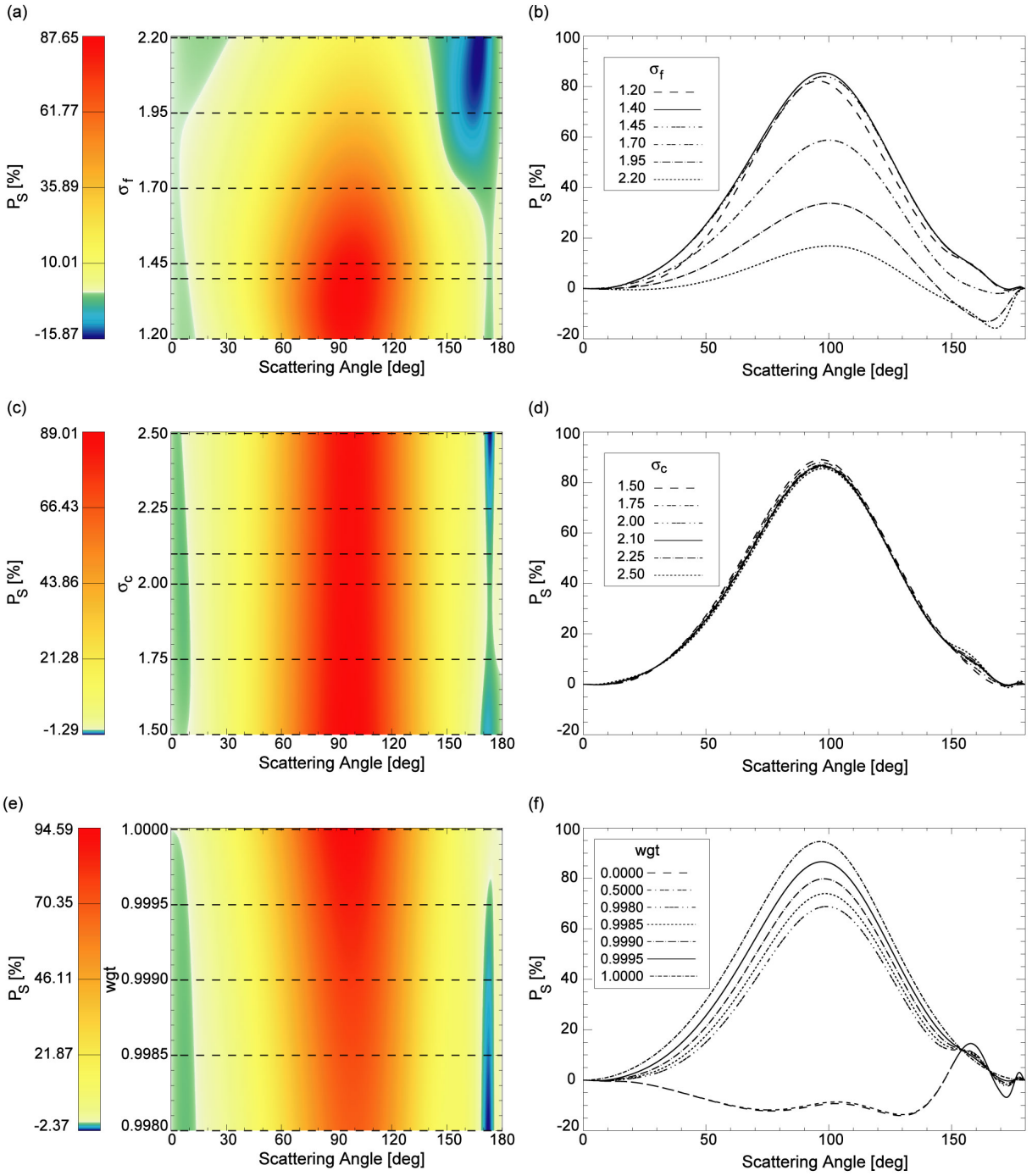

Figure 2.4: Same as in Figure 2.2, but for the standard deviation of (a), (b), the fine mode; the standard deviation of (c), (d), the coarse mode; (e), (f), the weighting factor of the fine mode.

2.3.3 Radiative transfer model and input parameters

The DAK [doubling–adding Royal Netherlands Meteorological Institute (KNMI)] model is designed for the line-by-line calculations of radiance, polarization, and irradiance at the top of the atmosphere (TOA) inside the atmosphere. It consists of an atmospheric shell around a monochromatic multiple scattering kernel, based on the polarized doubling–adding method [de Haan, 1987] ,[Stammes, 2001]. The calculation of the polarized internal radiation field of the atmosphere is described by de Haan [de Haan, 1987]. The atmosphere may consist of an arbitrary number of plane-parallel layers, each of which can have Rayleigh scattering, gas absorption, aerosol and or cloud particle scattering, and absorption. Polarization is fully taken into account. The atmospheric shell describes the optical parameters of each layer: optical thickness, single-scattering albedo, and scattering matrix [de Haan, 1987]. To be used in DAK, the scattering matrix must be expanded in so-called generalized spherical functions, which is done by the Mie scattering code [de Rooij and van der Stap, 1984]. Because of the strong forward peak of the aerosol phase function (which can amount to 3 orders of magnitude in F_{11} between 0° and 10°), the number of expansion coefficients needed for an accurate representation of the phase function is too high for practical purposes (computation time). For this reason, a delta approximation is used before the expansion is started for all the phase functions (see Appendix 2.A).

The degree of linear polarization is computed by using multiple-scattering simulations (DAK). The input parameters required for the DAK simulations include (see Table 2.2): a mid-latitude summer atmospheric profile, aerosol altitude *h*, aerosol optical thickness τ_{aer}, surface albedo A, Mie scattering matrices, and single-scattering albedo ω. The aerosol was placed in the lowest kilometer of the atmosphere. The ozone absorption in the Chappuis band was included in the calculations. The standard value of the aerosol optical thickness at 675 nm was chosen according to sunphotometer measurements made on a clear day (11 October 2004) in Cabauw, The Netherlands. The surface albedo of the surrounding grassland was chosen according to the database of [Koelemeijer et al, 2003] for October at a wavelength of 675 nm. The Mie-scattering matrices, selected from the sensitivity study in Subsection 2.3.2 and shown in the right panels of Figures 2.2–2.4, served as aerosol input parameters for the DAK simulations. The Cabauw case aerosol was used as the standard aerosol model (Table 2.1). For a comparison of the different figures of the sensitivity study, the Cabauw case is indicated by a solid black curve in Figures 2.5 and 2.6.

Table 2.2: Input Parameters for the DAK Multiple Scattering Simulations. The third column gives the standard Cabauw case values for 11 October 2004. The fourth column gives the range in which the parameters are varied in the sensitivity study.

DAK input parameter	Symbol	Standard value (Cabauw, The Netherlands)	Range
Wavelength	λ (μm)	0.675	constant
Surface albedo	A	0.100	0.05-0.20
Atmospheric profile		Midlatitude summer, AFGL (1986)	-
Number of atmospheric layers	N	32	constant
Aerosol altitude	h (km)	0-1	0-16
Mie input parameters		See Table 2.1	-
Aerosol optical thickness	τ_{aer}	0.065	0.045-0.400

2.3.4 Multiple-scattering Simulations of polarization of skylight

The focus for the multiple scattering simulations turns on the same four aspects of the sensitivity of skylight polarization on aerosol microphysical parameters as in Subsection 2.3.2: the sensitivity of the polarization in the forward-scattering direction, the sensitivity of the polarization in the backscattering direction, the sensitivity of the maximum polarization, and the sensitivity of the position of the maximum degree of linear polarization. The standard input parameters for this sensitivity study refer to very clear-sky conditions (the Cabauw case, Table 2.3).

For $P_s(\theta)$ in the forward-scattering direction, the strongest influence is found for variations of the fine mode median radius and the fine mode standard deviation [see Figs. 2.5(c) and 2.5(e)]. The influence of the real part of the refractive index, the weighting factor of the fine mode, and the aerosol optical thickness are less significant [see Figs. 2.5(b), 2.6(a), and 2.6(c)]. The other input parameters have a minor or insignificant influence on the polarization in the forward-scattering direction. The maximum degree of linear polarization is strongly influenced by nearly all the input parameters. The only exceptions are the coarse mode radius, the coarse mode standard deviation, the imaginary part of the refractive index, and

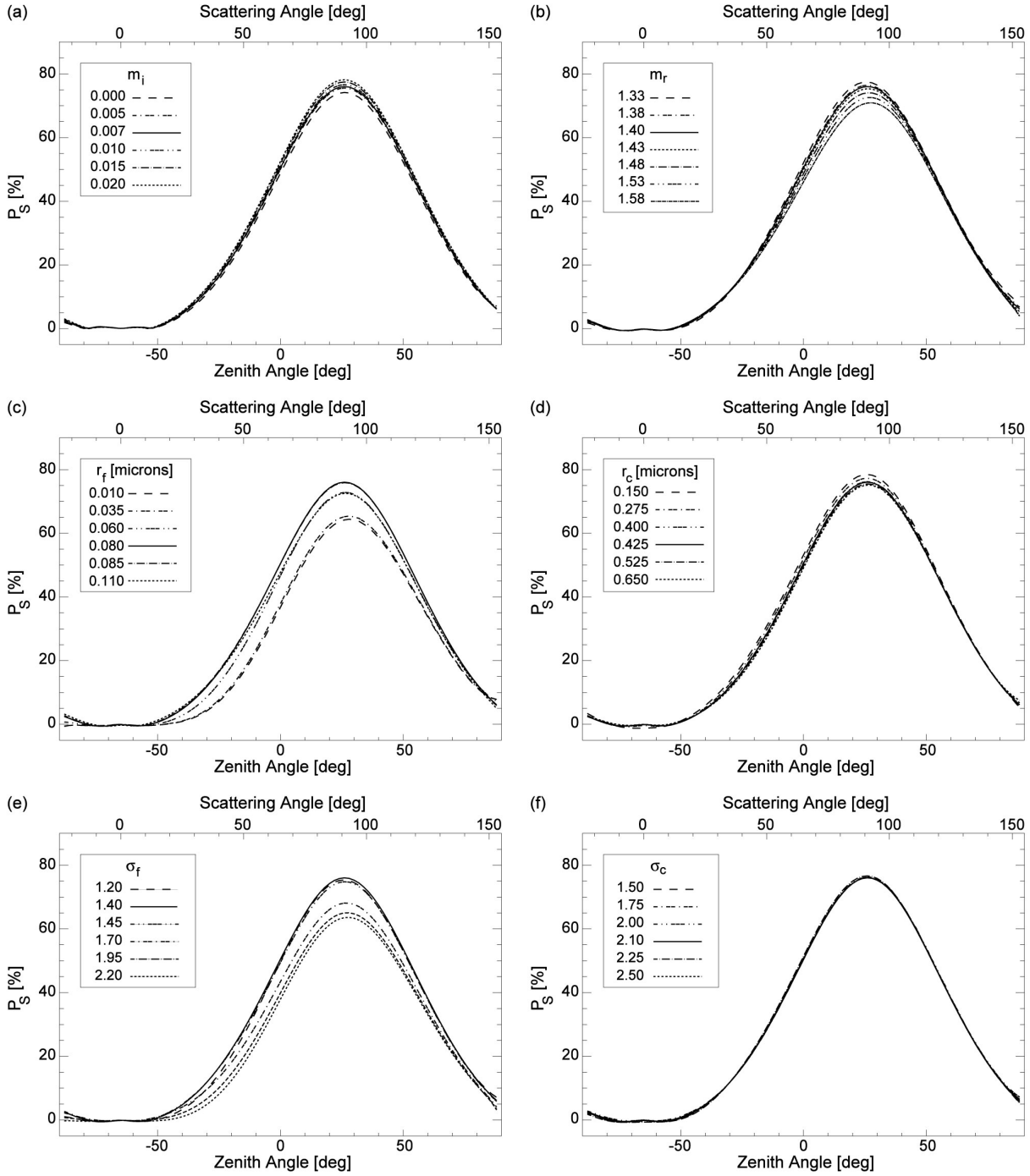

Figure 2.5: Multiple scattering simulations, using DAK, of the degree of linear polarization P_s at $\lambda = 675$ nm as a function of the zenith and scattering angles in the principal plane at a solar zenith angle of $\theta_0 = 65°$. Negative zenith angles refer to $\phi - \phi_0 = 0°$, and positive zenith angles to $\phi - \phi_0 = 180°$ (see Subsection 2.2.3). The Cabauw case (solid curve) was used as standard input, and one parameter was varied, while the others remain unchanged (see Tables 2.1 and 2.2). The varied parameters are (a) the imaginary part of the refractive index, (b) the real part of the refractive index, (c) the median radius of the fine mode, (d) the median radius of the coarse mode, (e) the standard deviation of the fine mode, (f) the standard deviation of the coarse mode.

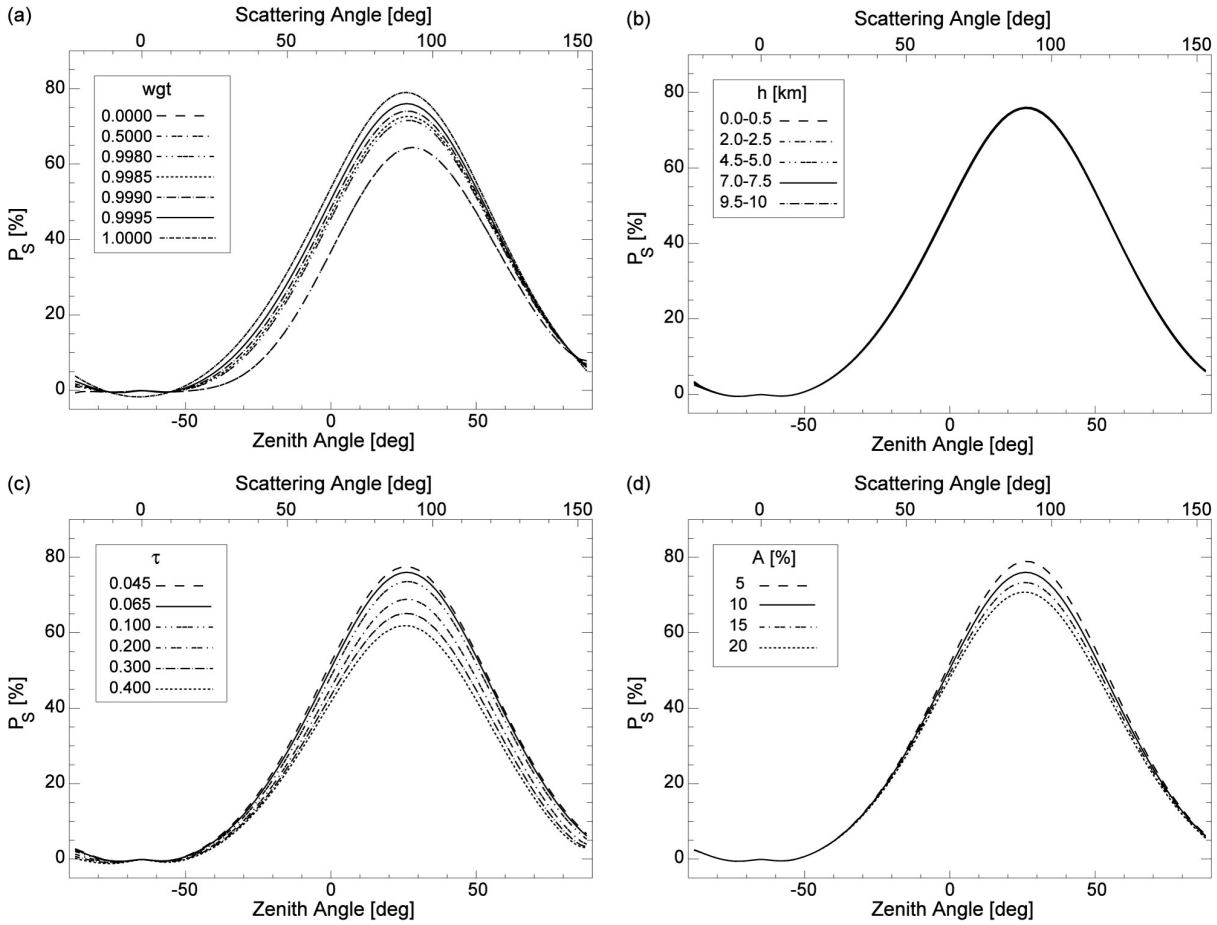

Figure 2.6: Same as in Figure 2.5, but for the weighting factor of (a) the fine mode, (b) the aerosol altitude, (c) the aerosol optical thickness, (d) the surface albedo.

the aerosol altitude, which have a minor or insignificant influence [see Figs. 2.5(a), 2.5(d), 2.5(f), and 2.6(b)]. For the position of the maximum degree of linear polarization, influences can be found for the real part of the refractive index, the fine mode median radius, and the standard deviation [see Figs. 2.5(b), 2.5(c), and 2.5(e)]. $P_s(\theta)$ in the backscattering direction is influenced mainly by the fine mode median radius, the standard deviation of the fine mode, and by the optical thickness [see Figs. 2.5(c), 2.5(e), and 2.6(c)]. The variations of the weighting factor and surface albedo have a weaker effect [see Figs. 2.6(a) and 2.6(d)]. The other parameters have an insignificant influence on the degree of linear polarization in the backscattering direction.

We also studied the sensitivity of $P_s(\theta)$ for very hazy-sky conditions. For hazy-sky aerosol parameters, derived on 8 May 2003 (Table 2.3), we found an increase in the sensitivity P_s for the real and imaginary parts of the refractive index, whereas the sensitivity of $P_s(\theta)$, because of the changes in the weighting factor, decreased strongly as compared with the clear-sky case. The strong influence of the fine mode median radius and the fine mode standard deviation remained, as did the influence of the aerosol optical thickness on $P_s(\theta)$. The influence of all the input parameters on the degree of linear polarization of skylight for both sky conditions (very clear and hazy) is summarized in Table 2.4. For classification of the input parameters we examined the impact of a relative parameter change of 10% based on the parameter ranges (see Tables 2.1 and 2.2) compared to the Cabauw case. We classified parameters with an absolute effect on the maximum degree of linear polarization $\Delta P_{s,\max}$ as follows: $\Delta P_{s,\max} \geq 1\% \equiv ++$ (very significant), $0.5 \leq \Delta P_{s,\max} < 1\% \equiv +$ (significant), $0.1 \leq \Delta P_{s,\max} < 0.5\% \equiv -$ (minor), $\Delta P_{s,\max} < 0.1\% \equiv --$ (insignificant).

For the position of the maximum polarization $\Delta\Theta_{P,\max}$ we took the following criteria: $\Delta\Theta_{P,\max} \geq 0.5^\circ \equiv ++$, $0.25^\circ \leq \Delta\Theta_{P,\max} < 0.5^\circ \equiv +$, $0.1^\circ \leq \Delta\Theta_{P,\max} < 0.25^\circ \equiv -$, and $\Delta\Theta_{P,\max} < 0.1^\circ \equiv --$. For the classification of input parameters and their effect on polarization in the forward- and backscattering directions, we followed a more qualitative approach by comparing the relative impact of all the input parameters. The results of this sensitivity study are used for the interpretation of measurements of skylight polarization in Section 2.5. The instrumental setup is described first in Section 2.4.

2.4 Instrument description

Here we give an overview of the polarization spectrometer FUBISS–POLAR (see Fig. 2.7 and Table 2.5) [Ruhtz et al., 2002], [Boesche, 2003] FUBISS–POLAR is designed to measure the degree of linear polarization of scattered skylight with a medium spectral resolution in the visible spectral range 400–700 nm and with a high spectral resolution in the near infrared (700–900 nm), including the O_2A band. Its optical front end consists of two identical entrance units. One entrance unit is linked via fiber optics with broadband spectrometers (with a spectral resolution of 7 nm) for the visible spectral range, and the

Table 2.3: Summary of the aerosol model parameters for clear (11 October 2004) and hazy (8 May 2003) sky conditions.

Parameter	Symbol	Cabauw Standard Case	Best Fit for 11 October 2004	Best Fit for 8 May 2003
Aerosol microphysical parameters (Mie)				
Wavelength	λ (μm)	0.675	0.675	0.675
Imaginary part of the refractive index	m_i	0.007	0.0007	0.0000
Real part of the refractive index	m_r	1.400	1.400	1.380
Median radius of the fine mode	r_f (μm)	0.080	0.080	0.120
Median radius of the coarse mode	r_c (μm)	0.425	0.425	0.700
Standard deviation of the fine mode	σ_f	1.400	1.300	1.950
Standard deviation of the coarse mode	σ_c	2.200	2.200	2.200
Weighting factor of the fine mode	w	0.9995	0.9996	0.9992
Average Volume	V	0.0055	0.0069	0.0725
Average Volume fine mode	V_f	0.0036	0.0029	0.0538
Macrophysical parameters (DAK)				
Aerosol altitude	h (km)	1	1	1
Aerosol optical thickness	τ_{aer}	0.065	0.065	0.390
Surface albedo	A	0.100	0.100	0.150
Mean deviation of the degree of polarization (fit-measurement)	(%)	1.490	0.300	-0.811
RMSE of the degree of polarization (fit-measurement)	(%)	1.350	0.760	0.910
Single-scattering albedo	ω	0.887	0.977	1.000
Fine mode fraction of τ_{aer}	(%)	70	51	17

Table 2.4: Input parameters for the DAK multiple scattering simulations. The third column gives the standard Cabauw case values for 11 October 2004. The fourth column gives the range in which the parameters are varied in the sensitivity study.

Parameters		Forward Polarization		Maximum Polarization		Position of Maximum		Backward Polarization	
		Clear	Hazy	Clear	Hazy	Clear	Hazy	Clear	Hazy
Microphysical aerosol parameters (Mie)									
Imaginary part of the refractive index	m_i	-	+	-	+	- -	- -	- -	+
Real part of the refractive index	m_r	+	+ +	+	+ +	-	+	- -	+ +
Median radius of the fine mode	r_f	+ +	+ +	+ +	+ +	- -	-	+	+
Median radius of the coarse mode	r_c	-	- -	-	- -	-	- -	- -	- -
Standard deviation of the fine mode	σ_f	+ +	+ +	+ +	+ +	+	+ +	+	+
Standard deviation of the coarse mode	σ_c	- -	- -	- -	- -	- -	- -	- -	- -
Weighting factor of the fine mode	w	+	- -	+	- -	-	- -	-	- -
Macrophysical parameters (DAK)									
Aerosol altitude	h	- -	- -	- -	- -	- -	- -	- -	- -
Aerosol optical thickness	τ_{aer}	+	+ +	+ +	+ +	- -	- -	+ +	+ +
Surface albedo	A	- -	- -	+	-	- -	- -	-	-

other with high spectral resolution spectrometers (with spectral resolution of 2.4 nm) for the near-infrared spectral range. Each entrance optical unit is equipped with four entrance tubes. Each tube contains a Glan–Thompson polarization prism with a different orientation of its polarization axis (0°, 45°, 90°, and 135°) and baffles for stray light suppression. The design allows arbitrary positioning of the entrance optics within the upper hemisphere. The possible measurement geometries are the principal plane and the almucantar (see also Fig. 2.1). The measured intensity I at a polarization prism axis orientation angle is related to Stokes parameters I, Q, and U as follows:

$$I_\alpha = \frac{1}{2} \cdot \left[I + Q \cos 2(\gamma + \alpha) + U \sin 2(\gamma + \alpha) \right] \tag{2.13}$$

where γ is the initial position of the polarization prism axes in the reference plane, which can be set to zero without loss of generality.

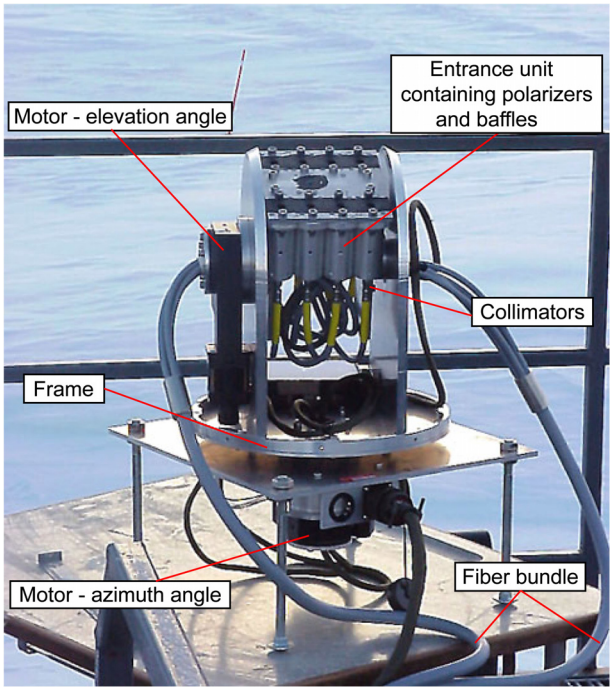

Figure 2.7: Setup of the polarization spectrometer FUBISS–POLAR. The instrument measures Stokes parameters I, Q, and U simultaneously at each scan angle.

To calculate Stokes parameters I, Q, and U, only three intensity measurements at different polarization prism axis angles are needed. However, a fourth measurement leads to an overdetermined system of equations and to a redundancy that allows a rough error estimation [Boesche, 2003]. The axis orientations of the FUBISS–POLAR polarization prisms are 0°, 45°, 90°, and 135°. The optical front end also comprises a four-quadrant diode to track the Sun position. This information is used to correct the alignment of the entrance optics by motors that are mounted at the frame construction. Measurements during a sky scan can be done continuously or at defined directions. FUBISS–POLAR is able to scan the principal plane or the almucantar within minutes, depending on the integration time, so that the Sun's relative position changes marginally. Since FUBISS–POLAR measures the intensities $I_{0°}$, $I_{45°}$, $I_{90°}$, and $I_{135°}$ simultaneously, it can be used for measurements of temporally varying objects. The system works autonomously, i.e., it takes the variation of the Sun's position into account. These are important advantages compared with other polarization measurement systems [Beaglehole and Carter, 1992], [Preusker et al., 1995], [Fitch and Coulson, 1997], [Takashima et al., 1999]. From the investigation of the random errors (signal-to-noise ratio and calibration standard stability) and the systematic errors (pointing error, fiber optics error, instrument polarization, and polarization prism accuracy) the

absolute polarimetric accuracy is estimated to be 1% and the alignment error is estimated to be 0.5° [Ruhtz et al, 2002], [Boesche, 2003].

2.5 Comparison of measurements and model results

Here we compare the multiangle measurements of the degree of polarization of skylight with the radiative transfer simulations. Conclusions about the aerosol refractive index, the aerosol size distribution, and the fine mode fraction of the aerosol optical thickness are drawn from the comparison. As an indication of whether the derived aerosol size parameters were oriented in the right direction, we looked at the spectral behavior of the maximum degree of polarization (see Fig. 2.8) and the Angström coefficient derived from the sunphotometer measurements and the Mie simulations. The Angström coefficient is the exponent of a power-law fit to the aerosol optical thickness: $\tau_{\mathrm{aer}}(\lambda) \propto \lambda^{-\alpha}$, or equivalently to the Mie extinction cross section. Using only two wavelengths for determining α, we have $\alpha = (\ln(\tau_{aer}(\lambda_1)) - \ln(\tau_{aer}(\lambda_2)))/(\ln(\lambda_2) - \ln(\lambda_2))$. The smaller the Angström coefficient, the bigger the aerosol particle size.

The measurements were taken with the polarization spectrometer FUBISS–POLAR described in Section 2.4. The measurement site was located at Cabauw, The Netherlands (51.58° N, 4.56° E). The measurements of polarization in the principal plane were taken under cloudless conditions on 8 May 2003 and 11 October 2004.

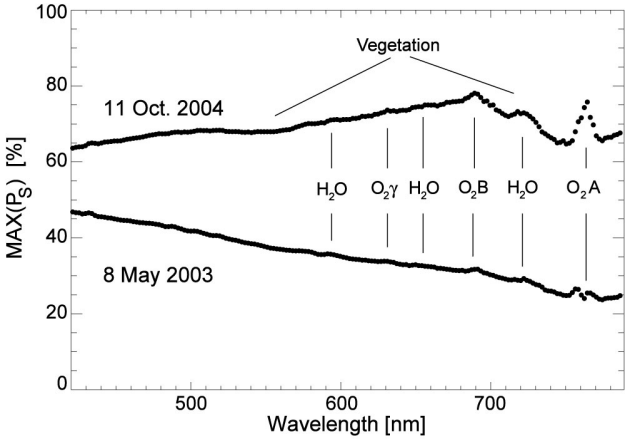

Figure 2.8: Maximum degree of polarization as a function of wavelength as measured at Cabauw, The Netherlands on 11 October 2004 at a solar zenith angle of $\theta_0 = 65°$ and on 8 May 2003 at a solar zenith angle of $\theta_0 = 71°$.

The measurements on 8 May 2003 were taken at 06:15 UTC at a solar zenith angle of $\theta_0 = 71°$ in 0.4° steps of viewing zenith angle θ. The integration time was 410 ms, and one sky scan took less than 4 min. The aerosol optical thickness was $\tau_{\text{aer}} = 0.39$ at $\lambda = 675$ nm, as measured in Cabauw by the SPUV sunphotometer (Yankee Environmental Systems, Turners Falls, Massachusetts) [Stammes and Henzing, 2000]. During the measurements the sky was cloudless, but it remained hazy the whole morning. At approximately noon, convective clouds started to develop. The surface albedo A of Cabauw in May at 675 nm was assumed to be 0.10 [Koelemeijer et al, 2003]. The measurements on 11 October 2004 were taken at 09:55 UTC at a solar zenith angle of $\theta_0 = 65°$ in 2.5° steps of viewing zenith angle θ. The integration time was 500 ms, and one sky scan took less than 1 min. The aerosol optical thickness was $\tau_{\text{aer}} = 0.065$ at $\lambda = 675$ nm. The whole day was very clear and cloudless. As a comparison, the multiyear average aerosol optical thickness at $\lambda = 675$ nm in Cabauw was approximately 0.15. The surface albedo A of Cabauw in October at 675 nm was assumed to be 0.15 [Koelemeijer et al, 2003]. The most important meteorological conditions for the two measurement days are combined in Table 2.6.

The skylight polarization measurements $P_s(\theta)$ at 675 nm for both days are shown in Figures 2.9(a), 2.9(b), and 2.10(a). The observations are shown with their absolute error bars, i.e., 1% for polarization and 0.5° for the viewing direction.

Table 2.6: Meteorological conditions during the measurements.

Date and Time	Solar Zenith Angle (deg.)	Temperature [°C]	Pressure (hPa)	Relative humidity (%)	Wind speed (m/s)
8 May 2003 06:15 UTC	70.81	10.9	1017.8	100	4.2
11 October 2004 09:55 UTC	65.02	9.5	1021.2	81	6.9

2.5.1 Clear-sky comparison for 11 October 2004

A lookup table of the calculated degree of skylight polarization (see also Section 2.3) for different aerosol microphysical properties was searched automatically to find the best fit to the data. The aerosol model parameters found from this lookup table were then used as a starting point for manual investigation to find a better fit between the observed and the

calculated $P_s(\theta)$. The single-scattering albedo of the model fits is included in Table 2.3, as well as the fine mode fraction of the aerosol optical thickness, calculated from the Mie extinction cross sections.

In Figure 2.9(a) the lookup table fit (the Cabauw case) to the measurements of the degree of linear polarization as a function of viewing zenith angle is shown as a solid line. The mean deviation between the measurement and the simulation is 1.49%, and the root-mean-square error (RMSE) is 1.35%. The model parameters of this fit are shown in Table 2.3. Furthermore, a pure Rayleigh simulation (no aerosol) is shown to point out the influence of the added aerosol. Two simulations using aerosol microphysical parameters according to the AERONET climatology for Greenbelt, USA, and Paris, France, are also shown [Dubovik et al., 2001]. The aerosol microphysical parameters of the Greenbelt and Paris climatology are shown in Table 2.1. The decrease of polarization between the no-aerosol and aerosol-loaded simulations is attributable to scattering by aerosols, which gives a lower $P_s(\theta)$ than scattering by molecules (see Subsection 2.3.2). A shift in the position of the maximum degree of polarization takes place as well. The decrease is seen mainly in the backscattering

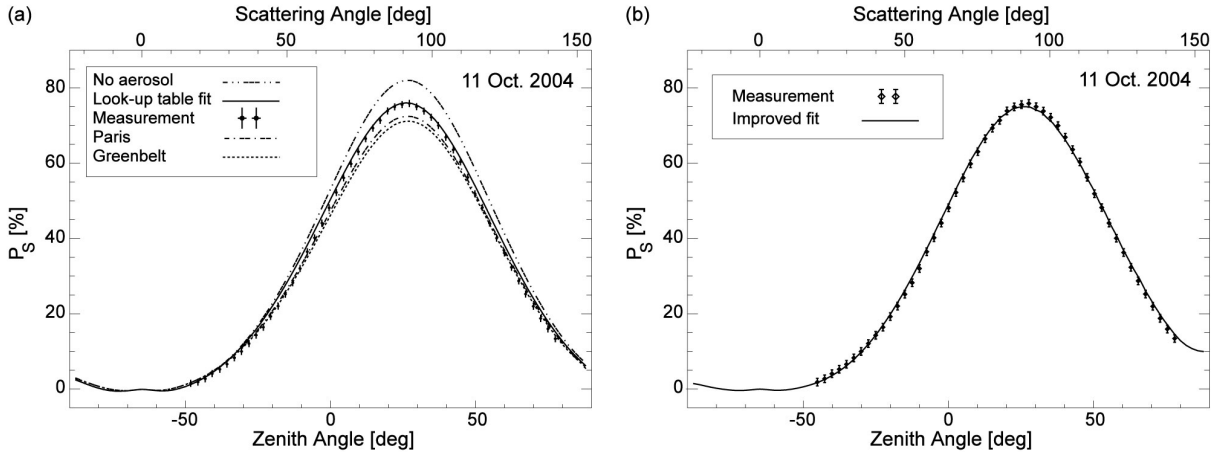

Figure 2.9: Degree of linear polarization P_s at $\lambda = 675$ nm as a function of the viewing zenith and scattering angles in the principal plane at a solar zenith angle of $\theta_0 = 65°$, as measured on 11 October 2004 at Cabauw, The Netherlands. (a) Comparison with multiple scattering calculations for a pure molecular atmosphere (maximum of P_s = 82.2% at $\theta = 25°$), as well as for aerosol loaded atmospheres. All the input parameters are shown in Tables 2.1 and 2.2. The best fit between measurement and model result is indicated by a solid curve. (b) Comparison with an improved model fit (see Table 2.3).

direction and in the maximum degree of polarization. The simulations using the Greenbelt and the Paris aerosol microphysical parameters have a lower maximum degree of polarization than those with the lookup table fit.

The lookup table fit could be improved by varying the imaginary part of the refractive index, the weighting factor of the fine mode, and the standard deviation of the fine and coarse modes [see Fig. 2.9(b)]. After the improvement, the mean deviation between simulation and measurement is only 0.30% and the RMSE is reduced to 0.76%. The aerosol microphysical parameters of this improved fit are also shown in Table 2.3. The absolute deviation of P_s between the measurements and the model fit is shown in Figure 2.10(b). Compared with the measurement, both model fits have a higher degree of linear polarization in the forward- and backscattering directions and a lower maximum degree of polarization. Given the fact that the measurement accuracy is 1%, the deviation is acceptable.

The effect on polarization because of the ozone absorption in the Chappuis band had been taken into account. The difference in the degree of polarization with and without ozone absorption is approximately -0.17% and affects mainly the backscattering direction.

As an indication of whether the aerosol size parameters were oriented in the right direction, we looked at the wavelength behavior of the maximum degree of polarization. The maximum degree of polarization at 675 nm was higher than at 465 nm (see Fig. 2.8). This is an indication of small particles [Aben et al., 1999]. Further, we looked at the Angström coefficient. From the sunphotometer measurements we derived an α of 1.1 between 550 and 675 nm and of 2.3 between 675 and 780 nm. From the Mie extinction cross sections we calculated an α of 1.7 between 550 and 675 nm and of 2.5 between 675 and 780 nm. Thus the sun photometer measurements also indicated the presence of small particles, which strengthens the conclusion of the presence of small particles as found by the polarization measurements.

2.5.2 Hazy-sky comparison for 8 May 2003

Because of a higher aerosol optical thickness τ_{aer} and a higher surface albedo A, and because of a larger solar zenith angle θ_0 on the hazy day, we already expected a lower degree of linear polarization, compared with the measurements of the clear day. The increase of τ_{aer} resulted in an increase of the radiance and a decrease of $P_s(\theta)$. This is the

result of more aerosol scatterers and hence more scattering in the line of sight by the less polarizing aerosols, compared with the molecules. The larger *A* decreases $P_s(\theta)$ because of an increase of depolarized light from the surface, whereas the larger θ_0 causes a shift in the position of the maximum degree of linear polarization to lower viewing zenith angles and a decrease of the effect of A (weaker illumination of the surface). As we have already seen in Section 2.3 we do not expect any influence on $P_s(\theta)$ because of the aerosol altitude. The comparison with the measurements of the clear day shows the expected shift of the position of the maximum to lower viewing zenith angles and a much lower degree of linear polarization [see Figs. 2.9(a), 2.9(b), and 2.10(a)]. Furthermore, we assume the presence of hygroscopic aerosols at the measurement site in Cabauw. With increasing relative humidity, it is generally expected that hygroscopic particles get larger and that the real and imaginary parts of the refractive index decrease. The relative humidity during the measurements was approximately 100%, compared to 81% on the clear day. Taking the microphysical parameters of the clear day as a starting point for the investigation, we increased the fine mode standard deviation and the median radii of the fine and coarse modes, whereas we decreased the real and imaginary parts of the refractive index, as well as the weighting factor of the fine mode. In Figure 2.10(a) the best fit to the FUBISS–POLAR measurements of the degree of linear polarization as a function of the viewing zenith angle in the principal plane is shown by a solid curve. The mean deviation between measurements and simulations is 0.81%, and the RMSE is 0.91%. The model parameters for this fit are shown in Table 2.3. The absolute difference of $P_s(\theta)$ between the model fit and the measurement is shown in Figure 2.10(b). The model fit has a higher degree of polarization at approximately the maximum and a lower degree of polarization in the forward-scattering and backscattering directions. The difference between the measurements and the model for the hazy day is similar in magnitude and shape to that of the clear day, but reversed in sign. The reason for this is not clear because the difference is mostly below 1%, which is within the limits of measurement accuracy. The difference in the degree of polarization with and without ozone absorption in the Chappuis band is approximately -0.11%, and also affects mainly the backscattering direction.

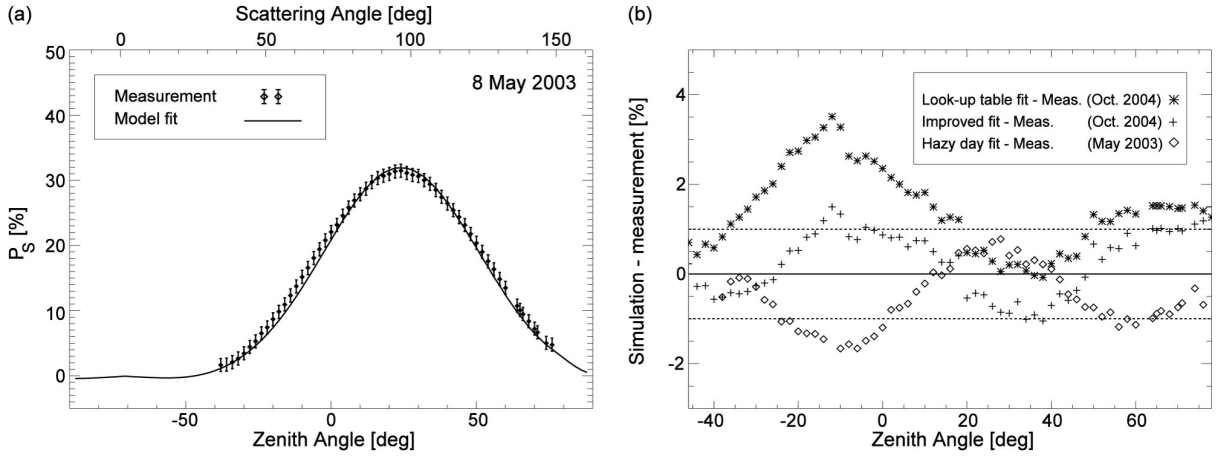

Figure 2.10: (a) Degree of linear polarization P_s at $\lambda = 675$ nm as a function of the zenith and scattering angles in the principal plane at a solar zenith angle of $\theta_0 = 71°$ as measured on 8 May 2003 at Cabauw, The Netherlands, compared with the best fit. For the pure molecular atmosphere we derive a maximum of P_s = 81.1% at $\theta = 19°$. (b) Deviation between the measurement and the model fits. Dotted lines indicate a deviation of 1%.

As an indication of whether the aerosol size parameters are oriented in the right direction, we reexamined the wavelength behavior of the maximum degree of polarization. For this day we find a lower maximum degree of polarization at 675 nm than at 465 nm (see Fig. 2.8), which is an indication of larger particles [Aben et al., 1999]. The Angström coefficient α, derived from the sunphotometer measurements, is 0.5 between 550 and 675 nm and 0.8 between 675 and 780 nm. From the Mie extinction cross sections we calculated an of 0.7 between 550 and 675 nm and of 0.9 between 675 and 780 nm. Thus the sunphotometer measurements also indicated the presence of larger particles on the hazy day than on the clear day.

2.6 Summary and Conclusions

The analysis of the dependence of the degree of linear polarization of skylight in the Sun's principal plane as a function of aerosol microphysical parameters using Mie calculations and multiple-scattering simulations shows that for a clear sky the degree of polarization is strongly influenced by the parameters of the fine mode of the aerosol size distribution (the median radius and geometric standard deviation), the real part of the aerosol refractive index, and the aerosol optical thickness. The other aerosol parameters show less influence. The sensitivity study was extended to hazy-sky conditions, where we found an increase of the sensitivity for the real and imaginary parts of the refractive index, whereas the sensitivity

attributable to changes in the weighting factor of the fine mode decreases strongly. The strong influence of the fine mode parameters as well as of the aerosol optical thickness remains. The determination of some parameters, such as the imaginary parts of the refractive index, is complicated by the fact that we can have nonunique solutions. We find similar results for a different combination of aerosol parameters, for instance, by lowering the imaginary part and increasing the weighting factor, or the other way around. However, this results in two strongly differing single-scattering albedos. An accurate determination of the imaginary part of the refractive index does not seem to be possible if only polarimetry is used.

From this sensitivity study in the continuum (outside the absorption bands) we conclude that the number of free input parameters for the polarization radiative transfer simulations can be reduced from ten to seven (see Table 2.3), namely, the real and imaginary parts of the refractive index, the median radius and the geometric standard deviation of the fine mode, the aerosol optical thickness, the weighting factor of the fine mode, and the surface albedo. The parameters of the coarse mode of the size distribution and the aerosol altitude can be regarded as nonfree parameters, because of their minor influence on skylight polarization. The aerosol optical thickness should be measured together with the polarization of skylight because of the strong influence of the aerosol optical thickness and to further reduce the number of free input parameters.

From skylight polarization measurements in Cabauw, The Netherlands, we derived microphysical aerosol parameters by comparing the calculated degree of polarization with the measured degree of polarization. The best fit was found manually, by adjusting every input parameter until we found the best comparison between measurement and simulation. To avoid local minima problems, we took the whole zenith angle range into account for the comparison. Furthermore, we calculated the fine mode fraction of the aerosol optical thickness from the microphysical aerosol parameters derived from the comparison. The measurements were taken at clear- and hazy-sky conditions with FUBISS–POLAR, a ground-based multispectral and multiangle polarization spectrometer. The aerosol optical thickness was measured with a sunphotometer. The comparison of the measurements and simulations of the degree of linear polarization shows very good agreement. For the comparison we used a bimodal lognormal aerosol size distribution because simulations with a single-mode approach showed that it was not possible to match the position of the

maximum degree of polarization of the measurements while finding an agreement in the forwardscattering and backscattering directions. As a measure of the quality of the solution we took the mean deviation and the RMSE. The difference between the model fits and the measurements of polarization was within the range of a measurement accuracy of 1% in degree of polarization. The RMSE between the model fit and the measured data was less than 0.92% for both test days. The model fit of the clear day seemed to overestimate the polarization measurements in the forward-scattering direction as well as in the backscattering direction, and underestimate it around the maximum degree of polarization. The model fit of the hazy day looks nearly mirror inverted to the clear-day model fit. The very good agreement between measurements and the simulations suggests that the basic assumption of Mie theory is applicable for the cases chosen here. If the sphericity assumption would not have been applicable it would not have been possible to achieve a satisfactory fit to the polarization measurements [Dubovik and King, 2000]. Furthermore, we see that the resulting size distribution, derived from the comparison between the polarization measurements and the simulations tended to be in the same direction as suggested by the sunphotometer measurements and the investigation of the wavelength dependence measurements of the maximum degree of linear polarization.

From the sensitivity study and the comparison between the simulations and the measurements, we find that it is not sufficient to measure and or simulate the degree of linear polarization only at a single-scattering angle in the principal plane, e.g., 90°. To estimate the aerosol properties reliably one has to find an agreement between the simulation and the measurement of polarization in the forward-scattering direction, in the backscattering direction, and the maximum, as was done here.

Based on this polarization study and previous studies [Cairns et al., 1997], [Dubovik and King, 2000], [Vermeulen et al., 2000], [Dubovik, 2004] a retrieval algorithm will be developed to automatically retrieve aerosol microphysical and optical properties from skylight polarization measurements at multiple wavelengths.

Appendix 2.A Delta Approximation

The delta approximation consists of truncating the forward peak of F_{11} at a certain scattering angle Θ_c [Joseph et al., 1976]. By doing so, the energy which is scattered in near-forward directions, is not considered to be scattered at all. Therefore, the scattering cross-section is reduced, and consequently also the extinction cross section, single-scattering albedo and optical thickness are changed. The truncated phase function has to be normalized. The truncation is done such that $F_{11}(\Theta) = F_{11}(\Theta_c)$ for $0 \le \Theta < \Theta_c$. The same is done for the other scattering matrix elements. The relative amount of energy, which is truncated is

$$\delta = \int_0^{\theta_c} F_{11}(\Theta)\mathrm{d}\Omega - F_{11}(\Theta_c)\int_0^{\theta_c} \mathrm{d}\Omega \tag{A1}$$

The scattering and extinction cross section now reduce to:

$$\sigma_s' = \sigma_s(1-\delta)\,, \tag{A2}$$

$$\sigma_e' = \sigma_e(1-\delta\omega)\,. \tag{A3}$$

The new single scattering albedo is now

$$\omega' = \omega\frac{1-\delta}{1-\delta\omega}\,. \tag{A4}$$

The optical thickness is adjusted according to

$$\tau' = (1-\delta\omega)\tau\,. \tag{A5}$$

The new phase function, together with the whole scattering matrix, is renormalized by:

$$F_{11}'(\Theta) = \frac{1}{1-\delta}F_{11}(\Theta)\,. \tag{A6}$$

Chapter 3

Polarization of skylight in the O_2A band: effects of aerosol properties

E. Boesche, P. Stammes, R. Preusker, R. Bennartz, W. H. Knap, and J. Fischer, *Applied Optics* **47**, 3467-3480 (2008).

Abstract

Motivated by several observations of the degree of linear polarization of skylight in the oxygen A (O_2A) band that do not yet have a quantitative explanation, we analyze the influence of aerosol altitude, microphysics, and optical thickness on the degree of linear polarization of the zenith skylight in the spectral region of the O_2A band, between 755 to 775 nm. It is shown that the degree of linear polarization inside the O_2A band is particularly sensitive to aerosol altitude. The sensitivity is strongest for aerosols within the troposphere and depends also on their microphysical properties and optical thickness. The polarization of the O_2A band can be larger than the polarization of the continuum, which typically occurs for strongly polarizing aerosols in an elevated layer, or smaller, which typically occurs for depolarizing aerosols or cirrus clouds in an elevated layer. We show that in the case of a single aerosol layer in the atmosphere a determination of the aerosol layer altitude may be obtained. Furthermore, we show limitations of the aerosol layer altitude determination in case of multiple aerosol layers. To perform these simulations we developed a fast method for multiple scattering radiative transfer calculations in gaseous absorption bands including polarization. The method is a combination of doubling-adding and k-binning methods. We present an error estimation of this method by comparing with accurate line-by-line radiative transfer simulations. For the O_2A band, the errors in the degree of linear polarization are less than 0.11% for transmitted light, and less than 0.31% for reflected light.

3.1 Introduction

Polarization observations of reflected or transmitted skylight in absorption bands, such as the oxygen A (O_2A) band or water vapor bands, show prominent features due to molecular absorption. For ground-based polarization measurements of transmitted skylight in the spectral region of the O_2A band these features are apparent in observations taken by [Stammes et al., 1994], [Preusker et al., 1995], [Aben et al., 1997], [Aben et al., 1999]. These authors have shown that on cloudless days the degree of linear polarization within the O_2A absorption band, around 760 nm, can be significantly higher or lower than the absorption-free continuum polarization (see Fig. 3.1). According to Stammes et al. (1994), the strong molecular absorption within the absorption band can explain the difference in polarization between continuum and absorption band. The strong absorption is shielding lower layers of the atmosphere from incident sunlight. Therefore most of the light has been scattered at high altitudes, whereas in the continuum no such shielding occurs. Thus, if the polarization properties of the lower atmospheric layers differ from those of the upper layers, a change of polarization can occur between the polarization in the continuum and the absorption band. Aerosol layers could especially cause such a change. Ground-based measurements of the polarization of the clear zenith sky in the O_2A band may offer information on the aerosol altitude profile [Stammes et al., 1994], [Preusker et al., 1995], [Stam et al., 1999].

In this paper we analyze the sensitivity of the degree of linear polarization of transmitted skylight in the spectral region of the O_2A band, between 755 and 775 nm, to changes of aerosol altitude, aerosol microphysics, and aerosol optical thickness (in the troposphere and lower stratosphere), extending the above mentioned work. To adequately study the effect of aerosol altitude on polarization of skylight in the O_2A band, we combined two existing radiative transfer methods to significantly improve the calculation time while maintaining a high accuracy compared to line-by-line simulations. As a spectral approximation technique we use the k-binning method, which is similar to a k-distribution approach, but overcomes shortcomings of a conventional k-distribution [Bennartz and Preusker, 2007], [Bennartz and Fischer, 2000]. We integrate this method in monochromatic doubling-adding multiple scattering calculations, including polarization, for vertically inhomogeneous atmospheres. An advantage of our combined method approach is that an implementation of a different response function is straightforward and does not require a new set of multiple scattering simulations. For our study we use spectral response functions with a resolution of 0.36 nm at

full width at half-maximum (FWHM) and an equal spacing of 0.21 nm. As atmospheric scatterers, we use Rayleigh scattering molecules and spherical aerosols as well as nonspherical ice crystal particles, using Mie-theory and the geometric-optics (GO) approximation. In Section 3.2 the definition of relevant polarization parameters, such as Stokes parameters, and the scattering matrix, are briefly discussed. Furthermore, we describe our combined method for fast radiative transfer simulations in absorption bands including polarization and give an error estimation of this method by comparing with accurate line-by-line radiative transfer simulations. In Section 3.3 we show the sensitivity of the degree of linear polarization of the zenith skylight to aerosol altitude and aerosol optical thickness within the O_2A absorption band and for the absorption-free continuum. Furthermore, we show the influence of the solar zenith angle, and spectral response function on the degree of linear polarization of the zenith skylight. The summary and conclusions follow in Section 3.4.

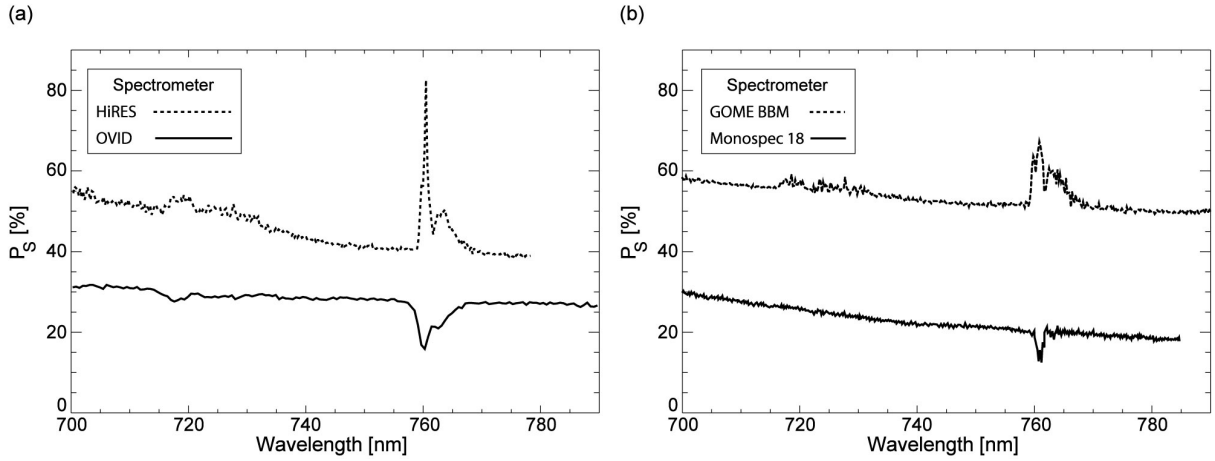

Figure 3.1: Ground-based measurements of the degree of linear polarization P_s of the cloud free sky as a function of wavelength. (a) As measured at the Institute for Space Sciences, in Berlin, Germany (52.5° N, 13.3° E) on May 11 1994 with the spectrometer OVID (solid line), with a spectral resolution of 2.0 nm, and as measured on June 24 1994 with the spectrometer HiRES (dotted line), with a spectral resolution of 0.3 nm [Preusker et al., 1995]. Geometry at both days: solar zenith angle $\theta_0 \approx 40^\circ$, viewing zenith angle $\theta = 60^\circ$, azimuth angle $\phi - \phi_0 = 180^\circ$, and scattering angle $\Theta = 100^\circ$. (b) As measured at SRON, Utrecht, the Netherlands (52.1° N, 5.2° E) on April 7 1997 with the spectrometer GOME BBM, with a spectral resolution of 0.33 nm, at a solar zenith angle of $\theta_0 = 79^\circ$, viewing zenith angle of $\theta = 0^\circ$, and scattering angle of $\Theta = 79^\circ$ (dotted line) [Aben et al., 1999], and as measured on October 19 1993 at KNMI, in De Bilt, the Netherlands (52.1° N, 5.2° E) with a Jarrell Ash Monospec 18 spectrometer, with a spectral resolution of 0.3 nm, at a solar zenith angle of $\theta_0 = 66^\circ$, viewing zenith angle of $\theta = 0^\circ$, and scattering angle of $\Theta = 66^\circ$ (solid line) [Stammes et al., 1994].

3.2 Combined method for fast simulations of the degree of polarization in absorption bands

3.2.1 Stokes parameters and polarization

The state of polarization of a light beam can be defined through the components of the Stokes vector $\mathbf{I}$ [Chandrasekhar, 1960], [van de Hulst, 1981], by measuring the relative intensities I_α of the light beam after it has passed through polarization devices at different orientation angles α of their transmission axes [Shurcliff, 1962]:

$$\mathbf{I} = \begin{pmatrix} I \\ Q \\ U \\ V \end{pmatrix} = \begin{pmatrix} I_{0^\circ} + I_{90^\circ} \\ I_{0^\circ} - I_{90^\circ} \\ I_{45^\circ} - I_{135^\circ} \\ I_+ - I_- \end{pmatrix} \tag{3.1}$$

where 0°, 45°, 90° and 135° denote the orientation angle of the polarization transmission axis with respect to a reference plane, and + and – are the right- and left-handed circular polarization components. The Stokes parameter I describes the total intensity, Q and U the linear polarization and V the circular polarization of the light beam. The degree of linear polarization in terms of Stokes parameters is defined as follows [Hovenier et al., 2004]:

$$P = \frac{(Q^2 + U^2)^{1/2}}{I} \tag{3.2}$$

In case $U = 0$, the following alternative definition for the degree of linear polarization will be used:

$$P_s = -\frac{Q}{I} \tag{3.3}$$

For $P_s < 0$ and for $P_s > 0$ the light is polarized parallel and perpendicular to the reference plane, respectively.

3.2.2 Scattering matrix at 765 nm

The scattering matrix $\boldsymbol{F}$ describes the change of direction, intensity, and polarization of a light beam caused by a single scattering event. The Stokes parameters of the scattered beam at scattering angle Θ can be written as a linear transformation of the Stokes parameters of the incident beam. We consider independent light scattering by an ensemble of randomly oriented particles, which have a plane of symmetry. Then the scattering matrix of the ensemble takes the following form [Chandrasekhar, 1960], [Shurcliff, 1962], [Hovenier et al., 2004]:

$$\begin{pmatrix} I_{sca} \\ Q_{sca} \\ U_{sca} \\ V_{sca} \end{pmatrix} = \begin{bmatrix} F_{11} & F_{12} & 0 & 0 \\ F_{12} & F_{22} & 0 & 0 \\ 0 & 0 & F_{33} & F_{34} \\ 0 & 0 & -F_{34} & F_{44} \end{bmatrix} \begin{pmatrix} I_{in} \\ Q_{in} \\ U_{in} \\ V_{in} \end{pmatrix} \tag{3.4}$$

where the subscripts “sca” and “in” stand for scattered and incoming beams. The scattering matrix elements F_{ij} are functions of the scattering angle. The function F_{11} is called the phase function and is normalized to 1. For unpolarized incident light only the first column of the scattering matrix suffices to determine the intensity and state of polarization of the light scattered once. In this case F_{11} is proportional to the scattered intensity as a function of the scattering angle and, furthermore, the degree of linear polarization is represented by the ratio $-F_{12}/F_{11}$. $\boldsymbol{F}$ depends on the wavelength, the refractive index, the size distribution, and the shape of the scattering particles and contains all polarizing properties of the ensemble of randomly oriented particles.

For spherical particles, we use Mie theory and for nonspherical ice crystal particles, the GO approximation to calculate the scattering matrix [de Rooij and van der Stap, 1984], [Hess et al., 1998].

3.2.3 Combined method for fast radiative transfer simulations in absorption bands including polarization

The disadvantage of accurate line-by-line radiative transfer simulations for gaseous absorption bands is the time consumption of such codes, especially if taking polarization into account. To overcome this drawback we combine two methods to significantly improve the calculation time, while maintaining a high accuracy compared to line-by-line simulations.

For the monochromatic multiple scattering simulations of polarized light in a vertically inhomogeneous atmosphere, we use the doubling-adding method (DAK – Doubling-Adding KNMI) [de Haan et al., 1987], [Stammes et al., 1989], [Stammes, 2001], and combine this with the k-binning method, which is similar to a k-distribution approach, but overcomes shortcomings of a conventional k-distribution [Bennartz and Fischer, 2000], [Bennartz and Preusker, 2007]. The idea of a conventional k-distribution method is to put absorption lines, within a certain wavelength interval, in order of absorption strength rather than of wavelength, resulting in a smooth dependence of absorption coefficient. This, in turn, makes spectral integration much easier and less time consuming. This is done for each channel of a given instrument. The significant difference between k-binning and a conventional k-distribution is that the entire absorption band is simulated and afterwards the radiances for each channel are reconstructed from the simulations that represent the entire spectral band. Thus no assumptions about the shape of the sensor weighting function have to be considered *a priori* for a given spectral interval. Any sensor response function can be constructed from a set of radiative transfer simulations for a spectral interval. This requires, to some extent, different constraints on the way the subdivision in spectroscopically similar intervals is performed. It has to be ensured that not only the band-averaged transmission is resembled to high accuracy, but also the transmission in each spectroscopically similar k-binning interval.

In the following we outline our combined method for fast simulations of radiance and polarization in absorption bands:

Step 1: k-binning. We calculate the molecular absorption coefficient k_i (or molecular absorption optical thickness τ_i^{abs}) for the i = 1, …, N k-binning intervals and each atmospheric layer using the k-binning method. As molecular spectroscopic database we used HITRAN 2001 [Rothman et al., 2003]. The sensor's spectral response function $f(\lambda)$ is

not considered *a priori*, instead the entire spectral band is subject to the k-binning analysis. The number of resulting k-binning intervals depends on the considered band interval, the resolution steps with which k-binning samples the spectroscopic database, the band-averaged transmission accuracy and the transmission accuracy in each spectroscopically similar k-binning interval. The resulting k-terms $k_i(\gamma)$ are no longer in the wavelength space, but rather in the **Γ**-space, in which the wavelengths are sorted in order of increasing gas absorption coefficient $k(\lambda)$. There is a bijective mapping function between λ and γ with $B(\lambda) = \gamma$ and $B^{-1}(\gamma) = \lambda$. This function is called the index function and maps from wavelength space into **Γ**-space.

Step 2: Mie/GO calculations. We calculate the single scattering properties of the atmospheric scatterers (aerosols, cirrus clouds) at a given wavelength λ_c using Mie-theory and/or the GO approximation (see also Subsections 3.2.2 and 3.3.1). The wavelength λ_c is used for the monochromatic radiative transfer simulations following Steps 3 and 4.

Step 3: DAK calculations. We use DAK to calculate the molecular scattering properties (molecular scattering coefficient σ_{sca} or molecular scattering optical thickness τ_{sca} and the depolarization factor δ) at λ_c. The scattering properties are assumed to be constant over the entire band. The chosen wavelength λ_c lies within the absorption band and stays constant throughout the calculations, e.g. 765 nm if considering the O_2A band. Subsequent to the calculations of the molecular scattering properties, we use DAK for the monochromatic multiple scattering simulations of the Stokes vector $\mathbf{I}_i$ for the i = 1, …, N k-binning intervals, in which the underlying surface is assumed to be Lambertian, and thus the reflected light is assumed to be unpolarized and isotropic.

Step 4: Weighting. We calculate the components of the Stokes vector $\mathbf{I}$ for arbitrary instrument channels within the considered band. Considering the results above and an instrument response function $f(\lambda)$ we only have to know how much each k-binning interval i contributes to the total spectral response of the channel. This fraction can be calculated by:

$$w_i = \int_{\Delta\gamma_i} f(B^{-1}(\gamma))d\gamma \tag{3.5}$$

The weights constitute the weighting of an instrument channel with response function $f(\lambda)$ in the k-binning. Now the components of the Stokes vector $\mathbf{I}$ of this channel can be constructed using:

$$\mathbf{I} = \sum_{i=1}^{N} w_i I_i \tag{3.6}$$

where $\mathbf{I}$ is the Stokes vector of the designated instrument channel and I_i are the results of the monochromatic radiative transfer simulations for the i = 1, …, N k-binning intervals. For example, if one particular channel is fully within one k-binning interval, e.g., an absorption-free channel, the corresponding weight $w_i = 1$. From this consideration it is obvious that not only the broad-band transmission, but also the transmission within each k-binning interval, has to be accurate. This approach significantly reduces the number of necessary simulations for different sensors and therefore reduces the computational cost.

3.2.4 Error estimation of the combined method

In this Subsection we show the error in the Stokes component I and P_s of transmitted and reflected light within the O_2A band between 755 and 775 nm, using the combined method. We determine the error by comparing the intensity I^{lbl} and the degree of linear polarization P_s^{lbl} as calculated using the line-by-line method, with I^{com} and P_s^{com} calculated using the combined method. We used a spectral response function with a resolution of 0.36 nm at FWHM and an equal spacing of 0.21 nm, which is similar to satellite spectrometers such as the Global Ozone Monitoring Experiment (GOME and GOME-2) or the Scanning Imaging Absorption Spectrometer for Atmospheric Cartography (SCIAMACHY) [Burrows et al., 1999], [Bovensmann et al., 1999]. The error of the degree of linear polarization is defined as:

$$\varepsilon_P = P_s^{com} - P_s^{lbl} \tag{3.7}$$

and the error of I as:

$$\varepsilon_I = \left(I^{com} - I^{lbl}\right) / I^{lbl} \tag{3.8}$$

Here the superscripts “com” and “lbl” refer to the combined method and the line-by-line method, respectively.

The line-by-line calculations of I and P_s for diffusely transmitted and reflected light are performed using DAK at a solar zenith angle of $\theta_0 = 65^\circ$, a viewing zenith angle of $\theta = 0^\circ$, a spectral resolution of 0.01 nm, a surface albedo of A_s = 0.2, and a standard mid-latitude summer atmosphere. In addition to molecular Rayleigh scattering we assume two types of aerosols, aerosol$_1$ and aerosol$_2$ (see Tables 3.1). The aerosols are located in the boundary layer (0-1km). In case of aerosol$_1$ the optical thickness is $\tau = 0.048$, resembling clear sky conditions, and in case of aerosol$_2$ $\tau = 0.350$, resembling hazy sky conditions. Figure 3.2 shows line-by-line calculations and convoluted spectra of the transmitted radiance and degree of linear polarization in the O_2A band. For the error analysis, we use the results obtained using aerosol$_1$. In this case the diffuse transmission is lower, compared to aerosol$_2$, which results in a higher sensitivity of the error to small differences between line-by-line and the combined method calculations.

For the combined method calculations we used 37 k-binning intervals, thus reducing the calculation time by a factor of 54, as compared to the line-by-line calculations. For further k-binning input parameters, see Table 3.3.

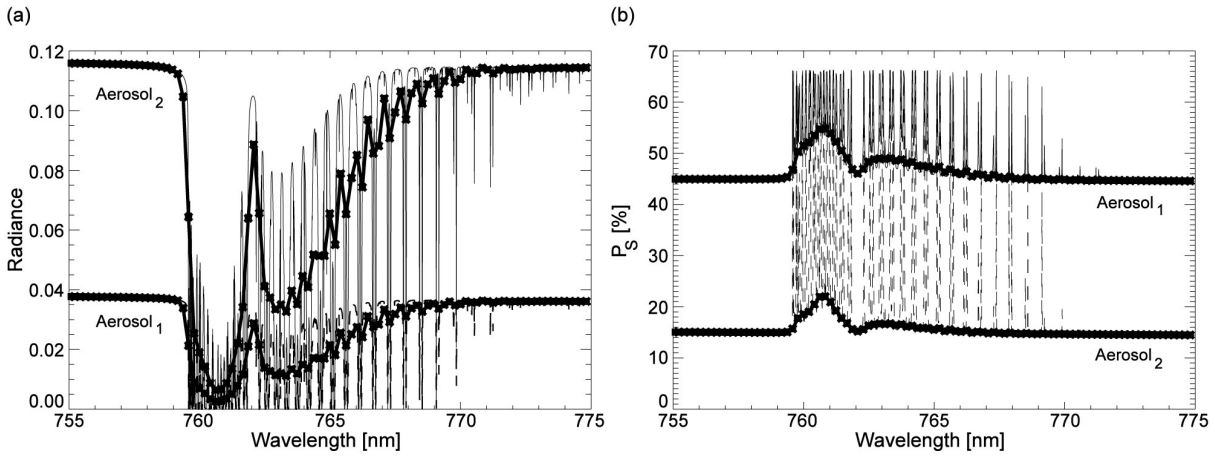

Figure 3.2: Simulations of the O_2A band as a function of wavelength for the zenith sky at a solar zenith angle of $\theta_0 = 65^\circ$ for different aerosol types (see Table 3.1) using line-by-line calculations with a spectral resolution of 0.01 nm (thin lines), and the spectrum convolved using a slit function with a spectral resolution of 0.36 nm FWHM and an equal spacing of 0.21 nm (thick lines). The aerosol is located in the BL of the atmosphere with an aerosol optical thickness of $\tau_{BL} = 0.048$ in case of aerosol$_1$ and $\tau_{BL} = 0.350$ in case of aerosol$_2$. The asterisk (*) indicates the convolved spectrum. The surface albedo is $A_s = 0.20$. (a) Transmitted radiance. (b) Degree of linear polarization P_s of transmitted light.

Table 3.1: Aerosol model parameters used in the radiative transfer simulations. The spherical aerosol types are representative for clear and hazy sky conditions in the Netherlands [Boesche et al., 2006].

Aerosol Parameter	Symbol	$Aerosol_1$ (clear sky)	$Aerosol_2$ (hazy sky)
Wavelength	λ [μm]	0.765	0.765
Imaginary part of the refractive index	m_i	0.0000	0.0007
Real part of the refractive index	m_r	1.400	1.380
Median radius of the fine mode	r_f [μm]	0.080	0.120
Median radius of the coarse mode	r_c [μm]	0.425	0.700
Standard deviation of the fine mode	σ_f	1.300	1.950
Standard deviation of the coarse mode	σ_c	2.200	2.200
Weighting factor of the fine mode	w	0.9996	0.9992

Table 3.2: Ice crystal model parameters used in the radiative transfer simulations. The imperfect hexagonal ice crystal C_1 represents cirrus cloud particles [Knap et al., 2005].

Ice crystal Parameter	Symbol	Ice crystal C_1
Wavelength	λ [μm]	0.765
Imaginary part	m_i	0.783E-07
Real part	m_r	1.306
Length	L [μm]	30
Radius	R [μm]	10
Effective radius	r_{eff} [μm]	12.2997
Aspect ratio		1.5
Orientation		random

Table 3.3: K-binning parameters. The minimum and maximum wavelengths define the spectral region under consideration. The wavelength resolution specifies the resolution with which the spectral database is sampled. The threshold refers to the user defined threshold for the total atmospheric transmittance error. The value in brackets refers to the additional threshold applied to the atmospheric transmission error for each layer. The maximum error refers to the maximum error of the atmospheric transmittance in each of the k-binning intervals [Bennartz and Fischer, 2000], [Bennartz and Preusker, 2007].

K-binning parameter	Symbol	Input
Atmospheric Profile		Mid-latitude Summer, AFGL (1986)
Filter function		rectangular
Minimum wavelength	[nm]	755
Maximum wavelength	[nm]	775
Wavelength resolution	[nm]	0.01
Threshold	[%]	0.01 / (0.005)
Maximum error	[%]	0.001
Intervals needed		37

Figures 3.3(a) and 3.3(b) show results of the convoluted line-by-line and the combined method for I and P_s for transmitted light as a function of wavelength λ, at $\theta_0 = 65^\circ$ and $\theta = 0^\circ$. Figures 3.3(c) and 3.3(d) show the error ε_I and ε_P for transmitted light as a function of wavelength λ. Figures 3.3(e) and 3.3(f), on the other hand, show the error ε_I and ε_P for reflected light as a function of wavelength λ. The largest errors in I and P_s occur around $\lambda = 760$ nm, where we find strong absorption [Figs. 3.3(c)-3.3(f) (solid line)]. For transmission, the error in the degree of linear polarization is $\varepsilon_P \leq 0.11\,\%$ and in the radiance $\varepsilon_I \leq 3.1\,\%$, while for reflection, the error in the degree of linear polarization is $\varepsilon_P \leq 0.31\,\%$ and in the radiance $\varepsilon_I \leq 3.1\,\%$. The errors in the degree of linear polarization are an order of magnitude smaller than in the radiance. Since P_s is a relative result [see Eq. (3.3)], it appears that the errors in I and Q largely cancel each other.

To further increase the accuracy of the combined method we can increase the number of k-binning intervals for the chosen band interval, or we can limit the simulations to individual channels of the chosen instrument.

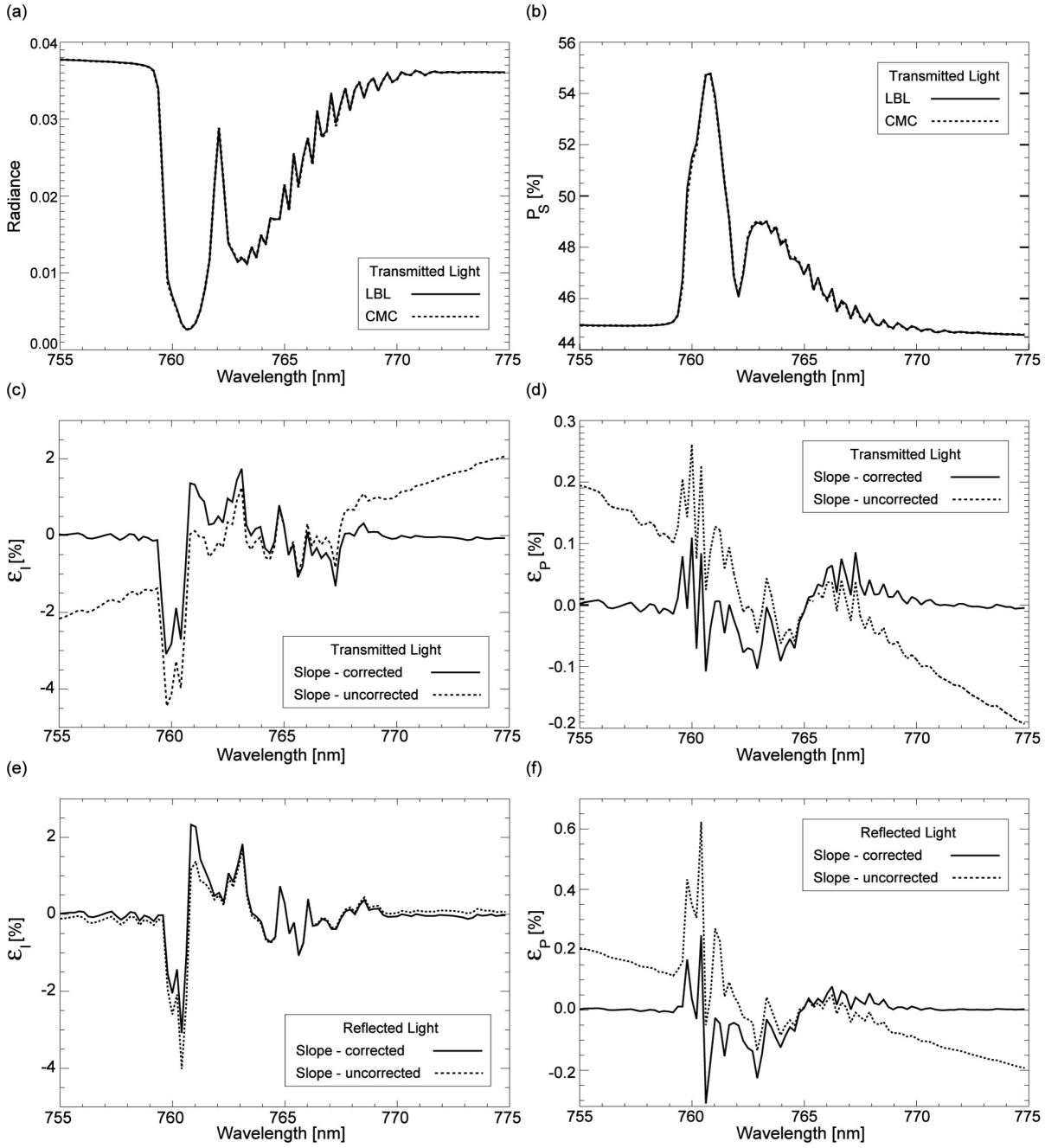

Figure 3.3: Comparison of line-by-line (LBL) and combined method calculations (COM) of radiance and degree of linear polarization P_s within the O_2A band as a function of wavelength for zenith/nadir view at a solar zenith angle of $\theta_0 = 65^\circ$. The surface albedo is A_s = 0.20. The BL contains aerosol$_1$ with $\tau_{BL} = 0.048$. (a) Transmitted radiance of zenith skylight. (b) Degree of linear polarization of the zenith skylight. (c) Error of the transmitted radiance ε_I [see Eq. (3.8)]. The dotted line shows ε_I without slope-correction and the solid line with slope-correction. (d) Error of the degree of linear polarization of the zenith skylight ε_P [see Eq. (3.7)]. The dotted line shows ε_P without slope-correction and the solid line with slope-correction. (e) As in (c), but for reflected light at top-of-atmosphere in nadir view. (f) As in (d), but for reflected light in nadir viewing direction.

Furthermore, a slope occurs in ε_I and ε_P, which can be explained as follows: In the combined method, as outlined in Subsection 3.2.3, we use a constant wavelength λ_c for the calculations, which should be representative for the whole absorption band. This assumes that the scattering properties of the atmosphere are wavelength independent within the absorption band. Apparently this assumption does not apply for the whole absorption band as can clearly be seen in the spectral slope of ε_I and ε_P [see Figs. 3.3(c), 3.3(d), and 3.3(f)]. The slope of ε_I in Figure 3.3(e) is less pronounced. Still we find a pronounced slope in ε_P [see Fig. 3.3(f)]. This is caused by a slope occurring in Q, not shown here.

To overcome this problem we apply the following solution: Let λ_1, λ_2, and λ_3 be three wavelengths that all have contributions from one particular k-binning interval. In its current form k-binning will pick one of them, e.g., λ_2 as representative for all three. But if the scattering properties are wavelength dependent, the actual components of the Stokes vector $\mathbf{I}$ at λ_3 will not be equal to the one at λ_2. Assuming that the scattering optical thickness exhibits a linear spectral behavior for the absorption band, we can find the minimum and maximum wavelengths where a certain k-binning interval contributes to the radiance, in this case λ_1 and λ_3. Now we simulate the k-binning interval at λ_1 and λ_3, not only at λ_2 as done previously. Let the outcome be $\mathbf{I}(\lambda_1)$ and $\mathbf{I}(\lambda_3)$. To get the components of the Stokes vector $\mathbf{I}(\lambda_2)$, we interpolate linearly in λ between $\mathbf{I}(\lambda_1)$ and $\mathbf{I}(\lambda_3)$.

The above can potentially be done with all k-binning intervals that cover a wide spectral range, which would double the calculation time. Applying this to 2-5 intervals that have the least absorption we already solve the problem of the wavelength dependency; see the corrected slopes in Figure 3.3.

3.3 Sensitivity of the degree of linear polarization of the zenith skylight in the O_2A band to aerosol altitude

In this Section we analyse the sensitivity of the degree of linear polarization of the zenith skylight in the spectral region of the O_2A band to changes of aerosol altitude, aerosol microphysics, and aerosol optical thickness τ_{aer} in the troposphere and lower stratosphere. For the simulations we used the combined method, which combines both a high accuracy ($\varepsilon_P \leq 0.11\,\%$) and short computing time. We used a spectral response function with a resolution of 0.36 nm at FWHM and an equal spacing of 0.21 nm. Throughout this study we

use two different types of atmospheric scatterers, namely spherical aerosols according to Mie scattering theory and nonspherical ice crystal particles according to the GO approximation method. If not mentioned otherwise, the viewing geometry is as follows: solar zenith angle $\theta_0 = 65^\circ$ and viewing zenith angle $\theta = 0^\circ$. The microphysical properties of the spherical aerosol particles were derived from actual measurements at clear sky conditions ($aerosol_1$) and hazy sky conditions ($aerosol_2$) taken in Cabauw, The Netherlands (see Table 3.1) [Boesche et al., 2006]. The microphysical properties of the nonspherical ice crystals correspond to C_1 imperfect hexagonal ice crystals (IMP), which are randomly oriented (see Table 3.2) [Hess et al., 1998], [Knap et al., 2005]. The tilt angle α, which can be considered as the degree of the distortion of the surface of the ice crystals, is set to 30°. For this choice of tilt angle the phase function varies rather smoothly with scattering angle and does not show the sharp angular features of a pristine hexagon phase function, e.g., halo peaks. This tilt angle value is suitable for the representation of natural (irregular) ice crystals in clouds. The size of a hexagonal crystal is given by its length L and so called radius r. Depending on the magnitude of the aspect ratio (L/2r), the crystal is a column (L/2r > 1) or a plate (L/2r < 1). The effective radius r_{eff} of the ice crystal is defined here as the radius of a sphere that has the same volume as the hexagon:

$$r_{eff} = \left(\frac{9\sqrt{3}}{8\pi} r^2 L \right)^{1/3} \tag{3.9}$$

Figure 3.4 shows calculations of the phase function F_{11} and single scattering polarization $-F_{12}/F_{11}$ for all three types of scatterers. As expected, we find higher polarization for the small aerosol type, compared to the large aerosol and ice crystals [Knap et al., 2005], [Boesche et al., 2006].

3.3.1 Processes determining the degree of linear polarization in the O_2A band

For a general interpretation of the processes that determine the degree of linear polarization in the O_2A band we consider four processes that account for the Stokes vector elements I and Q and the resulting degree of linear polarization P_s of the cloud free sky: (1) single

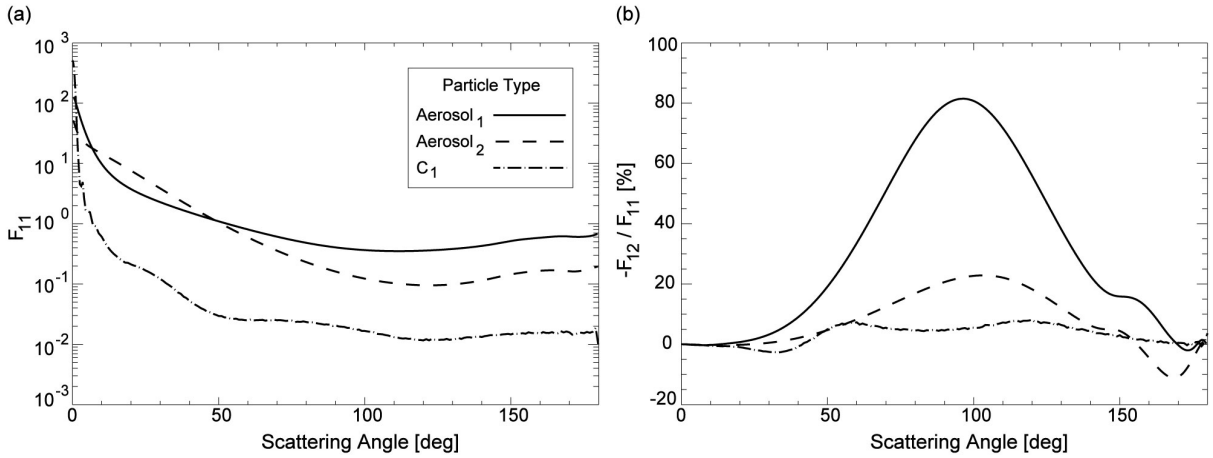

Figure 3.4: Scattering matrix elements F_{11} and $-F_{12}/F_{11}$ as computed at $\lambda = 765$ nm for different types of scatterers (see Tables 3.1 and 3.2). Mie theory was used for the simulations of the spherical aerosols and the GO approximation method for the nonspherical ice crystal. (a) Phase function F_{11} as a function of scattering angle. (b) Single scattering polarization $-F_{12}/F_{11}$ as a function of scattering angle.

scattering in the atmosphere (either by molecules or aerosols); (2) direct transmission to the surface, subsequent reflection by the depolarizing surface, and single scattering in the atmosphere; (3) multiple scattering in the atmosphere; (4) higher order surface reflection and atmospheric scattering. These four processes provide the contributions to skylight measurements.

To understand the role of these processes we analyse, below, the influence of molecular scattering, aerosol scattering, surface albedo, aerosol altitude, and vertical distribution of aerosols on the degree of linear polarization in the O_2A band (see Fig. 3.5):

(a). Molecular scattering, A_s = 0.00 [Fig. 3.5 (solid line)]: For a purely Rayleigh scattering atmosphere we find a high degree of linear polarization in the continuum due to scattering by strongly polarizing molecules. Since the Rayleigh optical thickness at 765 nm is only 0.0255 there is not much multiple scattering in the continuum. However, inside the O_2A band the small amount of multiple scattering is further reduced by means of absorption. Therefore we find a slightly higher degree of linear polarization inside the absorption band (P_b), as compared to the continuum (P_c).

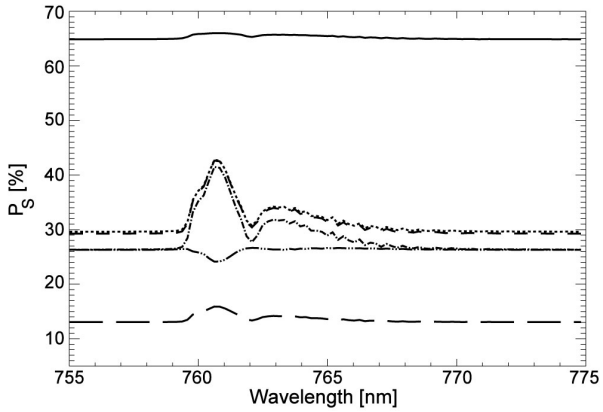

Figure 3.5: Degree of linear polarization of zenith skylight as a function of wavelength at a solar zenith angle of $\theta_0 = 65^\circ$ showing processes which determine the polarization in the O_2A band: pure Rayleigh scattering (solid line) without surface reflection; inclusion of aerosol$_2$ to the boundary layer with a geometrical thickness of 1 km and an optical thickness of 0.1 (dotted line); adding a surface albedo of A_s = 0.02 (dashed line) and of A_s = 0.20 (dashed-dotted line); elevation of the aerosol layer up to 16 km (dashed double dotted line); and inclusion of aerosol$_2$ to the boundary layer with an optical thickness of 0.35 (long dashed line).

(b). Molecular and aerosol scattering, A_s = 0.00 [Fig. 3.5 (dotted line)]: Adding weakly polarizing aerosols with $\tau_{aer} = 0.10$ to the boundary layer (0-1 km) strongly decreases P_c, while P_b decreases less strongly. The decrease of P_c is stronger for higher aerosol optical thicknesses (increase of multiple scattering). Inside the O_2A band, light is mainly scattered at higher altitudes, because the strong gaseous absorption prevents light to reach lower parts of the atmosphere, thus molecular scattering dominates polarization inside the O_2A band, which results in a higher P_b.

(c). Molecular- and aerosol scattering, A_s = 0.02 [Fig. 3.5 (dashed line)] and 0.20 [Fig. 3.5 (dashed-dotted line)]: Adding surface reflection with a low albedo of A_s = 0.02 (resembling water surfaces) shows little effect on P_c and nearly no effect on P_b. Inside the absorption band the surface is shielded due to the gaseous absorption and this causes the lower effect on P_b. Increasing the surface albedo to A_s = 0.20 we see a further decrease of P_c and P_b. In these cases the decrease of the degree of linear polarization is mainly because the atmosphere is bounded by a depolarizing Lambertian surface. Increasing surface reflection decreases the degree of linear polarization because I increases and Q remains unchanged. The decrease in P_s is more pronounced for small solar zenith angles. This increase of surface influence with smaller solar zenith angles is due to the more efficient transmission of

the direct beam through the atmosphere and the consequently stronger illumination of the surface. At the same time, the more efficient transmission causes less multiple scattering [Coulson, 1988]. Inside the O_2A band the surface is shielded due to the gaseous absorption.

(d). As (c), but increasing the aerosol layer altitude [Fig. 3.5 (dashed double dotted line)]: An altitude increase from 1 to 16 km of the aerosol layer shows a negligible influence on P_c, whereas the influence on P_b is strong. The influence of aerosol altitude on P_b is due to the strong O_2A band absorption, which prevents light to reach lower parts of the atmosphere. Because most of the sunlight inside the absorption band is scattered at higher altitudes, an increase in aerosol altitude increases the probability of aerosol scattering as compared to molecular scattering and is thus decreasing P_b. For weakly polarizing aerosols this can lead to a band polarization which is lower than the continuum polarization. Whereas in the continuum, sunlight can interact with all scatterers in the entire atmosphere, provided that the scatterers are nonabsorbing and that the optical thickness of the scatterers is below 1. Inside the band, as a result of the strong absorption, sunlight only interacts with the upper part of the atmosphere. Aerosol absorption affects molecular scattering below the aerosol layer, and the underlying Rayleigh scattering produces only a small signal. In that case we find a small decrease of P_c with increasing aerosol altitude.

(e). As (d), but adding a second aerosol layer [Fig. 3.5 (long dashed line)]: Adding a second aerosol layer between 0 and 1 km with weakly polarizing aerosol having an optical thickness of $\tau_{aer} = 0.35$ increases multiple scattering and further decreases the degree of linear polarization of P_c and P_b, as in process (b). Adding a second scattering layer can strongly alter the effect of process (d), depending on the single scattering properties and aerosol optical thickness of the added layer. This is studied in the next Subsection.

3.3.2 Simulations of the effect of aerosol altitude on the degree of linear polarization of the zenith skylight

In this Section we study the influence of aerosol altitude, microphysical properties and aerosol optical thickness changes on the degree of linear polarization P_s within the O_2A band. This is done for different types of model atmospheres (see Fig. 3.6). The basic atmosphere is a Rayleigh scattering atmosphere with oxygen as the only absorbing gas. In this atmosphere we place a boundary layer (BL), which comprises aerosols, and/or an elevated layer (EL), which comprises aerosols or ice crystals (see Tables 3.1 and 3.2). The

boundary layer is located between 0 and 1 km. The aerosol optical thickness of the boundary layer is $\tau_{BL} = 0.048$, resembling clear sky conditions, or $\tau_{BL} = 0.350$, resembling hazy sky conditions. The elevated layer, with a geometrical thickness of 1 km, is shifted through the atmosphere in steps of 2 km. The optical thickness of the elevated layer is $\tau_{EL} = 0.03$, or $\tau_{EL} = 0.10$. Referring to C_1 ice crystals this resembles a range from subvisible to thin cirrus clouds [Sassen et al., 1989]. The surface albedo is chosen to be A_s = 0.20.

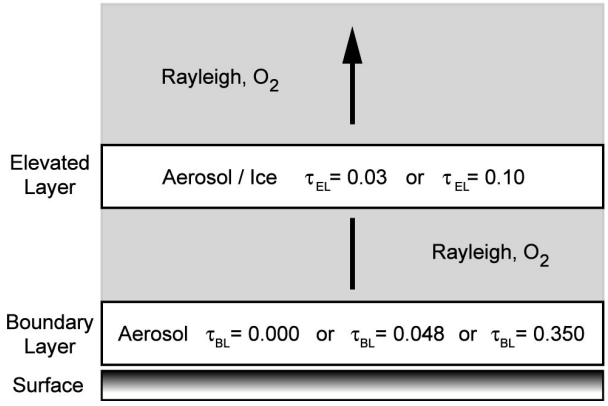

Figure 3.6: Schematic representation of the model atmosphere. The model atmosphere comprises molecules, aerosols and ice crystals (see Tables 3.1 and 3.2). The molecules are homogeneously mixed throughout the atmosphere according to the pressure profile, while the aerosols are located within the boundary layer, between 0 and 1 km, and inside an elevated layer. The aerosols in the elevated layer can be replaced by ice crystals and the altitude of the elevated layer is variable between 2 and 16 km. Furthermore, the optical thickness of the boundary layer and the elevated layer are variable. The atmosphere is bounded by a Lambertian surface.

3.3.2.1 Basic atmosphere plus an elevated scattering layer

Figure 3.7(a) shows P_s as a function of wavelength for the basic model atmosphere with an added scattering layer at different altitudes and for different types of scatterers. The aerosol optical thickness of the elevated layer is $\tau_{EL} = 0.10$. Furthermore, we included P_s for pure Rayleigh scattering to illustrate the processes (a) and (b) of Subsection 3.3.1, which describes the effect on P_s by adding aerosol to a Rayleigh atmosphere. To illustrate the influence of aerosol layer altitude changes on the degree of linear polarization in the continuum P_c and within the absorption band P_b in a more pronounced way, we show P_c and the polarization difference $P_b - P_c$ as function of the aerosol layer altitude [see Fig. 3.7(b)]. The polarization inside the O_2A band can be larger or smaller than in the continuum [see Subsection 3.3.1 (d)]. This is indicated by a change of sign of $P_b - P_c$. The circles in

Figure 3.7(a) indicate P_c, selected at 757.9 nm and P_b, selected at 760.6 nm. Figure 3.7(b) shows P_c, marked by an asterisk, and $P_b - P_c$ as a function of altitude for three different types of scatterers. As outlined in Subsection 3.3.1 (d), we find a decrease of P_b with increasing aerosol altitude for all scatterers, while P_c remains nearly unaffected if the scatterer is non-absorbing. In case of the absorbing aerosol$_2$, we see a decrease of P_c with increasing aerosol altitude, as outlined in Subsection 3.3.1 (d). We also see that the decrease of P_b is more pronounced for weakly polarizing scatterers (aerosol$_2$ and C_1).

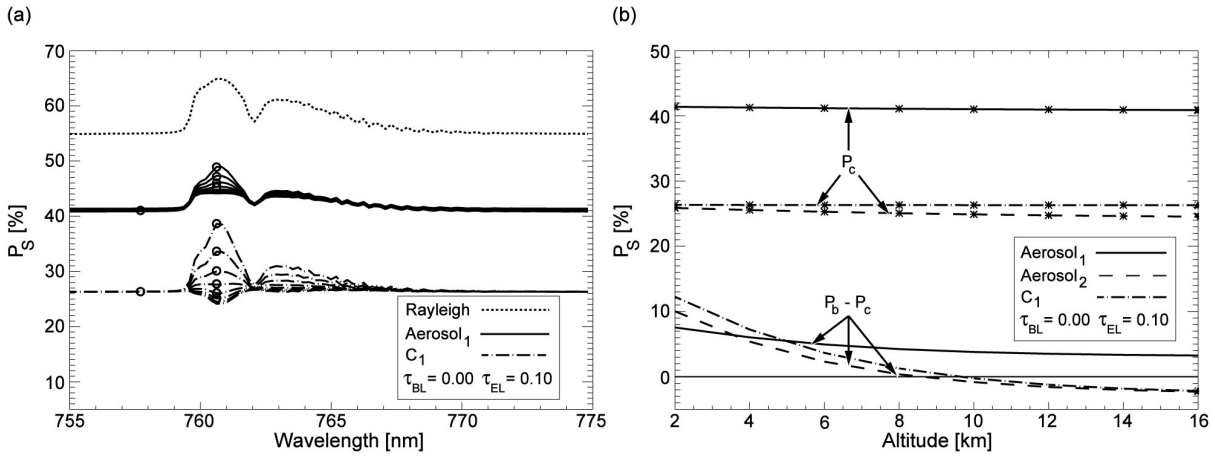

Figure 3.7: (a) Degree of linear polarization of the zenith skylight as a function of wavelength at a solar zenith angle of $\theta_0 = 65^\circ$ for a pure Rayleigh atmosphere and for an atmosphere including an elevated scattering layer at different altitudes. The elevated layer contains different types of scatterers, while the boundary layer contains no aerosol. The surface albedo is A_s = 0.20. The circles indicate the continuum polarization P_c, selected at 757.9 nm, and O_2A band polarization P_b, selected at 760.6 nm. (b) Continuum polarization (asterisk) and difference between band and continuum polarization $P_b - P_c$ as a function of the elevated layer altitude.

3.3.2.2 Basic atmosphere plus boundary- and elevated scattering layers

Figure 3.8 shows P_c and $P_b - P_c$ as a function of aerosol altitude for the basic model atmosphere with an added boundary scattering layer and an elevated scattering layer. Both the boundary and the elevated layer contain scatterers of the same type: strongly polarizing aerosol$_1$ [Figs. 3.8(a) and 3.8(b)] and weakly polarizing aerosol$_2$ [Figs. 3.8(c) and 3.8(d)]. In Figs. 3.8(a) and 3.8(c) the optical thickness of the boundary layer is $\tau_{BL} = 0.048$ and in 3.8(b) and 3.8(d) $\tau_{BL} = 0.350$. Adding the same kind of scatterer in the boundary layer has a similar effect as an increase of the aerosol optical thickness and causes a decrease of P_c and P_b, compared to the case without boundary layer aerosol [see Subsection 3.1 (e)].

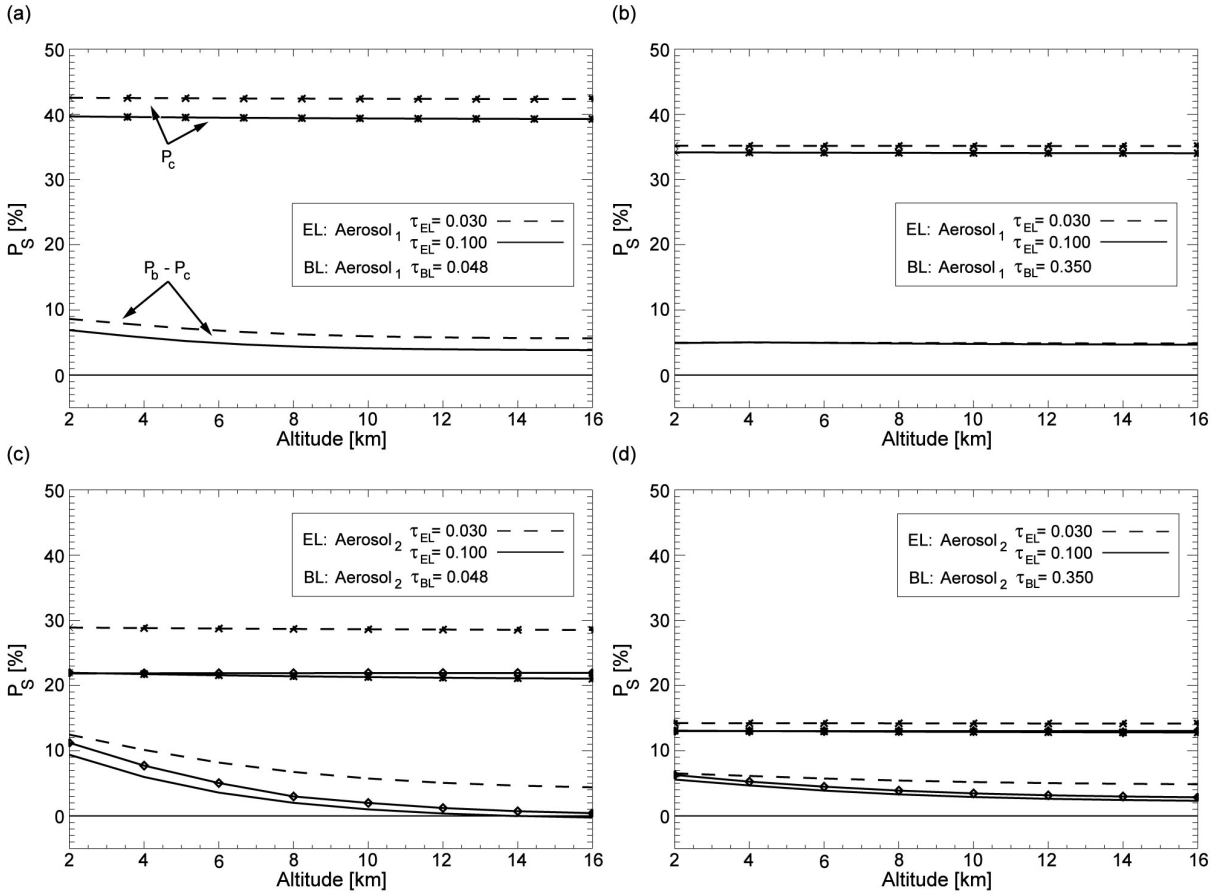

Figure 3.8: Continuum polarization P_c (asterisk) and band-continuum polarization $P_b - P_c$ as a function of the elevated layer altitude for zenith skylight at a solar zenith angle of $\theta_0 = 65^\circ$, with a surface albedo of A_s = 0.20, and different optical thicknesses of the boundary and elevated layer. The boundary and elevated layer contain aerosols of the same type. The boundary layer optical thickness of $\tau_{BL} = 0.048$ resembles clear sky conditions and $\tau_{BL} = 0.350$ resembles hazy sky conditions. (a) and (b): BL and EL comprise aerosol1. (c) and (d): BL and EL comprise aerosol2. Here we also included results using scatterer C1 in the elevated layer with an optical thickness of $\tau_{BL} = 0.10$ (denoted by diamonds).

Furthermore we show the results for weakly polarizing C_1 ice crystals added to the elevated layer, to simulate the influence of cirrus clouds [see Figs. 3.8(c) and 3.8(d)]. No sign change of $P_b - P_c$ occurs in case of weakly polarizing aerosol$_2$ or C_1. We find that the influence of the elevated layer altitude on P_b decreases if the aerosol optical thickness of the boundary layer increases. This can be explained as follows: I_b as function of aerosol layer altitude h can be written as

$$I_b(h) \cong I_{BL,b} + I_{mol,b} + I_{EL,b}(h) \tag{3.10}$$

where $I_{BL,b}$ is determined by aerosol scattering in the boundary layer, $I_{mol,b}$ is determined by Rayleigh scattering and $I_{EL,b}(h)$ by scattering in the elevated layer. Analogously we can write

$$Q_b(h) \cong Q_{BL,b} + Q_{mol,b} + Q_{EL,b}(h) \tag{3.11}$$

An increase of the boundary layer aerosol optical thickness τ_{BL} causes more multiple scattering, which leads to a decrease of P_b, due to a stronger increase of Stokes parameter $I_{BL,b}$ as compared to $Q_{BL,b}$. Assuming that the absolute changes of $\Delta I_{EL,b}$ and $\Delta Q_{EL,b}$ with increasing aerosol layer altitude are independent to changes of τ_{BL}, we find that the relative increase of $I_b(h)$ with increasing altitude of the elevated layer reduces strongly in case of high τ_{BL}, while in comparison the relative increase of $Q_b(h)$ reduces less, as compared to the case of low τ_{BL}. Thus, in case of high τ_{BL} the degree of linear polarization $P_b = -Q_b / I_b$ decreases less strongly with increasing altitude of the elevated scattering layer than in the case of low τ_{BL}.

Figure 3.9 shows P_c and $P_b - P_c$ as a function of aerosol altitude for the basic model atmosphere with an added boundary and elevated aerosol layer. In this case the boundary and the elevated layer comprise different types of scatterers: Strongly polarizing aerosol$_1$ in the boundary layer and weakly polarizing aerosol$_2$ in the elevated layer [Figs. 3.9(a) and 3.9(b)]; Weakly polarizing aerosol$_2$ in the boundary layer and strongly polarizing aerosol$_1$ in the elevated layer [Figs. 3.9(c) and 3.9(d)]. In the left panel of Figure 3.9 the optical thickness of the boundary layer is $\tau_{BL} = 0.048$ and in the right panel $\tau_{BL} = 0.350$. Adding aerosol scatterers with different polarization properties (see Fig. 3.4) in the boundary layer can cause an increase as well as a decrease of P_c and P_b, as compared to the basic model atmosphere with only an elevated aerosol layer added (see Fig. 3.7). Furthermore we show the results for weakly polarizing C_1 ice crystals added to the elevated layer, to simulate the influence of cirrus clouds [see Figs. 3.9(a) and 3.9(b)].

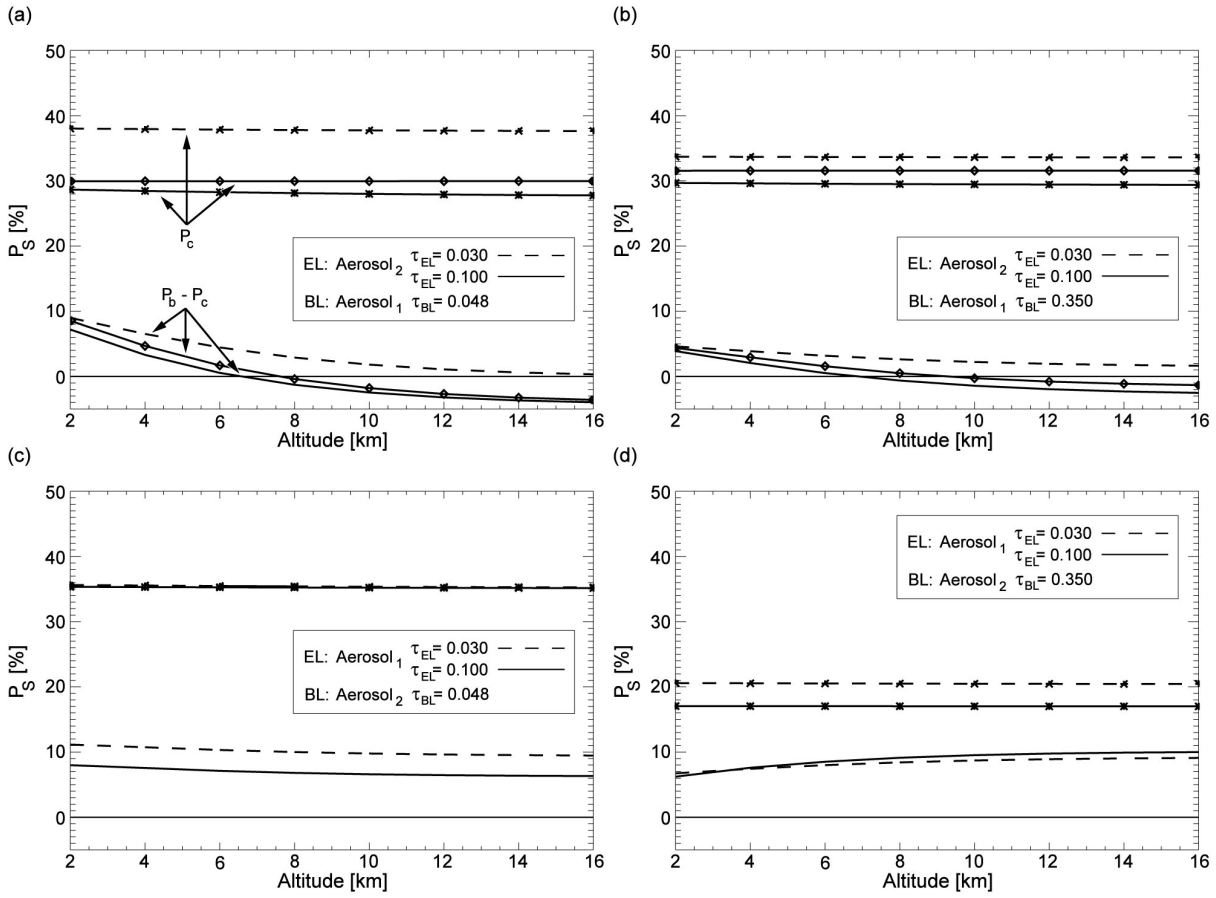

Figure 3.9: as Figure 3.8, but now the boundary and elevated layer contain different types of aerosol. (a) and (b): BL comprises aerosol$_1$ and EL comprises aerosol$_2$; here we also included results using scatterer C_1 in the elevated layer with an optical thickness of $\tau_{BL} = 0.10$ (denoted by diamonds). (c) and (d): BL comprises aerosol$_2$ and EL comprises aerosol$_1$.

In case of strongly polarizing aerosol$_1$ located in boundary layer and weakly polarizing aerosol$_2$ or C_1 in the elevated layer a sign change of $P_b - P_c$ occurs [see Figs. 3.9(a) and 3.9(b)]. For low τ_{BL} we see an increase of P_c, while P_b changes less as compared to the basic model atmosphere with only an elevated aerosol layer added. Thus, the sign change of $P_b - P_c$ occurs at lower altitudes and $P_b - P_c$ is lower at higher altitudes. As can be seen in Figure 3.8, an increase of τ_{BL} to 0.350 leads to a decrease of P_c and P_b, due to an increase of multiple scattering, and, also, the effect of aerosol altitude is reduced.

In the case of weakly polarizing aerosol$_2$ located in the boundary layer and strongly polarizing aerosol$_1$ in the elevated layer, we find that an altitude increase of the elevated layer can also cause an increase in P_b [see Figs. 3.9(c) and 3.9(d)]. For low τ_{BL} we find the expected

decrease in P_b with increasing altitude of the elevated layer, whereas for high τ_{BL} we find that an altitude increase of the elevated layer causes an increase of P_b instead of a decrease. In the case of strongly polarizing aerosol located in the elevated layer, the absolute change of $\Delta Q_{EL,b}$ is larger and $\Delta I_{EL,b}$ is smaller, as compared to the case with weakly polarizing aerosol located in the elevated layer [Fig. 3.8(d)]. This leads to a stronger relative increase of Q_b, while the relative change of I_b increases less [see Eq. (3.10) and (3.11)]. If τ_{BL} is high enough, the relative increase of Q_b becomes larger than that of I_b, resulting in an increase of P_b with increasing aerosol layer altitude.

Based on the above presented simulations of the influence of aerosol altitude on the degree of linear polarization of the zenith skylight in the O_2A band we may conclude the following, regarding the measurements taken on May 11 1994 [Fig. 3.1(a) solid line] and on October 19 1993 [Fig. 3.1(b) solid line]: It seems likely that the observed decrease of P_b inside the O_2A band was caused by a second scattering particle layer in the upper troposphere, probably thin cirrus, since the stratospheric aerosol scattering optical thickness is generally very low, except shortly after volcanic events. During the time of the measurements (1993, 1994) the stratospheric optical thickness was still increased due to effects of the Pinatubo eruption ($\tau_{strat} \leq 0.05$) [Mishchenko et al., 2003]. However, this alone is unlikely to have caused the observed low P_b but might have influenced the measurements of the degree of linear polarization in this period.

3.3.2.3 Dependence on solar zenith angle and spectral resolution

The results shown above pertain to zenith sky observations with $\theta_0 = 65^\circ$. Figure 3.10 shows P_s as a function of wavelength for different solar zenith angles. For solar zenith angles θ_0 tending towards the zenith (smaller scattering angle Θ), we find a decrease of P_c (see also Fig. 3.4) [Coulson, 1988]. Furthermore we find that P_b converges towards P_c [Stammes et al., 1994]. The scattering angle difference can be an explanation of the considerably larger differences of $P_b - P_c$ observed by Preusker et al. (1995) [Fig. 3.1(a) solid line], as compared to the observations by Stammes et al. (1994) [Fig. 3.1(b) solid line]. Furthermore the results depend on the spectral resolution of the spectrometer (see Fig. 3.11). A higher resolution provides a more detailed spectral fine-structure in the polarization and thus the polarization effects, as shown in this Section, are more pronounced.

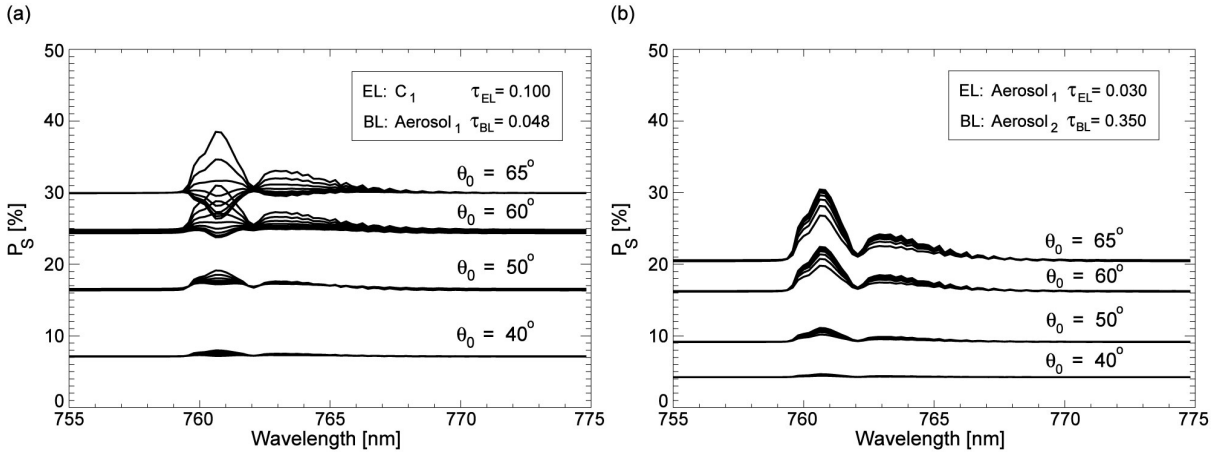

Figure 3.10: Degree of linear polarization of zenith skylight as a function of wavelength for different solar zenith angles θ_0 and different altitudes of the elevated scattering layer. The elevated layer is shifted through the atmosphere from 2 to 16 km in steps of two kilometers. The surface albedo is A_s = 0.20. (a) BL comprises aerosol$_1$ and EL comprises C_1. P_b decreases with increasing altitude of the elevated layer. (b) BL comprises aerosol$_2$ and EL comprises aerosol$_1$. P_b increases with increasing altitude of the elevated layer.

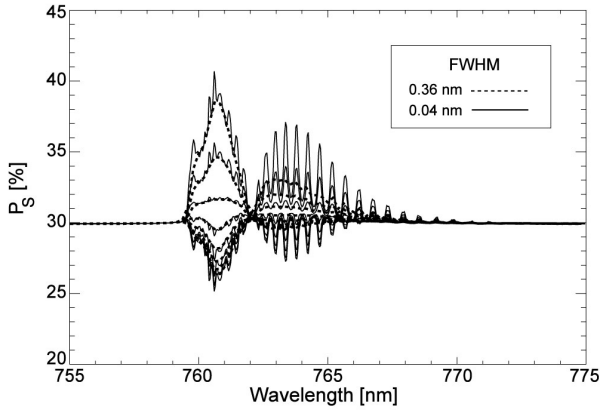

Figure 3.11: Degree of linear polarization of zenith skylight as a function of wavelength at a solar zenith angle of $\theta_0 = 65^\circ$ for two different spectral response functions and different altitudes of the elevated scattering layer. The boundary layer comprises aerosol$_1$ with an optical thickness of $\tau_{BL} = 0.048$ and the elevated layer comprises scatterer C_1 with $\tau_{EL} = 0.100$. The elevated layer is shifted through the atmosphere from 2 to 16 km in steps of two kilometers, resulting in a decrease of P_b with increasing altitude of the elevated layer.

3.4 Conclusions and Outlook

In this paper we studied the influence of aerosol altitude, aerosol microphysics, and aerosol optical thickness on the degree of linear polarization of the zenith skylight in the spectral region of the O_2A band. We developed a combined method for fast radiative transfer simulations in absorption bands including polarization. As a spectral approximation technique we used the k-binning method, and integrated this method in monochromatic doubling-adding multiple scattering calculations. For both reflected and diffusely transmitted light we compared the radiance and the degree of linear polarization as calculated using the combined method with the results of accurate line-by-line simulations. Furthermore, we corrected for the spectral dependency of the scattering properties within the O_2A band. Based on the comparison we conclude that the radiance error due to the assumptions of the k-binning approach is smaller than 3.1% for both the reflected and the transmitted radiation. For the degree of linear polarization, this error is smaller than 0.31% for reflected light and smaller than 0.11% for transmitted light. These maximum errors hold for instrument channels around 760 nm. The errors are smaller for other instrument channels.

Regarding the sensitivity of the degree of linear polarization of the zenith skylight within the O_2A band to changes of aerosol altitude and aerosol optical thickness we can conclude the following: Increasing the altitude of an elevated aerosol layer within a Rayleigh scattering atmosphere decreases the degree of linear polarization inside the oxygen absorption band for all scatterers under consideration. The magnitude of this effect depends on the polarization properties of the chosen aerosol or ice crystal. Adding another scattering layer (boundary layer), including aerosols of the same type, decreases the sensitivity of P_b to changes of the scattering layer altitude. A strongly polarizing scatterer in the boundary layer and a weakly polarizing scatterer in the elevated layer increases the sensitivity of P_b to changes of the scattering layer altitude. A weakly polarizing scatterer in the boundary layer and a strongly polarizing scatterer in the elevated layer decreases the sensitivity of P_b to changes of the scattering layer altitude. The higher the optical thickness of the boundary layer, the less sensitive P_b is to changes of the scattering layer altitude. In the case of weakly polarizing aerosol in the boundary layer and strongly polarizing aerosol in the elevated layer we find an increase of P_b with increasing scattering layer altitude. The sensitivity of P_b to changes of the scattering layer altitude is strongest inside the troposphere and decreases with increasing altitude. The polarization inside the O_2A band can be larger or smaller than

the continuum polarization. In the absence of boundary layer aerosols $P_b < P_c$ is only observed for weakly polarizing aerosols or ice crystals within the troposphere and lower stratosphere. In the presence of boundary layer aerosol we find this effect only for a combination of strongly polarizing scatterers located in the boundary layer together with weakly polarizing scatterers in an elevated scattering layer. For all other cases we find that $P_b > P_c$. Decreasing the optical thickness of the elevated scattering layer decreases the scattering altitude effect on P_b. The polarization in the continuum and inside the absorption band strongly depends on the viewing geometry.

We may tentatively conclude that a retrieval of the aerosol profile from ground-based measurements of the polarization of the cloud free zenith sky in the O_2A band region seems too ambitious in the case of multiple aerosol layers without additional information on the microphysical aerosol properties and optical thickness of the individual layers. Only in case of a single aerosol layer, a determination of the aerosol layer altitude may be obtained due to the fact that the retrieval of microphysical aerosol properties and optical thickness is achievable from the continuum. The detection of the presence of a second aerosol or ice crystal layer from polarization measurements might be possible as well. Polarization measurements at a high-altitude site or airplane-based measurements might offer altitude information on aerosols or sub-visible cirrus in the upper troposphere / lower stratosphere.

Based on this study of ground-based polarization observations we expect that it is also necessary to include the effect of aerosol altitude in simulations of top-of-atmosphere radiance and polarization in absorption bands. The influence of aerosol altitude and other aerosol properties on the degree of polarization inside gaseous absorption bands will affect the measurements of polarization sensitive spectrometers such as the Medium resolution imaging spectrometer (MERIS) [Rast and Bezy, 1999], the Global Ozone Monitoring Experiment (GOME) [Stam et al., 2000b], [Hasekamp and Landgraf, 2002a], [Hasekamp et al., 2002b], the Scanning Imaging Absorption Spectrometer for Atmospheric Cartography (SCIAMACHY) [Bovensmann et al., 1999], [Schutgens and Stammes, 2002], [van Diedenhoven et al., 2005], the Polarization and directionality of the Earth's reflectance (POLDER) [Deuzé et al., 2000], [Duforet et al., 2007], or the upcoming Aerosol Polarimeter Sensor (APS) [Mishchenko et al., 2007], and the Orbiting Carbon Observatory (OCO) [O'Brien and Rayner, 2002], [Crisp et al., 2004], [Haring et al., 2005]. In the near future we plan to apply our method to OCO to study the aerosol influence on the polarization of oxygen and carbon dioxide absorption bands, as observed from space.

Chapter 4

Aerosol influence on polarization and intensity in near-infrared O_2 and CO_2 absorption bands observed from space

E. Boesche, P. Stammes, and R. Bennartz, *Journal of Quantitative Spectroscopy & Radiative Transfer* doi:10.1016/j.jqsrt.2008.09.019 (JQSRT 2008).

Abstract

We study the intensity and degree of linear polarization of reflected solar radiation at the top of the atmosphere within two carbon dioxide bands and one oxygen absorption band in the near-infrared. In particular, we are interested in the sensitivity of the degree of linear polarization and intensity to changes of aerosol and cirrus cloud layer heights, microphysical properties, and surface albedo. For the simulations we use spectral response functions representative of the Orbiting Carbon Observatory (OCO). Inside the O_2A band at 760 nm and strong CO_2 band at 2060 nm we find a strong influence of the aerosol and cirrus cloud layer height on the degree of linear polarization. An increase of the aerosol or cirrus cloud layer height can lead either to a decrease or increase of the polarization within the band, depending on the microphysical and optical properties of the scatterers, surface albedo, and absorption strength in the bands. The results for the O_2A band also indicate that even over land OCO enables an estimation of the height of an aerosol or cirrus cloud layer. Inside the weak CO_2 band at 1610 nm the influence of aerosol or cirrus cloud layer heights is lower as compared to the O_2A band and CO_2 band at 2060nm, due to the relatively stronger surface influence. Here an increase of aerosol or cirrus cloud layer height leads to an increase of the degree of linear polarization even in case of low surface albedo and for weakly polarizing scatterers. For the weak CO_2 band at 1610nm we also study the influence of the aerosol or cirrus cloud layer height on the column CO_2 estimate and the errors resulting from ignoring polarization in simulations of backscatter measurements by space-based instruments such as OCO. Depending on the surface albedo, misinterpretations of the height of atmospheric scatterers might strongly affect the column CO_2 estimates.

4.1 Introduction

The reflected radiation at top-of-atmosphere (TOA) contains information of optical and microphysical properties of atmospheric constituents due to scattering and absorption within the atmosphere. Spectroscopic observations within gaseous absorption bands such as the oxygen and carbon dioxide bands enable the estimate of, e.g. the height of atmospheric scatterers, the cloud top altitude, the surface pressure, and the CO_2 column and the near-surface CO_2 [Duforet et al., 2007], [O'Brien and Mitchell, 1992], [Kuze and Chance, 1994], [van Diedenhoven et al., 2005], [O'Brien and Rayner, 2002], [Mao and Kawa, 2004]. In the continuum and inside gaseous absorption bands polarization can play an important role in the accuracy of remote the continuum and inside gaseous absorption bands polarization can play an important role in the accuracy of remote as ozone, or aerosols [Mishchenko and Travis, 1997], [Levy et al., 2004], [Mishchenko et al., 2004], [Boesche et al., 2006], [Chowdhary et al., 2005]. Radiative transfer calculations including polarization are also important for the interpretation of satellite measurements such as from the medium resolution imaging spectrometer (MERIS) [Rast and Bezy, 1999], the global ozone monitoring experiment (GOME) [Hasekamp et al., 2002], [Burrows et al., 1999], [Stam et al., 2000], the scanning imaging absorption spectrometer for atmospheric cartography (SCIAMACHY) [van Diedenhoven et al., 2005], [Bovensmann et al., 1999], [Tilstra et al., 2007], the Polarization and Directionality of the Earth's Reflectance (POLDER) [Duforet et al., 2007], [Deschamps et al., 1994], or for the upcoming aerosol polarimeter sensor (APS) [Mishchenko et al., 2007], the Greenhouse gases Observing SATellite (GOSAT) [Hamazaki et al., 2004], and the Orbiting Carbon Observatory(OCO) [Crisp et al., 2004], [Haring et al., 2005]. These instruments are sensitive to the polarization of the reflected radiance, while not all of them are able to measure the polarization incident on the instrument. Thus it is necessary for accurate retrievals to consider the polarization in addition to the intensity of the light incident on the instrument [Levy et al., 2004], [Hasekamp et al., 2002], [Mishchenko et al., 2007].

In this article we analyze the sensitivity of the degree of linear polarization and intensity at TOA to changes of aerosol or cirrus cloud layer height, microphysical properties, and surface albedo. In particular we are interested in the spectral regions of oxygen and carbon dioxide absorption bands. As atmospheric scatterers we use spherical aerosols as well as non-spherical ice-crystal particles (resembling cirrus clouds) with their scattering properties being derived from Mie theory and geometric-optics-approximation (GO), respectively. We use spectral response functions representative for the OCO instrument [Haring et al., 2005]. OCO (scheduled for launch December 2008) is designed to measure reflected sunlight in the

spectral region of the O_2A band at 760 nm, the weak CO_2 band at 1610 nm and the strong CO_2 band at 2060 nm. OCO will operate in three observation modes: Nadir, Glint, and Target mode [Crisp et al., 2004]. The main objective of the OCO mission is to precisely measure the global distribution of carbon dioxide in the Earth's atmosphere. The weak CO_2 band at 1610 nm is highly sensitive to CO_2 alterations near the surface and is relatively free of other absorbing gases and thus well suited for column CO_2 estimates. Measurements in the O_2A band and the strong CO_2 band at 2060 nm provide information about surface pressure, surface albedo, atmospheric temperature, water vapor, as well as cloud and aerosol properties which are essential for adequate column CO_2 estimates. Regarding the weak CO_2 band between1594 and 1619 nm, we are interested in the influence of the aerosol or cirrus cloud layer height on the ratio of radiances at wavelengths of strong and weak absorption, which allows the estimation of column CO_2 [O'Brien and Rayner, 2002], [Mao and Kawa, 2004], and the influence on the degree of linear polarization. Furthermore, we are interested in the influence of aerosol or cirrus cloud layer height on the radiance and the degree of linear polarization in the O_2A band between 758 and 772 nm and the strong CO_2 band between 2040 and 2080 nm. Radiance ratios of reflected radiation in these bands for instance allow the estimation of the vertical structure of atmospheric scatterers [Duforet et al., 2007]. The high spectral resolution and high radiance sensitivity of OCO should enable a high sensitivity to the vertical structure of atmospheric scatterers also over land. An earlier study by Natraj et al. (2007) evaluated the errors resulting from ignoring polarization in analyzing simulations of backscatter measurements of the O_2A band by space-based instruments such as OCO with regard to beam and viewing geometry, surface reflectance and aerosol loading. We study the errors resulting from ignoring polarization in analyzing simulations of backscatter measurements of the O_2A band, weak CO_2 band at 1610 nm and the strong CO_2 band at 2060 nm with regard to aerosol and cirrus cloud layer height.

The definitions of Stokes parameters and ratio of radiances in absorption bands relevant for this paper are given in Section 4.2. In Section 4.3 we introduce the radiative transfer model and describe the scattering properties of ice clouds and aerosols, the model atmosphere, and the observation geometry. In Section 4.4 we outline the processes determining the TOA polarization and intensity in gaseous absorption bands. In Section 4.5 we show the results of the effect of aerosol and cirrus cloud layer height, aerosol microphysics and surface albedo on the degree of linear polarization and intensity at TOA. Conclusions are given in Section 4.6.

4.2 Definition of Stokes parameters and ratio of radiances relevant to OCO

4.2.1 Stokes parameters and polarization

Measurements of polarized light can be expressed by the Mueller matrix $\mathbf{M}$ and the Stokes vector $\mathbf{I}$ [Hovenier et al., 2004]:

$$\mathbf{I}_{\text{det}} = \mathbf{M} \cdot \mathbf{I}_0 \tag{4.1}$$

where on the left-hand side the Stokes vector describes the light as detected by the instrument, denoted by the subscript ''det'', and on the right hand side the Mueller matrix defines the response of the instrument to incoming light represented by a Stokes vector, denoted by ''0''. In the following discussion the circular component V of the Stokes vector is neglected, because numerous experiments and simulations show that V has a marginal influence on the total degree of polarization in the atmosphere [Stammes, 1989], [Egan, 1992]. Thus, Eq.(4.1) can be written as:

$$\begin{pmatrix} I \\ Q \\ U \end{pmatrix}_{\text{det}} = \begin{pmatrix} M_{11} & M_{12} & M_{13} \\ M_{21} & M_{22} & M_{23} \\ M_{31} & M_{32} & M_{33} \end{pmatrix} \cdot \begin{pmatrix} I \\ Q \\ U \end{pmatrix}_0 \tag{4.2}$$

where the first parameter of the Stokes vector, I, denotes the total intensity of the light. Q is a measure for the polarization along a chosen reference plane and can be described as $Q = I_x - I_y$. U is a measure for the polarization along a chosen direction which is 45° from the reference plane and is defined as $U = I_{45} - I_{-45}$. The total intensity can be written, e.g. as $I = I_x + I_y$. All Mueller matrix elements are dependent on wavelength and on the scattering angle of the light.

The detectors of the OCO instrument are only sensitive to intensity, thus reducing Eq. (4.2) to:

$$I_{\text{det}} = M_{11} \cdot I_0 + M_{12} \cdot Q_0 + M_{13} \cdot U_0 \tag{4.3}$$

where M_{11} is the radiometric sensitivity of the instrument, which can be set to 1, without loss of generality.

OCO is equipped with a linear polarizer within its optical path [Haring et al., 2005]. In nadir viewing direction, $\theta = 0^\circ$, the polarization axis of the instrument remains perpendicular to the principal plane (defined by the sun, surface target, and the instrument aperture) as OCO travels along its orbit track. Thus, OCO is only sensitive to the reflected radiation that is polarized perpendicular to this plane. In nadir viewing direction U equals zero. Assuming a Mueller matrix of an ideal polarizer [Gerrard and Burch, 1994]:

$$\mathbf{M} = \frac{1}{2} \cdot \begin{pmatrix} 1 & \cos 2\gamma & \sin 2\gamma \\ \cos 2\gamma & \cos^2 2\gamma & \cos 2\gamma \sin 2\gamma \\ \sin 2\gamma & \cos 2\gamma \sin 2\gamma & \sin^2 2\gamma \end{pmatrix} \tag{4.4}$$

we can write the intensity I detected at the instrument as follows:

$$I_{\text{det}} = \frac{1}{2} \cdot \left[I + Q \cdot \cos\left(2\gamma + 180^\circ\right) \right] \tag{4.5}$$

where γ is the orientation of the polarization axis in the reference plane, which can be set to 0, without loss of generality. This yields:

$$I_{\text{det}} = \frac{I - Q}{2} \tag{4.6}$$

In the following we define the intensity detected by the OCO instrument as follows:

$$I_{OCO} = 2 \cdot I_{\text{det}} = I - Q = I \cdot \left(1 + P_s\right) \tag{4.7}$$

where P_s is the degree of linear polarization of a light beam and is defined as follows [Hovenier et al., 2004]:

$$P_s = -\frac{Q}{I} \tag{4.8}$$

This shows that an error can be introduced if ignoring polarization in analyzing simulations of backscatter measurements of the O_2A band by space-based instruments such as OCO.

4.2.2 Ratio of radiances

Measurements of the (cloud free) radiance inside absorption bands at two wavelengths, one with strong, and the other with weak absorption, allow the retrieval of column CO_2 [O'Brien and Rayner, 2002]. The ratio of radiances, X_I, is defined as:

$$\mathrm{X}_I = \frac{I_b}{I_c} \tag{4.9}$$

and for the OCO instrument, which is sensing I-Q, the ratio of radiances, $\mathrm{X}_{I_{OCO}}$, is defined as:

$$\mathrm{X}_{I_{OCO}} = \frac{I_b - Q_b}{I_c - Q_c} \tag{4.10}$$

where $I_{b(c)}$ and $Q_{b(c)}$ are the radiance and linear polarization at wavelength $\lambda_{b(c)}$. The subscript "b" stands for strong absorption in the band and "c" for weak absorption in the continuum. If the radiation is scattered only at the surface (see I_r in Fig. 4.1) Eq. (4.9) can be approximated by $\mathrm{X}_I \cong \exp\left[-m\left(\tau_b - \tau_c\right)\right]$, where m is the air mass factor that accounts for slant paths followed by the photons, $m = \left|1/\cos\theta_i\right| + \left|1/\cos\theta_r\right|$ whereas θ_i and θ_r are the angles of incidence and reflection and $\tau_{b(c)}$ the optical thickness at wavelength $\lambda_{b(c)}$. The optical thickness difference $\tau_b - \tau_c$ can directly be related to e.g. the CO_2 column density [O'Brien and Rayner, 2002]. However, when aerosols or cirrus clouds are present in the atmosphere, scattering by particles will modify the mean photon path-length and thus change the total column CO_2 absorption. Besides the estimation of the column CO_2 it is possible to determine the height of atmospheric scatterers from radiance ratios X within the O_2A band, as done with POLDER or MERIS [Duforet et al., 2007]. Throughout the article we define changes in the radiance ratio, $\delta X_{I_{oco}}$ as:

$$\delta\mathrm{X}_{I_{OCO}} = \frac{\mathrm{X}_{I_{OCO}} - \mathrm{X}_{I_{OCO}(ref)}}{\mathrm{X}_{I_{OCO}(ref)}} \cdot 100\ \% \tag{4.11}$$

where ''ref'' denotes the reference value of $X_{I_{oco}}$.

The relative differences between the radiance ratio $X_I = I_b / I_c$, using only the total intensity, and $X_{I_{oco}} = (I-Q)_b / (I-Q)_c$, using the OCO signal can be expressed as follows (assuming no error in the intensity):

$$\varepsilon_{\mathrm{X}} = \left(\frac{1+P_c}{1+P_b} - 1 \right) \cdot 100 \ \% \tag{4.12}$$

where P_{c} and P_b are the degree of linear polarization in the continuum and with in the absorption band. The variable ε_{X} can be regarded as the error due to ignoring polarization in analyzing simulations of backscatter measurements of the O_2A band by space-based instruments such as OCO or as the relative differences between observations made by unpolarized instruments (e.g. MERIS) and OCO. An earlier study by Natraj et al. (2007) focused on evaluating the relative difference in intensity, whereas we are interested in the relative difference in radiance ratio.

4.3 Radiative transfer calculations

For the polarized radiative transfer calculations in gaseous absorption bands we combine two methods to significantly improve the calculation time while maintaining a high accuracy compared to line-by-line simulations [Boesche et al., 2008]. As spectral approximation technique we use the k-binning method, which is similar to a k-distribution approach, but overcomes shortcomings of a conventional k-distribution [Bennartz and Fischer, 2000], [Bennartz and Preusker, 2007]. We combine this method with monochromatic multiple scattering radiative transfer simulations, including polarization, for vertically inhomogeneous atmospheres (Doubling Adding KNMI – DAK) [de Haan et al., 1987], [Stammes et al., 1989]. An advantage of our combined method approach is that no assumptions about the shape of the sensor weighting function have to be considered a-priori for a given spectral interval. Any sensor response function can be constructed from a set of radiative transfer simulations for a spectral interval (for a detailed discussion see [Bennartz and Fischer, 2000], [Bennartz and Preusker, 2007], [Boesche et al., 2008]).

For our study we used spectral response functions which are representative for the OCO instrument with a high spectral resolution $(\lambda / \Delta\lambda)$ of > 17000 for the O_2A band and > 20000 for both of the CO_2 bands [Haring et al., 2005]. We assume a Gaussian spectral response function with a full-width at half-maximum (FWHM) of 0.04 nm inside the O_2A band, 0.07 nm

inside the CO_2 at 1610 nm and 0.09 nm inside the CO_2 band at 2060 nm, with an equal spacing.

The molecular absorption coefficients k_i (or molecular absorption optical thickness τ_i^{abs}) for the i = 1, …, N k-binning intervals are calculated using the k-binning method. As molecular spectroscopic database we use HITRAN 2004 [Rothman et al., 2005]. The Voigt profile is used for absorption line shapes to include Doppler-broadening in the whole column of the atmosphere.

DAK is used for the monochromatic multiple scattering radiative transfer simulations of the Stokes vector $\mathbf{I}_i$ for the i = 1, …, N k-binning intervals. The AFGL mid-latitude summer atmospheric profile is used up to 100 km. The model atmosphere is assumed to be plane parallel and divided into 32 layers with a vertical resolution of 1 km within the first 25 layers. The atmosphere is bounded by a Lambertian surface, thus the reflected light is assumed to be unpolarized and isotropic in the outward hemisphere. We assumed two different surface albedos in this study. For dark surfaces we assume a surface albedo of A_s = 0.02, and for brighter surfaces we assume A_s = 0.20. The surface albedos are assumed to be a fixed value for all absorption bands under consideration.

In this study, three different types of scatterer are included in the calculations, resembling scatterers as found under clear to hazy sky conditions: small, strongly polarizing spherical aerosols ($aerosol_1$); large, weakly polarizing spherical aerosols ($aerosol_2$); and weakly polarizing non-spherical ice-crystals (C_1). The microphysical properties of the spherical aerosol particles were derived from actual measurements at clear sky conditions ($aerosol_1$) and hazy sky conditions ($aerosol_2$), taken at Cabauw, The Netherlands [Boesche et al., 2006]. Their microphysical and optical properties correspond to urban-industrial aerosols [Dubovik et al., 2000]. We included cirrus clouds in this study because clouds cover large parts of the Earth. Statistics of four years of global High Resolution Infrared Radiation Sounder (HIRS) cloud data show a global preponderance of transmissive clouds of around 42% on the average and about three fourths of these are above 500 hPa and presumed to be cirrus [Wylie and Menzel, 1999]. In this study we used small imperfect hexagonal monocrystals (C_1), which are randomly oriented, resembling cirrus cloud particles [Hess et al., 1998], [Knap et al., 2005].

The single scattering properties of the chosen scatterers are calculated using Mie theory, in case of aerosols, and using the GO approximation, in case of non-spherical ice-crystals. The microphysical properties of the aerosols as well as cirrus clouds are assumed to be constant within the spectral region of the absorption bands. Tables 4.1 and 4.2 list the optical and microphysical properties of the aerosols and ice-crystals used in this study.

To study the influence of aerosol and cirrus cloud layer height, microphysical properties and surface albedo changes on the degree of linear polarization P and the intensity I_{OCO} in the O_2A and CO_2 absorption bands at TOA, we use the following model atmosphere. The basic model atmosphere is a Rayleigh scattering atmosphere with oxygen or carbon dioxide as the only absorbing gas. In this atmosphere we place an elevated scattering layer (EL), which comprises aerosols or ice-crystals (see Table 4.1 and 4.2). The scattering layer has a fixed geometrical thickness of 1 km. The scattering layer height (denoting the top of the layer) is changed in steps of 2 km. The optical thickness τ_{EL} of the scattering layer in the O_2A band is 0.10, resembling clear sky conditions. Using the relationship $\tau(\lambda_1)/\tau(\lambda_2) = \sigma_{ext}(\lambda_1)/\sigma_{ext}(\lambda_2)$, where σ_{ext} is the wavelength dependent extinction cross section, we can calculate the optical thickness at 1610 and 2060 nm. The resulting optical thickness in the CO_2 band at 1610 nm is 0.059, and in the CO_2 band at 2060 nm the is 0.049 (see Table 4.1).

4.4 Processes determining polarization and intensity in absorption bands as observed at TOA

Attenuation of solar radiation, penetrating the atmosphere, is caused by molecular (Rayleigh) scattering, absorption by O_2 and other gases such as O_3, H_2O, or CO_2, extinction (scattering and/or absorption) by aerosols and transmissive cirrus clouds, and reflection at the surface. The total radiance at TOA I_{TOA} is the sum of the following contributions (see Fig. 4.1): (1) the radiance transmitted through the atmosphere and reflected by the surface, I_r; (2) the radiance scattered once in the atmosphere, either by aerosols, cloud particles, or molecules, and transmitted back to space, I_{ss}; (3) the radiance scattered once in the atmosphere, then reflected at the surface, and transmitted back to space, I_{sr}; (4) the radiance reflected at the surface and then scattered once in the atmosphere, I_{rs} and (5) all higher order scattering processes, I_{ms} (multiple scattering):

$$I_{TOA} = I_r + I_{ss} + I_{sr} + I_{rs} + I_{ms} \tag{4.14}$$

The Stokes parameter Q at TOA can be written as:

$$Q_{TOA} = Q_{ss} + Q_{ms} \tag{4.15}$$

Q_{TOA} is only affected by the scattering contributions, because the surface is assumed to be Lambertian and thus the surface reflected radiation only contributes to the radiance signal. These contributions depend strongly on gaseous absorption, height of atmospheric scatterers, and viewing geometry.

To understand the role of these processes we now analyze the influence of molecular scattering, aerosol scattering, surface albedo, and height of atmospheric scatterers on the degree of linear polarization and intensity in the O_2A band as observed at TOA:

(a) Molecular scattering, with black surface A_s = 0.0 [Fig. 4.2 (red line)]: For a purely Rayleigh scattering atmosphere the TOA radiance I_{TOA} is composed of the backscattering components I_{ss} and I_{ms}. Compared to the continuum we find a higher degree of linear polarization in the absorption band because multiple scattering is reduced by means of absorption, and single scattering is enhanced. Therefore the degree of linear polarization inside the absorption band (P_b) is higher as compared to the continuum (P_c).

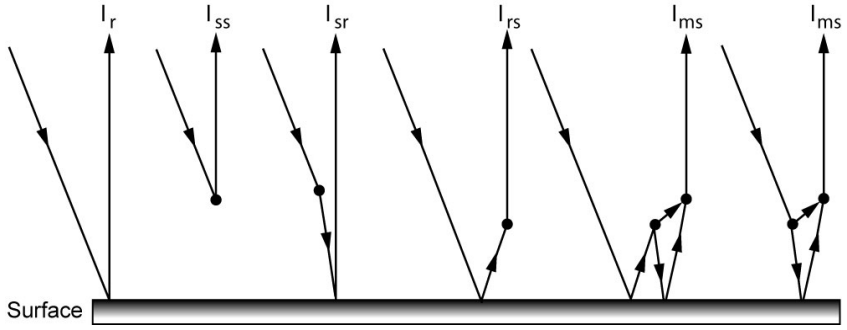

Figure 4.1: Illustration of the solar light paths in the atmosphere. I_r is the radiance transmitted through the atmosphere and reflected by the surface. I_{ss} is the radiance scattered once in the atmosphere, either by aerosols, cloud particles, or molecules back to space. I_{sr} is the radiance scattered once in the atmosphere, reflected at the surface, and transmitted back to space. I_{rs} is the radiance reflected at the surface and scattered once in the atmosphere. I_{ms} describes all higher order scattering processes (multiple scattering).

Table 4.1: Aerosol model parameters used in the radiative transfer simulations. The spherical aerosol types are representative for small and large continental aerosols [Boesche et al., 2006].

Aerosol Parameter	Symbol	$Aerosol_1$			$Aerosol_2$		
		765 nm	1610 nm	2060 nm	765 nm	1610 nm	2060 nm
Imaginary part of the refractive index	m_i	0.0000	0.0057	0.0017	0.0007	0.0030	0.0010
Real part of the refractive index	m_r	1.40	1.38	1.34	1.380	1.36	1.33
Scattering layer optical thickness	τ	0.10	0.059	0.049	0.10	0.059	0.049
Median radius of the fine mode	$r_f\,[\mu m]$		0.080			0.120	
Median radius of the coarse mode	$r_c\,[\mu m]$		0.425			0.700	
Standard deviation of the fine mode	σ_f		1.300			1.950	
Standard deviation of the coarse mode	σ_c		2.200			2.200	
Weighting factor of the fine mode	w		0.9996			0.9992	

Table 4.2: Ice crystal model parameters used in the radiative transfer simulations. The imperfect hexagonal ice crystal C_1 represents cirrus cloud particles [Hess et al., 1998].

Ice crystal Parameter	Symbol	Ice crystal C_1		
		765 nm	1610 nm	2060 nm
Imaginary part	m_i	0.783E-07	0.346E-03	0.126E-02
Real part	m_r	1.306	1.289	1.271
Scattering layer optical thickness	τ	0.1	0.059	0.049
Length	$L\,[\mu m]$		30	
Radius	$R\,[\mu m]$		10	
Effective radius	$r_{eff}\,[\mu m]$		12.2997	
Aspect ratio			1.5	
Orientation			random	

(b) Molecular and aerosol scattering, A_s = 0.0 [Fig. 4.2 (green line)]: Including large, weakly polarizing aerosol$_2$, with $\tau_{aer} = 0.10$, to the boundary layer (0-1 km) of the model atmosphere increases multiple scattering. The continuum polarization P_c decreases stronger than the polarizatio P_b in the region of strong absorption lines. Inside gaseous absorption bands light is mainly scattered at higher altitudes (gaseous absorption prevents light to reach lower parts of the atmosphere) thus molecular scattering dominates inside the absorption band, which results in a higher P_b and the increase of I_{TOA} is smaller inside the band.

(c) Molecular and aerosol scattering, A_s = 0.02 [Fig. 4.2 (blue line)] and 0.20 [Fig. 4.2 (orange line)]: Adding surface reflection with a low albedo of A_s = 0.02 has a strong impact on P_c, while P_b is less affected. Inside the absorption band the surface is shielded due to the gaseous absorption and this causes the lower impact on P_b. Increasing the surface albedo to A_s = 0.20 we see a further decrease of P_c and P_b. In these cases the decrease of degree of linear polarization is caused by the fact that the atmosphere in DAK is bounded by a Lambertian surface, thus the reflected light is assumed to be unpolarized and isotropic in the outward hemisphere. This results in an increase of I_{TOA}, while Q_{TOA} remains unchanged. The increase of I_{TOA} is dominated by surface reflected components I_r, I_{sr}, and I_{rs}. The effects are more pronounced for small solar zenith angles. This increase of surface influence with smaller solar zenith angles is due to the more efficient transmission of the direct beam through the atmosphere, and the consequent strong illumination of the surface. At the same time the efficient transmission causes less multiple scattering [Coulson, 1998];

(d): As (c), but increasing the aerosol layer height, A_s = 0.20 [Fig. 4.2 (black line)]: An altitude increase from 1 to 16 km of the aerosol scattering layer shows a negligible influence on P_c, whereas the influence on P_b is strong. The influence of aerosol layer height on P_b is caused by the strong O_2A band absorption which prevents light to reach lower parts of the atmosphere. Due to the fact that light inside the absorption band is scattered at higher altitudes, an increase in aerosol layer height increases the probability of aerosol scattering as compared to molecular scattering and is thus decreasing P_b. Whereas in the continuum light can interact with all scatterers in the entire atmosphere if the scatterers are assumed to be non-absorbing. Aerosol absorption affects molecular scattering below the aerosol layer, and the underlying Rayleigh scattering produces only a small signal. In that case we find a small

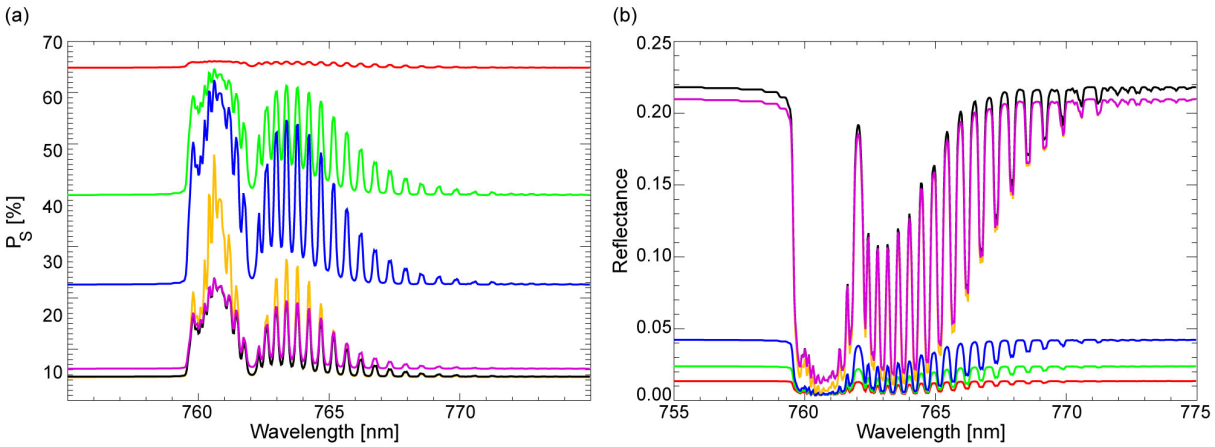

Figure 4.2: Degree of linear polarization and reflectance of reflected light as a function of wavelength at a solar zenith angle of $\theta_0 = 65^\circ$ showing processes which determine the polarization in the O_2A band: pure Rayleigh scattering (red) without surface reflection; inclusion of aerosol$_2$ to the boundary layer with a geometrical thickness of 1 km and an optical thickness of 0.1 at 765 nm (green); adding a surface albedo of A_s = 0.02 (blue) and of A_s = 0.20 (orange); elevation of the aerosol layer up to 16 km (black); inclusion of aerosol$_2$ to the boundary layer with an optical thickness of 0.35 (purple).

decrease of P_c with increasing aerosol scattering layer height. However, in case of increasing surface reflection the aerosol layer height influence on P_b decreases and furthermore can lead to an increase of P_b.;

(e): As (d), but adding a second aerosol layer, A_s = 0.20 [Fig. 4.2 (purple line)]: Adding a second aerosol layer between 0 and 1 km with weakly polarizing aerosol$_2$, having an optical thickness of $\tau_{aer} = 0.35$, slightly increases the continuum polarization, but due to the shielding effect this shows nearly no effect inside the band.

4.5 Effect of scattering layer height on polarization and intensity at TOA

In this Section we study the influence of scattering layer height, microphysics and surface reflectance on the degree of linear polarization P_s [Eq. (4.8)], and radiance ratio $X_{I_{OCO}}$ [Eq. (4.10)], for nadir observations inside the O_2A band, the weak CO_2 band at 1610 nm, and the strong CO_2 band at 2060 nm.

The simulations are carried out for a basic model atmosphere (see Section 4.3) comprising an elevated scattering layer with a geometrical thickness of 1 km which is shifted through the

atmosphere in steps of 2 km. The elevated scattering layer has an optical thickness of 0.10 in the O_2A band is 0.10, in the CO_2 at 1610 nm $\tau_{EL} = 0.059$, and in the CO_2 band at 2060 nm $\tau_{EL} = 0.049$. We include different types of scatterers in the elevated scattering layer: small, strongly polarizing aerosol$_1$; large, weakly polarizing aerosol$_2$ and weakly polarizing C_1 ice-crystals, see Tables 4.1 and 4.2 for the optical characteristics of the scatterers. As viewing geometry we chose a solar zenith angle of $\theta_0 = 65^\circ$ and a viewing zenith angle of $\theta = 0^\circ$ (nadir view), resulting in a scattering angle of $\Theta = 115^\circ$.

Figure 4.3 illustrates the TOA spectra of the degree of linear polarization (solid line) and reflectance I_{OCO} (dashed line) in the O_2A band, the weak CO_2 band and the strong CO_2 band. In this case the elevated scattering layer is located between 1 and 2 km and contains small, strongly polarizing aerosol$_1$. Regarding the degree of linear polarization, we see a much lower degree of linear polarization inside the weak CO_2 band around 1610 nm [Fig. 4.3 (b)], caused by the strong influence of the surface.

4.5.1 Oxygen A band

Interaction between absorption of incident light in the oxygen A band and scattering by particles can provide information about the vertical structure of scatterers in the atmosphere [Stammes et al., 1994], [Preusker et al., 1995], [Aben et al., 1999], [Stam et al., 1999], [Duforet et al., 2007], [Boesche et al., 2008]. Figure 4.4 (top panel) shows the degree of linear polarization P_s as a function of the scattering layer height for different types of scatterers and at different surface albedos. To illustrate the influence of height changes on the degree of linear polarization in the continuum P_c (at 757.92 nm) and within the absorption band P_b (at 760.60 nm) in a more pronounced way we show P_c and the polarization difference $P_b - P_c$ as function of scattering layer height. As discussed in Section 4.4 we find a decrease of P_b with increasing scattering layer height for low surface reflection. The decrease is strongest for the weakly polarizing aerosol$_2$ and C_1, while strongly polarizing aerosol$_1$ shows little influence of P_b. The continuum polarization P_c remains more or less unchanged. We find that the influence of the elevated scattering layer height on P_b decreases if the surface albedo increases. In case of strongly polarizing aerosol$_1$ we find that P_b increases with increasing scattering layer height.

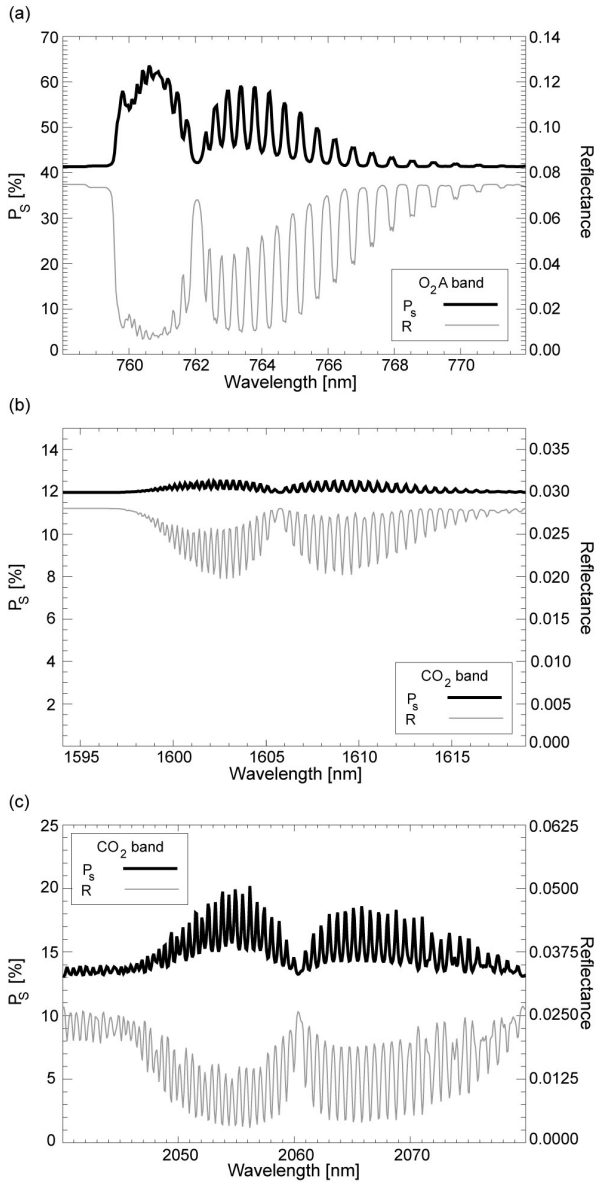

Figure 4.3: Top-of-the-atmosphere spectra of the degree of linear polarization and reflectance at a viewing zenith angle of $\theta = 0^\circ$ (nadir) and solar zenith angle of $\theta_0 = 65^\circ$. Aerosol$_1$ is included in the boundary layer between 0 and 1 km. The surface albedo is 0.02. (a) O_2A band at 760 nm with a scattering layer optical thickness of 0.10. (b) CO_2 band at 1610 nm with a scattering layer optical thickness of 0.059. (c) CO_2 band at 2060 nm with a scattering layer optical thickness of 0.049.

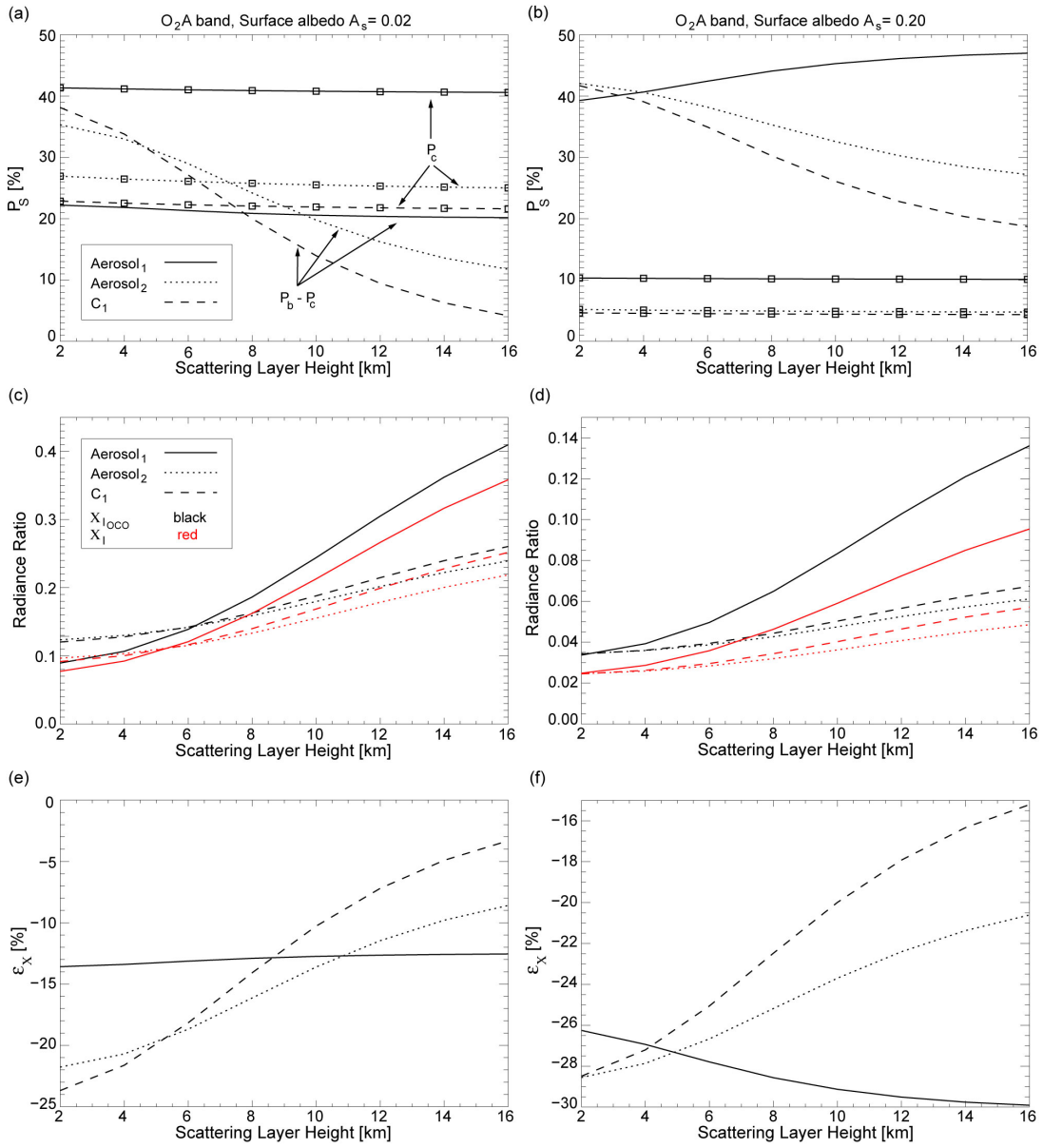

Figure 4.4: Top panel: Degree of linear polarization of the reflected radiation in the O_2A band as function of the scattering layer height for different types of scatterers. The solar zenith angle is $\theta_0 = 65^\circ$ and the viewing zenith angle is $\theta = 0^\circ$ (nadir). The optical thickness of the scattering layer is 0.10. The curves marked with boxes indicate the continuum polarization P_c, selected at 757.92 nm, while the unmarked curves show the difference between band polarization and continuum polarization, $P_b - P_c$. P_b was selected at 760.60 nm. (a) Surface albedo A_s = 0.02. (b) Surface albedo A_s = 0.20. Middle panel: Radiance ratio $X_{I_{OCO}} = I_{OCO}(760.60)/I_{OCO}(757.92)$ as a function of scattering layer height for different types of scatterers in the O_2A band (solar zenith angle $\theta_0 = 65^\circ$; viewing zenith angle $\theta = 0^\circ$, and $\tau_{scat} = 0.10$). The red lines show X_I and the black lines show $X_{I_{OCO}}$. (c) Surface albedo A_s = 0.02. (d) Surface albedo A_s = 0.20. Bottom panel: Relative radiance ratio difference ε_X as a function scattering layer height. (e) Surface albedo A_s = 0.02. (f) Surface albedo A_s = 0.20

This can be explained as follows: I_b as function of aerosol layer height h can be written as $I_b(h) \cong I_{surf,b} + I_{mol,b} + I_{EL,b}(h)$,where $I_{surf,b}$ is determined by the surface reflection, $I_{mol,b}$ is determined by Rayleigh scattering and $I_{EL,b}(h)$ by scattering in the elevated layer. Analogously we can write $Q_b(h) \cong Q_{mol,b} + Q_{EL,b}(h)$. An increase of surface reflection A_s increases the intensity I and Q remains unchanged. Assuming that the absolute changes of $\Delta I_{EL,b}$ and $\Delta Q_{EL,b}$ with increasing aerosol layer height are independent to changes of A_s, we find that the relative increase of $I_b(h)$ with increasing height of the scattering layer is reduced in case of higher A_s, while in comparison the relative increase of $Q_b(h)$ remains unchanged. Thus, in case of increasing A_s the degree of linear polarization $P_b = -Q_b / I_b$ decreases less strongly with increasing height of the scattering layer than in the case of lower A_s. If the influence of the surface reflection is high enough the relative increase of Q_b becomes larger than that of I_b, resulting in an increase of P_b with increasing aerosol layer height. A decrease of P_b below P_c, as observed for ground based polarization measurements, could only be found for A_s = 0.0 (see Refs. [Stammes et al., 1994], [Aben et al., 1999], [Boesche et al., 2008]). As shown in the top panel of Fig. 4.4 the sensitivity of P_b to changes of the scattering layer height is strongly affected by the microphysics of the scatterers. The influence of aerosol layer height is stronger for larger solar zenith angles. This is related to the higher concentration of absorbing and scattering particles within the light path, which is related to the geometric air mass factor $m = 1/\cos\theta_0 + 1/\cos\theta$.

Furthermore we examine the radiance ratio $X_{I_{OCO}}$. In this case we choose the radiance ratio to be $X_{I_{OCO}} = I_{OCO}(760.60) / I_{OCO}(757.92)$. The signal at 760.60 nm is strongly attenuated by oxygen absorption, whereas the attenuation of the signal at 757.92 nm is absent.

Figure 4.4 (middle panel) shows the radiance ratio $X_{I_{OCO}}$ as a function of the scattering layer height for different types of scatterers at different surface albedos. We also included the radiance ratio X_I. It is shown that the radiance ratio $X_{I_{OCO}}$ is sensitive to changes of the elevated scattering layer height. This is caused by changes in $I_{OCO}(760.60)$. The strong O_2A band absorption prevents light to reach lower parts of the atmosphere. Thus light inside the absorption band is scattered at higher altitudes. An increase in aerosol scattering layer height increases the probability of aerosol scattering as compared to molecular scattering and $I_{OCO}(760.60)$ increases. In the continuum light can interact with all scatterers in the entire atmosphere, if the scatterers are assumed to be non-absorbing, and therefore changes of the scattering layer height show minor influence on $I_{OCO}(757.92)$. The radiance ratio $X_{I_{OCO}}$ strongly depends on the surface albedo, the aerosol microphysics, and height of aerosols, as

also shown by [Vanbauce et al., 1998], [Dubuisson et al., 2001], or [van Diedenhoven et al., 2005]. The studies showed for instance that in the O_2A band for low surface albedos the surface pressure, which is well correlated to the radiance ratio, is underestimated in the retrieval. This is due to the relatively high contribution of the backscattered signal I_{ss}, shortening the mean photon path-length. While incase of high surface albedos, the surface pressure is generally overestimated in the retrieval. This is due to the contribution of the surface reflected components I_{sr}, I_{rs}, and partially I_{ms}, increasing the overall path-length of the scattered photons (see Subsection 4.5.2). Furthermore it is shown that the aerosol height has a significant impact on the surface pressure retrieval in case of low surface albedos, while for high surface albedos the impact decreases (see also Subsection 4.5.2). Table 4.3 shows the radiance ratio change $\delta X_{I_{OCO}}$ due to changes of the scattering layer height at different surface albedos. We find that the sensitivity of $X_{I_{OCO}}$ is strongest for the smaller, strongly polarizing aerosol$_1$ as compared to larger, weakly polarizing aerosol$_2$ and C_1. Increasing the surface albedo lessens the sensitivity of $X_{I_{OCO}}$ to changes of the scattering layer height.

The bottom panel of Fig. 4.4 shows the relative radiance ratio difference ε_X as a function of the scattering layer height for different types of scatterers and at different surface albedos. The relative difference ε_X decreases with increasing scattering layer height, for weakly polarizing aerosols and low surface albedo (A_s = 0.02). For strongly polarizing scatterers and strong influence of the surface albedo in the band we can also find an increase of ε_X with increasing scattering layer height. The relative radiance ratio difference ε_X resembles the behavior of the degree of linear polarization P_b (top panel of Fig. 4.4) as can be seen from Eq. (4.12).

Table 4.3: Sensitivity of the radiance ratio $X_{I_{OCO}}$ to changes of the scattering layer height in the O_2A band at 760 nm. The height indicates the top of the scattering layer.

	$\delta X_{I_{OCO}}$ (Aerosol$_1$) [%]		$\delta X_{I_{OCO}}$ (Aerosol$_2$) [%]		$\delta X_{I_{OCO}}$ (C_1) [%]	
Height [km]	A_s = 0.02	A_s = 0.20	A_s = 0.02	A_s = 0.20	A_s = 0.02	A_s = 0.20
2-4	19.25	16.51	5.26	4.39	9.25	5.29
4-6	30.29	26.47	9.06	7.69	16.01	9.36
6-8	34.13	30.59	12.09	10.30	20.31	12.46
8-10	30.98	28.44	13.11	11.27	20.60	13.44
10-12	24.94	23.31	12.21	10.62	18.05	12.47
12-14	18.77	17.75	10.20	8.97	14.41	10.41
14-16	13.12	12.50	7.68	6.81	10.50	7.83

4.5.2 Carbon Dioxide band at 1610 nm

To estimate the total column of CO_2 we can use the radiance ratio $X_{I_{OCO}}$ at wavelengths of strong and weak absorption [O'Brien and Rayner, 2002], [Mao and Kawa, 2004] (see also Section 4.4). Scattering of atmospheric radiation at aerosols or ice cloud particles can alter $X_{I_{OCO}}$ and hence affect the estimation of total column CO_2. Based on a Rayleigh atmosphere, Figures 4.5 (top panel) shows the radiance ratio changes $\delta X_{I_{OCO}}$ caused by a 1% increase of column CO_2 at different surface albedos as function of wavelength. The radiance ratio in the CO_2 band at 1610 nm $X_{I_{OCO}}(\lambda) = I_{OCO}(\lambda) / I_{OCO}(1594.06\ nm)$ decreases with increasing CO_2 concentration. Furthermore we show the radiance ratio changes due to inclusion of an aerosol layer and cirrus clouds at different surface albedos. For a surface albedo of 0.02 (left panel of Fig. 4.5), we find positive radiance ratio changes due to inclusion of aerosols or cirrus particles. The scatterers are located between 1 and 2 km. Scatterers in the atmosphere increase the effect of the backscattered signal I_{ss} which contributes to the total signal at TOA. This can lead to a shortening of the photon path-length and can lead to an underestimation of the total column CO_2. In this case, the aerosols and cirrus clouds lead to an underestimation of the total column CO. For a surface albedo of 0.20 (right panel of Fig. 4.5) we find a change of the aforementioned effect. For all scatterers under consideration we find a negative radiance ratio change. An increase of surface albedo increases the effect of the surface reflected components I_{sr}, I_{rs}, and partially I_{ms} which contribute to the total signal at TOA, compared to the backscattered signal I_{ss}. This leads overall to an increase of the path-length of the scattered photons, which leads to an overestimation of total column CO_2. Thus scatterers in the atmosphere can lead to both, an underestimate and an overestimate of column CO_2, depending on the microphysical and optical properties of the scatterers, the height of atmospheric scatterers, the surface albedo, and viewing geometry.

Figure 4.6 (top panel) shows the degree of linear polarization in the continuum P_c (at 1594.06 nm) and the polarization difference $P_b - P_c$ between the polarization in the band P_b (at 1602.88 nm) and the continuum polarization as function of scattering layer height for different types of scatterers and at different surface albedos. We find an increase of P_b with increasing scattering layer height for all types of scatterers, even at a low surface albedo of 0.02. This is caused by the strong influence of the surface albedo in the weaker absorbing CO_2 band at 1610 nm (see also Section 4.4 and Subsection 4.5.1). Furthermore the weak absorption in this band allows for more multiple scattering and thus the degree of linear polarization in the band is much weaker, as compared to the O_2A band or the CO_2 band at 2060 nm (see also Fig. 4.3).

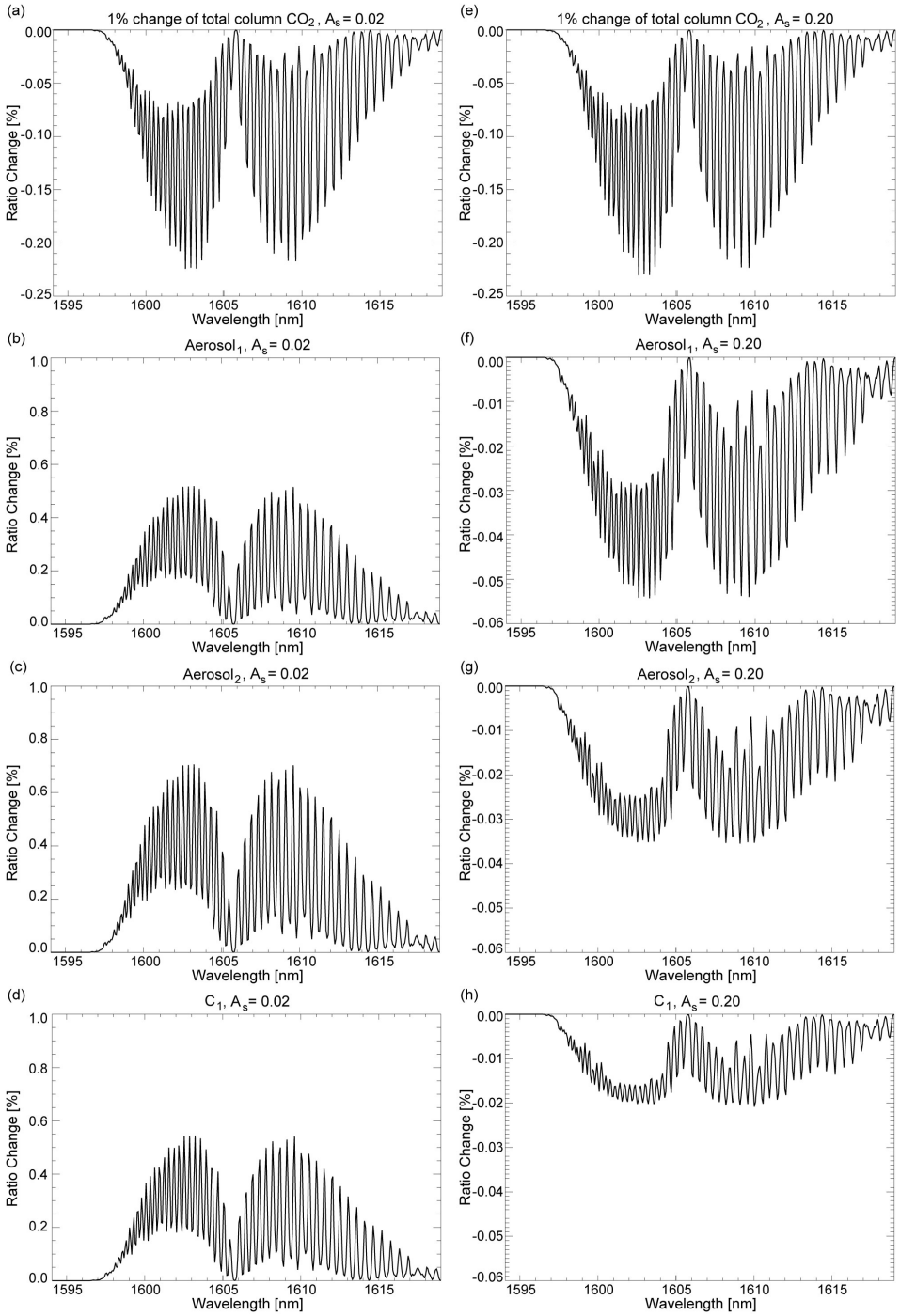

Figure 4.5: Left panel: Based on a Rayleigh atmosphere, (a) shows the radiance ratio changes $\delta X_{I_{OCO}}$ caused by a 1% increase of column CO_2 as function of wavelength (solar zenith angle $\theta_0 = 65^\circ$, viewing angle $\theta = 0^\circ$, and A_s = 0.02). The radiance ratio is chosen to be $X_{I_{OCO}}(\lambda) = I_{OCO}(\lambda) / I_{OCO}(1594.06nm)$. (b-d) Radiance ratio changes due to inclusion of different types of scatterers (aerosol$_1$, aerosol$_2$, and C_1) between 1 and 2 km. The optical thickness of the scattering layers is 0.059 and the surface albedo is 0.02. Right panel: Same as left panel but for a surface albedo of 0.20.

We also examine the influence of the scattering layer height on the radiance ratio $X_{I_{OCO}}$. We choose the radiance ratio to be $X_{I_{OCO}} = I_{OCO}(1602.88) / I_{OCO}(1594.06)$. The signal at 1602.88 nm is strongly attenuated by carbon dioxide absorption, whereas the attenuation of the signal at 1594.06 nm is absent. The middle panel of Figure 4.6 shows the radiance ratio $X_{I_{OCO}}$ as a function of the scattering layer height for different types of scatterers and at different surface albedos. An increase of the scattering layer height increases $X_{I_{OCO}}$ for all the scatterers under consideration and leads to an underestimation of column CO. This is due to a shortening of the overall path-length of the sunlight (the backscattering signal I_{ss} increases compared to the surface reflected components). The effect is stronger for a surface albedo of 0.02 (left panel of Fig. 4.6), as the influence of the surface-reflected components is lower. An increase of surface albedo (right panel of Fig. 4.6) leads to a decrease of the scattering layer height effect, by increasing the effect of the reflected components I_{sr}, I_{rs}, and partially I_{ms} which lengthen the path-length of the sunlight. We also X_I to point out the influence of neglecting polarization in simulations of backscattered measurements of the O2A band by space-based instruments such as OCO.

Table 4.4 shows the radiance ratio change $\delta X_{I_{OCO}}$ due to changes of the scattering layer height for different types of scatterers and at different surface albedos. At a surface albedo of A_S = 0.20 we find that a change of the scattering layer height from 2 to 4 km causes a change in radiance ratio between 0.05% and 0.12%. The small, strongly polarizing aerosol$_1$ shows the strongest influence. The radiance ratio change caused by a 1% change of total column CO_2 is about -0.23% (see top panel of Fig. 4.5). For low surface albedos, where the backscattering component I_{ss} has a stronger impact, the change in radiance ratio is of an order or two of magnitude larger. A change of the scattering layer height from 2 to 4 km for instance causes a change between 1.09 and 1.60%. In these cases the determination of the scattering layer height is even more crucial for the estimation of the column CO_2 amount.

The bottom panel of Fig. 4.6 shows the relative radiance ratio difference ε_X as a function of the scattering layer height for different types of scatterers at different surface albedos. Neglecting polarization leads to an overestimation of column CO_2 for all cases and the bias

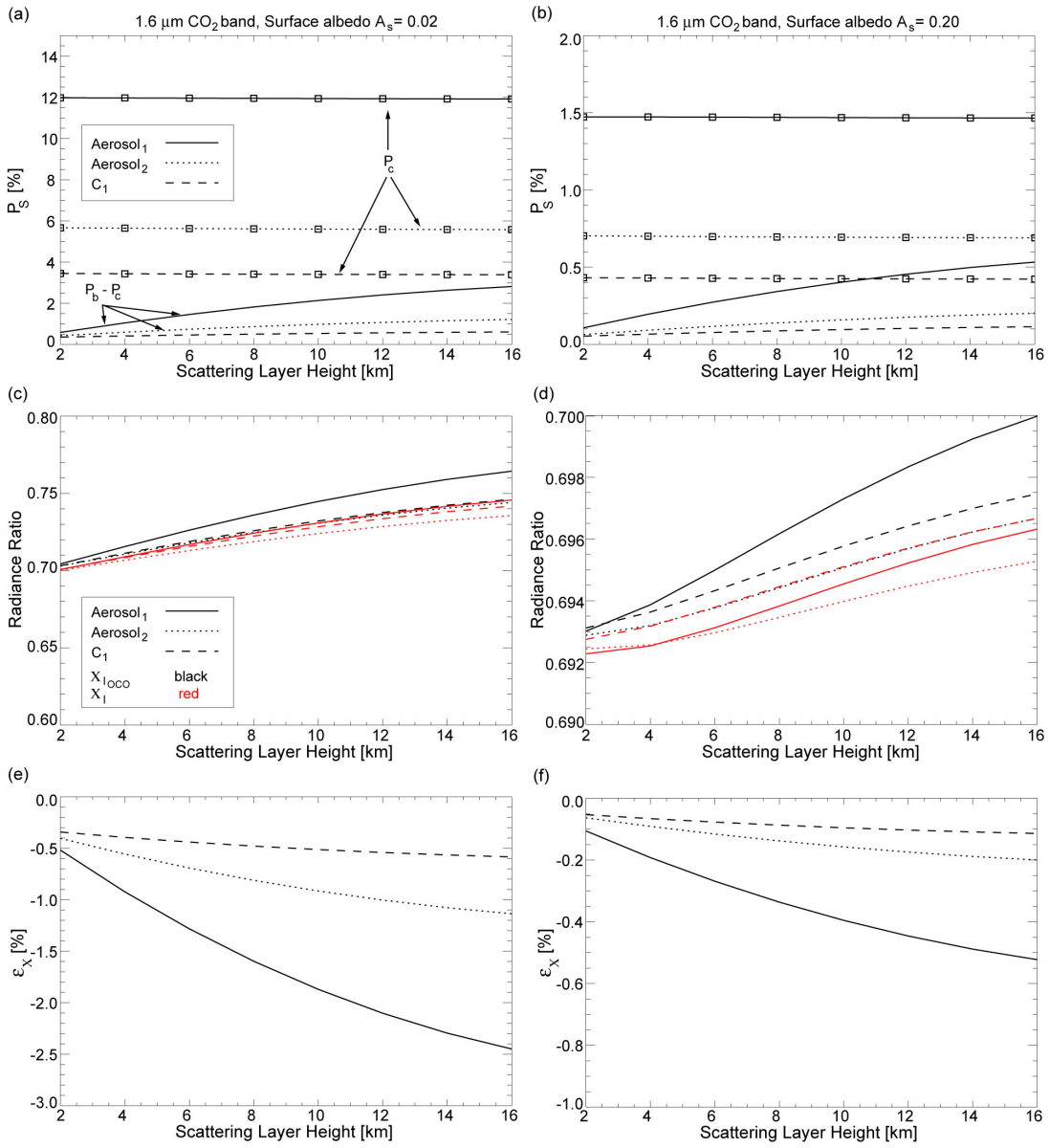

Figure 4.6: Top panel: Degree of linear polarization of the reflected radiation in the CO_2 band around 1610 nm as function of the scattering layer height for different types of scatterers. The solar zenith angle is $\theta_0 = 65^\circ$ and the viewing zenith angle is $\theta = 0^\circ$ (nadir). The optical thickness of the scattering layer is 0.059. The curves marked with boxes indicate the continuum polarization P_c, selected at 1594.06 nm, while the unmarked curves show the difference between band polarization and continuum polarization, $P_b - P_c$. P_b was selected at 1602.88 nm. (a) Surface albedo A_s = 0.02. (b). Middle panel: Radiance ratio $X_{I_{OCO}} = I_{OCO}(1602.88)/I_{OCO}(1594.06)$ as a function of scattering layer height for different types of scatterers in the weak CO_2 band around 1610 nm (solar zenith angle $\theta_0 = 65^\circ$; viewing angle $\theta = 0^\circ$, and $\tau_{scat} = 0.059$). The red lines show X_I and the black lines show $X_{I_{OCO}}$. (c) Surface albedo A_s = 0.02. (d) Surface albedo A_s = 0.20. Bottom panel: Relative radiance ratio difference ε_X as a function of Scattering layer height. (e) Surface albedo A_s = 0.02. (f) Surface albedo A_s = 0.20.

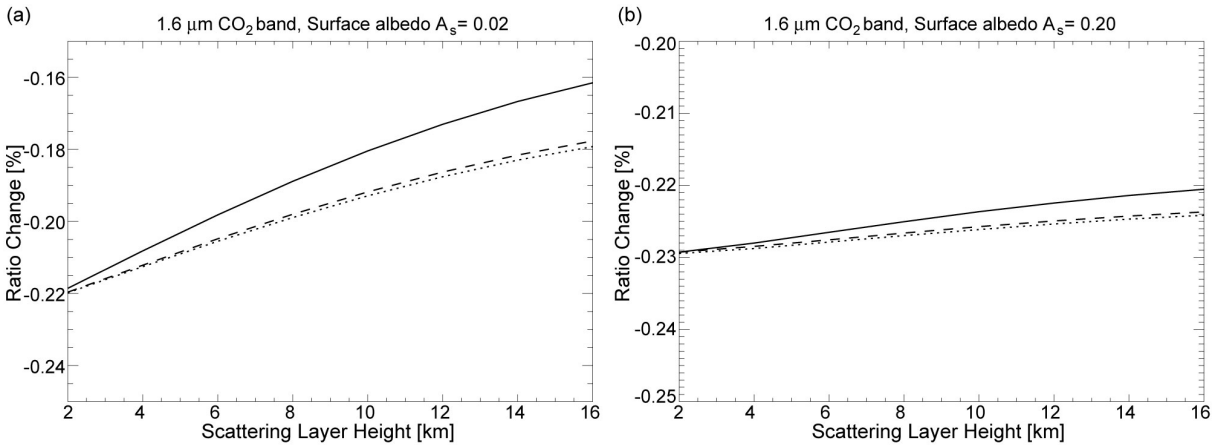

Figure 4.7: **.** Radiance ratio change to a 1 % increase of the CO_2 column amount as a function of scattering layer height for different types of scatterers in the weak CO_2 band around 1610 nm (solar zenith angle $\theta_0 = 65^\circ$; viewing angle $\theta = 0^\circ$, and $\tau_{scat} = 0.059$). (c) Surface albedo A_s = 0.02. (d) Surface albedo A_s = 0.20.

Table 4.4. Sensitivity of the radiance ratio $X_{I_{OCO}}$ to changes of the scattering layer height in the CO_2 band around 1610 nm. The height indicates the top of the scattering layer.

	$\delta X_{I_{OCO}}$ (Aerosol$_1$) [%]		$\delta X_{I_{OCO}}$ (Aerosol$_2$) [%]		$\delta X_{I_{OCO}}$ (C$_1$) [%]	
Height [km]	A_s = 0.02	A_s = 0.20	A_s = 0.02	A_s = 0.20	A_s = 0.02	A_s = 0.20
2-4	1.60	0.12	1.09	0.05	1.15	0.07
4-6	1.49	0.16	1.02	0.08	1.07	0.10
6-8	1.35	0.17	0.93	0.09	0.97	0.11
8-10	1.19	0.16	0.83	0.09	0.87	0.10
10-12	1.03	0.15	0.72	0.09	0.75	0.10
12-14	0.88	0.13	0.61	0.08	0.64	0.08
14-16	0.70	0.11	0.49	0.06	0.51	0.07

increases with increasing scattering layer height. Strongly polarizing aerosols show the largest impact and ε_X ranges from around -0.5% to -2.4% at A_s = 0.02 and from around -0.1% to -0.5% at A_s = 0.2. Weakly polarizing aerosols and cirrus clouds have a lower impact on ε_X. Especially for low surface albedos this effect has a strong influence on the estimation of total column CO_2.

Furthermore we are interested in the radiance ratio change $\delta X_{I_{OCO}}$ caused by a 1% increase of column CO_2 and its sensitivity to changes of scattering layer heights. Fig. 4.7 shows the radiance ratio change caused by a 1% increase of total column CO_2 as a function of the scattering layer height due to the already mentioned shortening of the overall path-length, thus the signal is not affected by the absorbing gas below the scattering layer and leads to an underestimation of the total column CO_2. The effect is lower for higher surface albedos.

4.5.3 Carbon Dioxide band at 2060 nm

Compared to the weaker CO_2 band at 1610 nm the influence of polarization is stronger. Figure 4.8 (top panel) shows the degree of linear polarization P_s as a function as function of the scattering layer height for different types of scatterers and different surface albedos. As in

case of the O_2A band we show the influence of changes of the scattering layer height on the degree of linear polarization at weak absorption P_c (at 2040.16 nm) and the polarization difference between strong absorption P_b (at 2056.18 nm) and weak absorption $P_b - P_c$ as function of scattering layer height. In case of A_s = 0.02 we find a strong increase of P_b with increasing scattering layer height for strongly polarizing aerosol$_1$. Weakly polarizing aerosol$_2$ and C_1 show a smaller increase of P_b with increasing scattering layer height. Compared to the O_2A band we find a much lower P_c. In case of A_s = 0.20 increase of P_b with increasing scattering layer height is less strong. Furthermore we find a decrease of P_c due to increasing surface influence.

We also examine the sensitivity of the radiance ratio $X_{I_{OCO}}$ to changes of the scattering layer height. In this case we choose the radiance ratio to be $X_{I_{OCO}} = I_{OCO}(2056.18) / I_{OCO}(2040.16)$. The signal at 2056.18 nm is strongly attenuated by carbon dioxide absorption, whereas the attenuation of the signal at 2040.16 nm is less. Figure 4.8 (middle panel) shows $X_{I_{OCO}}$ as a function of the scattering layer height for different types of scatterers, and at different surface albedos. It is shown that the radiance ratio $X_{I_{OCO}}$ is sensitive to changes of the scattering layer height. In this band $X_{I_{OCO}}$ also depends strongly on the surface albedo, the aerosol microphysics, and aerosol or cirrus cloud layer height. The radiance ratio change $\delta X_{I_{OCO}}$ due to changes of the scattering layer

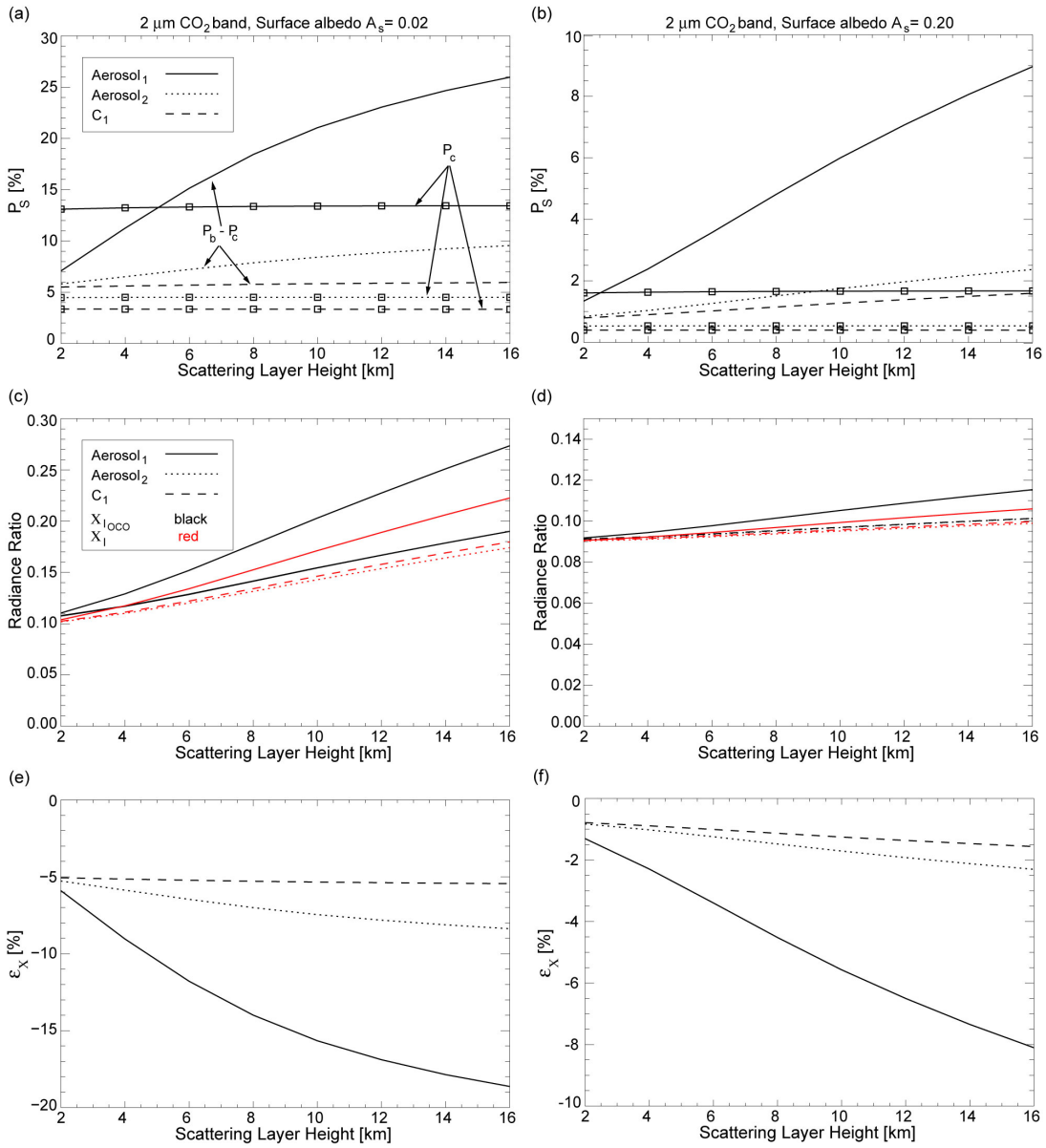

Figure 4.8: Degree of linear polarization of the reflected radiation in the strong CO_2 band around 2060 nm as function of the scattering layer height for different types of scatterers. The solar zenith angle is $\theta_0 = 65^\circ$ and the viewing zenith angle is $\theta = 0^\circ$ (nadir). The optical thickness of the scattering layer is 0.049. The curves marked with boxes indicate the continuum polarization, P_c, selected at 2040.16 nm, while the unmarked curves show the difference between band and continuum polarization $P_b - P_c$. P_b was selected at 2056.18 nm. (a) Surface albedo A_s = 0.02. (b) Surface albedo A_s = 0.20. Middle panel: Radiance ratio $X_{I_{OCO}} = I_{OCO}(2056.18)/I_{OCO}(2040.16)$ as a function of scattering layer height for different types of scatterers in the strong CO_2 band (solar zenith angle $\theta_0 = 65^\circ$; viewing angle $\theta = 0^\circ$, and $\tau_{scat} = 0.049$). The red lines show X_I using the scalar approximation and the black lines show $X_{I_{OCO}}$. (c) Surface albedo A_s = 0.02. (d) Surface albedo A_s = 0.20. Bottom panel: Relative radiance ratio difference ε_X as a function scattering layer height. (e) Surface albedo A_s = 0.02. (f) Surface albedo A_s = 0.20.

height at different surface albedos is shown in Table 4.5. For a surface albedo of A_s = 0.02 the radiance ratio shows a high sensitivity within the CO_2 band at 2060 nm to changes of the scattering layer height, while in case of A_s = 0.20 the sensitivity is less as compared to the O_2A band. In addition to the O_2A band, the CO_2 band can provide additional information on the vertical distribution of scatterers in the atmosphere. The bottom panel of Fig. 4.8 shows the relative radiance ratio difference ε_X as a function of the scattering layer height. As in case of the O_2A band and the CO2 band at 1610 nm we see that ε_X mirrors the behavior of the polarization in the band.

Table 4.5: Sensitivity of the radiance ratio $X_{I_{OCO}}$ to changes of the scattering layer height in the CO_2 band around 2060 nm. The height indicates the top of the scattering layer.

	$\delta X_{I_{OCO}}$ (Aerosol$_1$) [%]		$\delta X_{I_{OCO}}$ (Aerosol$_2$) [%]		$\delta X_{I_{OCO}}$ (C$_1$) [%]	
Height [km]	$A_s = 0.02$	$A_s = 0.20$	$A_s = 0.02$	$A_s = 0.20$	$A_s = 0.02$	$A_s = 0.20$
2-4	16.95	2.85	8.76	1.17	8.74	1.18
4-6	17.76	3.55	9.94	1.59	9.88	1.54
6-8	16.70	3.80	10.01	1.75	9.95	1.69
8-10	14.46	3.70	9.19	1.72	9.14	1.68
10-12	12.03	3.36	8.00	1.59	7.96	1.56
12-14	10.37	3.12	7.16	1.50	7.13	1.48
14-16	8.96	2.90	6.36	1.406	6.34	1.38

4.6 Conclusions

We studied the influence of scattering layer height, microphysics and surface albedo on TOA polarization and intensity in oxygen and carbon dioxide absorption bands. As scatterers we use aerosols as well as cirrus clouds.

Inside the O_2A band and the strong CO_2 band at 2060 nm we find a strong influence of the scattering layer height on the degree of linear polarization. An increase of the scattering layer height can lead either to a decrease or increase of the polarization within the band, depending on the microphysical and optical properties of the scatterers, as well as the surface albedo and absorption strength in the bands. Inside the weaker CO_2 band at 1610 nm the polarization influence is lower as compared to the O_2A band and the CO_2 band at 2060 nm, due to the relatively stronger influence of surface reflection and due to an increase

of aerosol multiple scattering by means of weaker absorption. Here an increase of scattering layer height leads to an increase of the degree of linear polarization even in case of a low surface albedo of 0.02 and weakly polarizing scatterers.

The radiance ratio $X_{I_{OCO}}$ inside the O_2A band and the strong CO_2 band at 2060 nm shows a high sensitivity to variations of the aerosol of cirrus cloud layer height. This indicates that aerosol or cirrus cloud layer height could be retrieved from these measurements. Even for a surface albedo of 0.20 the sensitivity to aerosol or cirrus cloud layer heights remains high for all cases considered here, which should allow a better estimation of scattering layer heights than in case of current instruments such as POLDER or MERIS.

Furthermore we analyze the differences of the radiance ratio between observations made by unpolarized instruments (e.g. MERIS), and OCO-like instruments in these bands.

Inside the weak CO_2 band at 1610 nm we show the radiance ratio changes $\delta X_{I_{OCO}}$ from a Rayleigh atmosphere for a 1% increase of the total column CO_2 and for an inclusion of aerosol layers or cirrus clouds at different surface albedos. We show that the inclusion of scatterers (aerosols or ice-crystals) can result in either an underestimate or an overestimate of total column CO_2, depending on the microphysical and optical properties of the scatterer, the absorption strength, and the surface albedo. Our results support findings reported by O'Brien and Rayner (2002), who show an underestimate of CO_2 due to scattering, and with the findings of Mao and Kawa (2004), who show an overestimate. Although there are several differences in the simulated conditions, Kawa and Mao already indicate that the high surface albedo of 0.3, used for their simulations, is the main cause for the differences between their results and the ones of O'Brien and Rayner. This could also be confirmed by Houweling et al. (2005), who shows an underestimation as well as an overestimation of CO_2 depending on the surface albedo.

The radiance ratio $X_{I_{OCO}}$ in the weak CO_2 band is sensitive to the scattering layer height and an increase of the scattering layer height leads to a strong underestimation of column CO_2 (shortening of the overall path-length of the sunlight). The radiance ratio change $\delta X_{I_{OCO}}$ due to an increase of the scattering layer from 2 to 4 km for instance is between 1.09% and 1.60% at A_s = 0.02, while the radiance ratio change from a Rayleigh atmosphere for a 1% perturbation of the total column CO_2 is around -0.23%. Thus the scattering layer height effect

has to be accounted for when estimating the total column CO_2. The bias is stronger for low surface albedos, as the influence of the surface-reflected components is lower. An increase of surface albedo leads to a decrease of the scattering layer height influence on $X_{I_{OCO}}$. Moreover the sensitivity of the radiance ratio to an increase of column CO_2 decreases with increasing scattering layer height, which also strongly depends on the surface albedo.

Ignoring polarization in simulations of backscatter measurements by space-based instruments such as OCO, leads to an overestimation of total column CO_2. This effect can be larger than the change caused by a 1% increase of total column CO_2, especially in cases of low surface albedo (A_s = 0.02) the error can be between -0.4% and -2.4%. [Natraj et al., 2007] evaluated the errors from ignoring polarization in analyzing spectroscopic measurements using OCO as a test case. Their analysis was carried out using the OCO Level2 algorithm [Kuang et al., 2002] and for different viewing geometries, surface reflectances and aerosol loadings and a fixed vertical distribution of aerosols in the atmosphere. They showed that the error can be as high as 10ppm. Our study shows that the error caused by neglecting polarization is also sensitive to the scattering layer height, especially for low surface albedos, and strongly polarizing scatterers. Compared to the O_2A band and the CO_2 band at 2060 nm we find a strong increase of ε_X with increasing scattering layer height. Because of the weaker absorption in the CO_2 band at 1610 nm, multiple scattering increases, and the influence of surface reflection is stronger. This leads to an increase of the degree of linear polarization in the band with increasing scatting layer height, while the continuum polarization remains unchanged. This results in an increase of ε_X with increasing scattering layer height.

The uncertainties induced by a poor determination of the height of atmospheric scatterers, their microphysical properties and due to ignoring polarization in simulations of backscattered measurements by space-based instruments such as OCO can cause large errors in the total column CO_2 estimation. These factors have to be accounted for to achieve a high accuracy in the total column CO_2 estimation as desired for OCO.

Chapter 5

Summary and Outlook

5.1 Summary

In this thesis aerosol microphysical and optical properties are studied by means of polarization observations and simulations of reflected or transmitted skylight in the continuum and in gaseous absorption bands, such as the O_2A band or carbon dioxide bands. The aerosol properties considered are aerosol optical thickness, aerosol layer altitude, aerosol refractive index, and aerosol size distribution. The presented work contributes to a better understanding of aerosol properties and their influence on radiation and polarization in the continuum and within gaseous absorption bands.

In Chapter 2 we study the influence of aerosol microphysical and optical parameters on the degree of linear polarization of diffusely transmitted skylight in the continuum. This study mainly focuses on the first research question (see Section 1.7 of Chapter 1). We use monochromatic multiple scattering calculations, including polarization, for vertically inhomogeneous atmospheres. Based on an extensive sensitivity study we identify the aerosol parameters with the strongest influence on the degree of linear polarization in the continuum, namely the fine mode of the aerosol size distribution (the median radius and geometric standard deviation), the real part of the aerosol refractive index, and the aerosol

optical thickness. We classify the aerosol properties according their impact on the degree of linear polarization.

From multispectral and multiangle polarization measurements at clear and hazy sky conditions in Cabauw, the Netherlands, we derive microphysical aerosol parameters by comparing the calculated degree of polarization with the measured degree of polarization. The derived aerosol size distribution in Cabauw is shown to be bimodal and the aerosols are weakly to nonabsorbing. The difference between the model fits and the polarization measurements is within the range of the measurement accuracy of the polarization spectrometer (~1%). The retrieved aerosol parameters are in accordance with aerosol climatology data derived from AERONET and can be classified as urban/industrial aerosol types. It appears that the retrieval of some parameters using only polarization observations, such as the imaginary part of the refractive index, remains ambiguous due to multiple solutions. Furthermore we found that it is necessary for a retrieval of aerosol parameters from polarization measurements to analyse the whole viewing zenith angle.

With the knowledge of the aerosol properties that can occur at clear and hazy sky conditions in the surroundings of an urban/industrial measurement location, we focus in Chapter 3 on the analysis of the aerosol altitude, aerosol microphysics, and aerosol optical thickness influences on the degree of linear polarization of the zenith skylight in the spectral region of the O_2A band. This study mainly focuses on the second research question (see Section 1.7 of Chapter 1). It is motivated by several ground-based observations of the degree of linear polarization of skylight in the O_2A band, taken by Stammes et al. (1994), Preusker et al. (1995) and Aben et al. (1997), which did not have a quantitative explanation yet. These measurements showed that in the O_2A band the degree of linear polarization can be larger or smaller than in the continuum. To adequately study the effect of aerosol altitude on polarization of skylight in the O_2A band we combine two existing radiative transfer methods to significantly improve the calculation time, while maintaining a high accuracy compared to line-by-line simulations. As a spectral approximation technique we use the k-binning method. We integrate this method in monochromatic doubling-adding multiple scattering calculations, including polarization, for vertically inhomogeneous atmospheres. Compared to line-by-line simulations of the O_2A band the combined method is around 54 times faster and the error in reflected and transmitted radiances is smaller than 3.1%, whereas in the degree of linear polarization the error is smaller than 0.31% for reflected light and smaller than 0.11% for

transmitted light. In case of a pure molecular atmosphere the polarization in the O_2A band is higher than in the continuum. If aerosols are added, our study shows that in general an increase of aerosol altitude causes a decrease of the degree of linear polarization inside the O_2A band. The observed case of a lower degree of polarization in the oxygen absorption band than in the continuum occurs for two cases. First, this effect occurs if the atmosphere contains besides Rayleigh scatterers and the absorbing O_2 molecules an elevated scattering layer at high altitude, containing weakly polarizing aerosols or cirrus clouds. This case is not likely to occur since in general there are also aerosols in the boundary layer of the atmosphere. Second, this effect occurs if we include strongly polarizing aerosols in the boundary layer and weakly polarizing aerosols or cirrus clouds in an elevated layer. This case is more likely to occur in the atmosphere. In all the other combinations, e.g. the same type of aerosol located in the boundary and in the elevated layer, or weakly polarizing aerosol in the boundary layer and strongly polarizing in the elevated layer, the degree of polarization in the oxygen absorption band remains higher than in the continuum. In case of weakly polarizing aerosol in the boundary layer and strongly polarizing in the elevated layer we can even find an increase of the degree of polarization in the band with increasing altitude of the elevated layer. We may tentatively conclude that a retrieval of the aerosol profile from ground-based measurements of the zenith sky polarization in the O_2A band region, without additional information on the microphysical aerosol properties and optical thickness, seems too ambitious in case of multiple aerosol layers. Only in case of a single aerosol layer a determination of the aerosol layer altitude may be obtained. The detection of the presence of a second aerosol or ice crystal layer from polarization measurements might be possible as well. Polarization measurements at a high-altitude site or airborne measurements might offer altitude information on aerosols or sub-visible cirrus in the upper troposphere.

Based on the study of the aerosol altitude influence on the degree of linear polarization of transmitted skylight inside the O_2A band, we analyse in Chapter 4 the influence of aerosol altitude, aerosol microphysics and surface albedo on top-of-atmosphere reflected radiance and polarization spectra in the O_2A band, the weak CO_2 band at 1610 nm, and the strong CO_2 band at 2060 nm. This study mainly focuses on the third and fourth research questions (see Section 1.7 of Chapter 1). For the study we use the previously developed combined method for fast radiative transfer simulation in absorption bands. The simulations were performed using spectral response functions which are representative for the Orbiting Carbon Observatory (OCO) satellite, which will be launched in 2008. Inside the O_2A band

and the CO_2 band at 2060 nm we find a large influence of the (aerosol/cirrus cloud) scattering layer altitude on the degree of linear polarization due to the strong gaseous absorption. An increase in scattering layer altitude can lead to a decrease or increase of the polarization within the bands, depending on the microphysical and optical properties of the scatterers, as well as on the surface albedo and viewing geometry. This is caused by different paths taken by the scattered and reflected light. The radiance ratio X (radiance in the band / radiance in the continuum) for the O_2A band and CO_2 band at 2060 nm shows a high sensitivity to the scattering layer altitude and allows an estimation of the altitude of scatterers. The assumed spectral resolution $(\lambda/\Delta\lambda)$ of >17000 for the O_2A-band and >20000 for both of the CO_2 bands offers a high radiance sensitivity and we may tentatively conclude that this leads to a higher accuracy of the estimation of the altitude of scatterers. Even for higher surface albedos the decrease of the scattering layer altitude sensitivity is low for the cases under consideration, thus allowing a much better estimation over land than in case of POLDER or MERIS. Furthermore we show that a neglect of polarization in radiative transfer calculations for OCO can lead to substantial errors in the estimation of column CO_2. For the weaker CO_2 band at 1610 nm the influence of the surface reflected intensity components contributing to the top-of-atmosphere is strong. The weak absorption and the accompanied weak shielding of lower layers of the atmosphere allows more multiple scattering in the absorption band as compared to the stronger CO_2 band at 2010 nm or the O_2A band. An increase of the scattering layer altitude at 1610 nm increases the band polarization inside the weak CO_2 band for all types of scatterers. The neglect of polarization in the estimation of column CO_2 biases the estimation of column CO_2 high. In case of low a surface albedo the bias is larger than the change caused by a 1% increase in CO_2 absorption and the bias increases with increasing scattering layer altitude. For higher surface albedos the bias due to neglect of polarization in the estimation of column CO_2 is lower, but still can exceed the change caused by a 1% increase of CO_2 absorption. Furthermore we find that scatterers in the atmosphere can lead to both, an underestimate and an overestimate of column CO_2, depending on the microphysical and optical properties of the scatterers, and the surface albedo. We also show that a poor determination of the scattering layer altitude strongly biases the estimation of column CO_2, especially in case of a low surface albedo. Thus, the possibility to detect a 1% change in CO_2 absorption is hindered if polarization is neglected and if the retrieval of the vertical structure of atmospheric scatterers is inaccurate.

5.2 Outlook

Multispectral and multiangle polarization measurements of transmitted and reflected skylight offer a unique way to retrieve aerosol microphysical and optical properties. Yet, polarization measurements alone are not the ultimate solution. Especially in the presence of multiple layers it proves difficult to derived parameters such as the aerosol layer height without additional information on the microphysical aerosol properties and optical thickness, as shown in Chapter 3. In combination with other methods such as sunphotometry, light detection and ranging (LIDAR) and radiance measurements, skylight polarimetry is a very accurate and versatile method.

From simulations and measurements of the polarization of skylight in the continuum, we find that it is not sufficient to measure the degree of linear polarization at a single viewing angle in the principal plane, e.g. 90° from the sun. As shown in Chapter 2, it is necessary for a reliable estimation of aerosol properties to find an agreement between the simulated and the measured polarization in the principal plane at the forward-scattering direction, at the backscattering direction, and at the maximum. This better constraints the retrieval of aerosol microphysical properties.

As shown in Chapter 3 and 4, it is necessary to include the effect of aerosol altitude in simulations of top-of-atmosphere radiance and polarization spectra in absorption bands. Due to the influence of aerosol altitude and other aerosol properties on the degree of polarization inside gaseous absorption bands, which are generally unknown, polarization sensitive spectrometers may yield incorrect values for retrievals of e.g. carbon dioxide, oxygen or water vapour. An estimation of aerosol height from ground-based polarization measurements in the O_2A band seems only possible in the presence of a single aerosol layer within the atmosphere. In the presence of two scattering layers it seems ambiguous to derive altitude information of an elevated aerosol layer from ground-based polarization observations. Still these measurements can enable the detection of cirrus clouds. However, in case of top-of-atmosphere polarization observations the influence of the boundary layer aerosol is minor and these observations may allow an estimation of multiple layer altitudes, if the aerosol microphysical properties are known. Furthermore this study should be extended to irregular shaped and absorbing aerosols, such as dust and soot particles.

Based on this study, in combination with earlier work [Cairns et al., 1997], [Dubovik and King, 2000], [Vermeulen et al., 2000], [Dubovik, 2004] a retrieval algorithm should be developed to automatically retrieve aerosol properties from multispectral and multiangle polarization observations of skylight in the continuum and in gaseous absorption bands. The presented combined method for fast radiative transfer simulations in absorption bands including polarization was shown to be able to significantly improve the feasibility of extensive studies of the influence of aerosol properties in gaseous absorption bands. It should be used to extend the study presented in this thesis (Chapter 4) to analyse the impact of clouds on top-of-atmosphere polarization observations in the oxygen and carbon dioxide bands. Nevertheless this method is still too slow for efficient retrievals of large amounts of data. The time-consuming part of the retrievals is the computation of the atmospheric transmission and reflection with the doubling-adding method. This could be improved by pre-calculated look-up-tables, optimal estimation techniques or a neural network approach.

Zusammenfassung

Diese Doktorarbeit befasst sich mit dem Einfluss von Aerosolteilchen auf die Polarisation atmosphärischen Streulichtes im Kontinuum und in Gas-Absorptionsbanden. Spektral- und winkelabhängige Messungen des Polarisationsgrades atmosphärischen Streulichtes liefern qualitative hochwertige Erkenntnisse über Eigenschaften von Aerosolteilchen wie den Brechungsindex, multimodale Größenverteilung, oder den Aerosoltyp. Polarisationsmessungen sind zum Teil sensitiver gegenüber Aerosoleigenschaften als reine Strahlungsmessungen und beinhalten somit wertvolle Informationen über Aerosole [Mishchenko et al, 1997].

Aerosole sind feste oder flüssige Schwebteilchen, suspendiert in Luft. Aerosole können durch natürliche Vorgänge in die Atmosphäre gelangen, wie zum Beispiel durch Vulkanausbrüche oder infolge von Aufwirbelung fester Teilchen durch Wind. Des Weiteren kann der Eintrag von Partikel in die Atmosphäre durch menschliche (anthropogene) Aktivitäten, wie die Verbrennung fossiler Brennstoffe, verursacht werden. Die Verweildauer von Aerosolteilchen liegt in der Regel zwischen Stunden und Tagen und hängt entscheidend von ihrer Größe ab. Der erwärmende Einfluss anthropogener Treibhausgase auf unser Klima, wie zum Beispiel Kohlendioxid (CO_2), ist seit langem bekannt. Der klimabeeinflussende Effekt der Aerosole hingegen, ist erst seit den 1990er Jahren verstärkt in den Fokus der Forschung getreten. Im Gegensatz zu den langlebigen und global gesehen gut durchmischten Treibhausgasen, sind Aerosole, aufgrund ihrer kurzen Lebensdauer,

regional sehr unterschiedlich verteilt. Die horizontale wie auch vertikale Verteilung von Aerosolen, kann sich durch regionale Wetterbedingungen schnell verändern. Des Weiteren können chemische Prozesse die Eigenschaften von Aerosolen stark verändern.

Aerosole beeinflussen unser Klima auf unterschiedliche Weise. Im Allgemeinen werden der direkte und der indirekte Effekt von Aerosolen auf den Strahlungshaushalt und das Klima unterschieden. Der direkte Aerosol-Effekt beruht darauf, dass Aerosolteilchen einen Teil der solaren Strahlung wieder in den Weltraum reflektieren. Dies hat einen kühlenden Effekt auf das Klima. Der direkte Effekt umfasst aber auch den Einfluss absorbierender Aerosole, wie zum Beispiel Rußpartikel. Durch Absorption wird die umgebende Atmosphäre erwärmt, aber die bodennahen Luftschichten abgekühlt. Der indirekte Effekt basiert auf dem Einfluss der Aerosole auf die Wolkenbildung. Veränderungen der Anzahl und Zusammensetzung von Aerosolen, die als Nukleationskeime dienen, beeinflussen die optische Dicke, die Albedo (Reflexion) und die Lebensdauer von Wolken und nehmen somit auch Einfluss auf den Niederschlag. Der Netto-Effekt des direkten und indirekten Aerosol-Einflusses auf das Klima ist aller Wahrscheinlichkeit nach negativ bzw. abkühlend. Es ist schwierig den Einfluss von Aerosolen auf unser Klima quantitativ zu erfassen. Das wissenschaftliche Verständnis des Aerosoleffektes wird laut dem *Intergovernmental Panel on Climate Change* (IPCC) als "mittel bis gering" eingestuft und es besteht großer Forschungsbedarf, um den Aerosoleffekt auf unser Klima, besser bestimmen zu können [Forster et al., 2007].

In dieser Arbeit werden drei Forschungsschwerpunkte behandelt. Der erste Forschungsschwerpunkt (Kapitel 2) richtet sich auf ein besseres Verständnis von Aerosoleigenschaften die vorherrschend sind in Cabauw, Niederlande. Cabauw befindet sich in einer urbanen Region, mit moderatem Einfluss von der Nordsee. Mittels Strahlungstransportsimulationen, unter Berücksichtigung von Polarisation, wird der Einfluss mikrophysikalischer und optischer Aerosoleigenschaften auf den Polarisationgrad untersucht. Ausgehend von dieser Studie, wird der Einfluss der wichtigsten Aerosoleigenschaften auf den Polarisationsgrad klassifiziert. Anhand von Polarisationsmessungen an Tagen mit geringer und starker Aerosolbelastung in Cabauw, Niederlande, werden mikrophysikalische Aerosoleigenschaften abgeleitet. Dies geschieht mittels Vergleich zwischen Messungen und Modellberechnungen. Im Hinblick auf den Aerosol-Brechungsindex und der Größenverteilung, zeigen die Aerosolmessungen in Cabauw Übereinstimmung mit

Aerosolklimatologien, berechnet anhand von langjährigen Messungen des *Aerosol Robotic Network* (AERONET) und können als urban/industriell eingestuft werden.

Mit Kenntnis über die Aerosoleigenschaften, die an klaren und trüben Tagen in dieser Region auftreten, richtet sich der zweite Forschungsschwerpunkt (Kapitel 3) auf den Einfluss der vertikalen Verteilung von Aerosolen, den Einfluss mikrophysikalischer Eigenschaften von Aerosolen und den Einfluss der Aerosol-optischen Dicke auf den linearen Polarisationsgrad des transmittierten Lichtes im Spektralbereich der Sauerstoff A-Absorptionsbande. Diese Studie ist motiviert durch Messungen des linearen Polarisationgrades transmittierten Lichtes in der Sauerstoff A-Bande, durchgeführt von Stammes et al. (1994), Preusker et al. (1995) und Aben et al. (1997). Die Messungen zeigen, dass der Polarisationsgrad innerhalb der Absorptionsbande sowohl größer als auch kleiner sein kann, als der Polarisationsgrad im Kontinuum. Kapitel 3 beschäftigt sich eingehend mit der Frage, unter welchen Umständen dieser Effekt auftreten kann und welche Aerosolinformationen daraus abgeleitet werden können. Ausgehend von einer Rayleigh-Atmosphäre, die unter anderem Sauerstoffmoleküle und eine einzelne Aerosolschicht enthält, kann gezeigt werden, dass eine Anhebung der Aerosolschicht eine Abnahme des Polarisationsgrades in der Absorptionsbande hervorruft. Die Stärke dieser Abnahme ist abhängig von den mikrophysikalischen Aerosoleigenschaften und der Aerosol-optischen Dicke. Die Polarisation im Kontinuum hingegen bleibt unverändert. Fügt man eine weitere Aerosolschicht in Bodennähe hinzu, so nimmt die Sensitivität des Polarisationsgrades gegenüber Höhenveränderungen der Aerosolschicht ab. Der beobachtete Fall eines geringeren Polarisationsgrades in der Absorptionsbande, gegenüber der Polarisation im Kontinuum, zeigt sich für zwei Fälle. Erstens im Falle einer einzelnen schwach polarisierenden Aerosolschicht in großer Höhe. Es ist jedoch unwahrscheinlich, dass kein Aerosol in Bodennähe anzutreffen ist. Zweitens im Falle von stark polarisierendem Aerosol in Bodennähe und einer schwach polarisierenden Aerosolschicht in größerer Höhe. Auch im Falle einer schwach polarisierenden Zirruswolke in großer Höhe zeigt sich dieser Effekt. Polarisationsmessungen in Absorptionsbanden enthalten Information über Aerosolhöhen. Im Falle von mehreren Aerosolschichten in der Atmosphäre zeigt es sich jedoch, dass es kaum möglich ist, aus bodengestützten Polarisationsmessungen die Höhe von Aerosolen abzuleiten, da der Einfluss des bodennahen Aerosols sehr ausgeprägt ist. Es fehlt Information über die unterschiedlichen Aerosoleigenschaften in verschiedenen Höhen und gerade diese Information ist notwendig im Fall von mehreren Aerosolschichten. Im Falle einer einzelnen Aerosolschicht ist eine

Bestimmung der Schichthöhe jedoch möglich. Strahlungstransportsimulationen in Absorptionsbanden, unter Berücksichtigung des Polarisationszustandes, sind sehr rechenintensiv. Für umfangreiche Studien ist es demnach wichtig, den Rechenaufwand zu reduzieren und gleichzeitig eine hohe Genauigkeit beizubehalten. Für diesen Zweck werden zwei bestehende Methoden kombiniert. Als spektrale Approximationstechnik wird die k-binning Methode benutzt. Diese wird mit monochromatischen Strahlungstransportsimulationen, beruhend auf der doubling-adding Methode für Mehrfachstreuungen, unter Berücksichtigung von Polarisation, kombiniert. Verglichen mit sehr präzisen line-by-line Berechnungen zeigt sich, dass diese Methode in den vorliegenden Simulationen ungefähr 54-mal schneller ist und dabei eine Ungenauigkeit bei der Berechnung von reflektierter und transmittierter Strahlung aufweist, die kleiner ist als 3.1%. Im Fall von Polarisationsberechnungen für reflektiertes Licht liegt diese Ungenauigkeit unter 0.31% und für transmittiertes Licht unter 0.11%.

Ausgehend von der vorangegangenen Studie, richtet sich der dritte Forschungsschwerpunkt (Kapitel 4) auf den Einfluss der vertikalen Verteilung von Aerosolen, den Einfluss mikrophysikalischer Eigenschaften von Aerosolen und den Einfluss der Bodenalbedo auf den linearen Polarisationsgrad reflektierten Lichtes im Spektralbereich der Sauerstoff A-Bande, der schwachen Kohlendioxidbande bei 1.610 nm und der starken Kohlendioxidbande bei 2.060 nm. Polarisationsmessungen reflektierten Lichtes in der Sauerstoff A-Bande, sowie in der starken Kohlendioxidbande, weisen, wie im vorangegangenen Kapitel, Aerosolhöheninformation auf. Hier zeigt sich, dass der Einfluss bodennahen Aerosols eine geringere Rolle spielt. Des Weiteren wird der Einfluss einer Vernachlässigung von Polarisation in Modellsimulationen auf die Abschätzung von Kohlendioxidkonzentrationen oder der vertikalen Verteilung von Aerosolen untersucht. Zudem richtet sich das Interesse auf die *Orbiting Carbon Observatory* (OCO) Satellitenmission der *National Aeronoutics and Space Administration* (NASA) [Crisp et al., 2004]. OCO liefert Daten über das atmosphärische Kohlendioxid, dem bedeutendsten anthropogenen Antriebsfaktor für den Klimawandel. Im Zusammenwirken mit Bodenmessungen erwartet man Aufschlüsse über natürliche und anthropogene Kohlendioxid-Quellen und -Senken. Veränderungen in der Kohlendioxidkonzentration sollen mit einer Genauigkeit von etwa 0.3% erfasst werden können. Wir untersuchen, welchen Einfluss die vertikale Verteilung von Aerosolen, mikrophysikalische Aerosoleigenschaften und Bodenalbedo auf die Abschätzung der Kohlendioxidkonzentration haben. Es zeigt sich, dass die Vernachlässigung von Polarisation

in Strahlungstransportsimulationen zu einer Überschätzung der abzuleitenden Kohlendioxidkonzentration führt. Dieser Effekt ist größer als die beabsichtigte Messgenauigkeit von etwa 0.3%, und wird mit zunehmender Höhe des Aerosols größer. Aerosole oder Zirruswolken in der Atmosphäre, können zu einer Über- oder Unterschätzung der Kohlendioxidkonzentration führen, abhängig von den mikrophysikalischen und optischen Eigenschaften der Streuer sowie der Bodenalbedo. Des Weiteren zeigen wir, dass eine ungenaue Bestimmung der vertikalen Schichtung von Streuern in der Atmosphäre die Abschätzung der Kohlendioxidkonzentration stark beeinflusst.

Bibliography

Abel S. J., Highwood, E. J., Haywood, J. M., and Stringer, M. A., “The direct radiative effect of biomass burning aerosols over southern Africa,” Atmos. Chem. Phys. **5**, 1999-2018 (2005).

Aben I., F. Helderman, D. M. Stam and P. Stammes, “Spectral fine-structure in the polarisation of skylight”, Geophys. Res. Lett. **26**, 591-594 (1999).

Aben I., F. Helderman, D. M. Stam, and P. Stammes, “High-spectral resolution polarization measurements of the atmosphere with the GOME-BBM,” Polarization: Measurement, Analysis, and Remote Sensing, Proceedings SPIE **3121**, 446-453 (1997).

Ackerman A. S., O. B. Toon, J. P. Taylor, D. W. Johnson, P. V. Hobbs, and R. J. Ferek, “Effects of aerosols on cloud albedo: Evaluation of Twomey’s parameterization of cloud susceptibility using measurements of ship tracks,” J. Atmos. Sci. 57, 2684-2695 (2000).

Albrecht B., “Aerosols, cloud microphysics and fractional cloudiness,” Science **245**, 1227–1230 (1989).

Barnaba F., and G. P. Gobbi, “Lidar estimation of tropospheric aerosol extinction, surface area, and volume: maritime and desert-dust cases,” J. Geophys. Res. **106**, 3005-3018 (2001).

Bates T. S., Anderson, T. L., Baynard, T., Bond, T., Boucher, O., Carmichael, G., Clarke, A., Erlick, C., Guo, H., Horowitz, L., Howell, S., Kulkarni, S., Maring, H., McComiskey, A., Middlebrook, A., Noone, K., O'Dowd, C. D., Ogren, J., Penner, J., Quinn, P. K., Ravishankara, A. R., Savoie, D. L., Schwartz, S. E., Shinozuka, Y., Tang, Y., Weber, R. J., and Wu, Y., "Aerosol direct radiative effects over the northwest Atlantic, northwest Pacific, and North Indian Oceans: estimates based on in-situ chemical and optical measurements and chemical transport modeling," Atmos. Chem. Phys. **6**, 1657-1732 (2006).

Beaglehole D., and G. G. Carter, "Antarctic skies 2. Characterization of the intensity and polarization of skylight in a high albedo environment," J. Geophys. Res. **97**, 2597-2600 (1992).

Bellouin, N., O. Boucher, J. Haywood, and M. S. Reddy, "Global estimates of aerosol direct radiative forcing from satellite measurements," Nature **438**, 1138-1141 (2005).

Bennartz R., and R. Preusker, "k-binning: A new approach to simulate narrow band satellite channels in layered atmospheres with variable gas absorption," submitted to J. Quant. Spectrosc. Radiat. Transfer (2007).

Bennartz R., and R. Preusker, "Representation of the photon pathlength distribution in a cloudy atmosphere using finite elements," J. Quant. Spectrosc. Radiat. Transfer **98**, 202-219 (2006).

Bennartz R., and J. Fischer, "A modified k-distribution approach applied to narrow band water vapour and oxygen absorption estimates in the near infrared," J. Quant. Spectrosc. Radiat. Transfer **66**, 539-553 (2000).

Berthier S., P. Chazette, P. Couvert, J. Pelon, F. Dulac, F. Thieuleux, C. Moulin, and T. Pain, "Desert dust aerosol columnar properties over ocean and continental Africa from Lidar in-Space Technology Experiment (LITE) and Meteosat synergy," J. Geophys. Res. **111**, D21202 (2006).

Boesche E., P. Stammes, R. Preusker, R. Bennartz, W. H. Knap, J. Fischer, "Polarization of skylight in the O_2A band: effects of aerosol properties," Applied Optics **47**, 3467-3480 (2008).

Boesche E., P. Stammes, T. Ruhtz, R. Preusker, J. Fischer, “Effect of aerosol microphysical properties on polarization of skylight: sensitivity study and measurements,” Applied Optics **45**, 8790-8805 (2006).

Boesche E., Aufbau und Beschreibung eines Polarisations Spektrometers fuer die Fernerkundung der Atmosphaere,” in Radiation in Atmosphere and Ocean **23**, J. Fischer, ed. (Institute for Space Sciences, Free University of Berlin, 2003).

Bovensmann H., J. P. Burrows, M. Buchwitz, J. Frerick, S. Noel, V. V. Rozanov, K. V. Chance, and A. P. H. Goede, “SCIAMACHY: Mission objectives and measurement modes,” J. Atmos. Sci. **56**, 127-150 (1999).

Brenguier J.-L., H. Pawlowska, and L. Schueller, “Cloud microphysical and radiative properties for parameterization and satellite monitoring of the indirect effect of aerosol on climate,” J. Geophys. Res. **108**, 8632 (2003).

Brenguier J.-L., H. Pawlowska, L. Schueller, R. Preusker, J. Fischer, and Y. Fouquart, “Radiative properties of boundary layer clouds: droplet effective radius versus droplet concentration,” J. Atmos. Sci. **57**, 803-821 (2000).

Breon F.-M., J.-L. Deuzé, D. Tanre, and M. Herman, “Validation of spaceborne estimates of aerosol loading from sun photometer measurements with emphasis on polarization,” J. Geophys. Res. **102**, 17187-17195 (1997).

Burrows J. P., M. Weber, M. Buchwitz, V.V. Rozanov, A. Ladstädter-Weissenmayer, A. Richter, R. de Beek, R. Hoogen, K. Bramstedt, K.-U. Eichmann, M. Eisinger and D. Perner, “The Global Ozone Monitoring Experiment (GOME): Mission Concept and First Scientific Results,” J. Atm. Sci. **56**, 151-175 (1999).

Cairns B., E. E. Russell, and L. D. Travis, “Research scanning polarimeter: calibration and ground-based measurements,” in Polarization: Measurement, Analysis, and Remote Sensing II, D. H. Goldstein and D. B. Chenault, eds., Proc. SPIE **3754**, 186-196 (1999).

Cairns B., B. E. Carlson, A. A. Lacis, and E. Russell, “An analysis of ground-based polarimetric sky radiance measurements,” in Proceedings of the Seventh Atmospheric Radiation Measurement (ARM) Science Meeting, ARM-CONF-1997 (San Antonio, Tex.), 51–57 (1997).

Chamaillard K., S. G. Jennings, C. Kleefeld, D. Ceburnis, and Y. J. Yoon, “Light backscattering and scattering by nonspherical sea-salt aerosols,” J. Quant. Spectrosc. Radiat. Transfer **79-80**, 577-597 (2003).

Chandrasekhar S., *Radiative Transfer* (Dover, 1960).

Chandrasekar S. and D. Elbert, “The illumination and polarization of the sunlit sky on Rayleigh scattering,” Trans. Am. Phil. Soc. **44**, 643-728 (1954).

Chandrasekar S. and D. Elbert, “Polarization of the sunlit sky,” Nature **167**, 51-4 (1951).

Charlson R. J., S. E. Schwartz, J. M. Hales, R. D. Cess, J. E. Coakley, J. E. Hansen, and J. D. Hofmann, “Climate forcing by anthropogenic aerosols,” Science **255**, 423-430 (1992).

Chowdhary J. B., B. Cairns, M. I. Mishchenko, P. V. Hobbs, G. F. Cota, J. Redemann, K. Rutledge, Holben B.N., and E. Russell, “Retrieval of aerosol scattering and absorption properties from photopolarimetric observations over the ocean during the CLAMS experiment,” J. Atmos. Sci. 62, 1093-1117 (2005).

Coulson K. L., Polarization and Intensity of Light in the Atmosphere (Deepak Publ., 1988).

Crisp D., R. M. Atlas, F.-M. Breon, L. R. Brown, J. P. Burrows, P. Ciais, B. J. Connor , S. C. Doney, I. Y. Fung, D. J. Jacob, E. C. Miller, D. O'Brien, S. Pawson, J. T. Randerson, P. Rayner , R. J. Salawitch, S. P. Sander, B. Sen, G. L. Stephens, P. P. Tans, G. C. Toon, P. O. Wennberg, S. C. Wofsy, Y. L. Yung, Z. Kuang, B. Chudasama, G. Sprague, B. Weiss, R. Pollock, D. Kenyon, and S. Schroll, “The Orbiting Carbon Observatory (OCO) mission,” Advances in Space Research **34**, 700-709 (2004).

d’Almeida G. A., P. Koepke, and E. P. Shettle, eds. *Atmospheric Aerosols–Global Climatology and Radiative Characteristics*, (Deepak, 1991).

de Haan J. F., P. B. Bosma, and J. W. Hovenier, “The adding method for multiple scattering calculations of polarized light,” Astron. & Astrophys. **183**, 371-391 (1987).

de Haan J. W., “Effects of aerosols on the brightness and polarization of cloudless planetary atmospheres,” Ph.D. dissertation (Free University of Amsterdam, 1987).

de Rooij W. A., and C. C. A. H. van der Stap, “Expansion of Mie scattering matrices in generalized spherical functions,” Astron. & Astrophys. **131**, 237-248 (1984).

Deschamps P.-Y., F.-M. Bréon, M. Leroy, A. Podaire, A. Bricaud, J.-C. Buriez, and G. Seze, “The POLDER Mission: instrument characteristics and scientific objectives,” IEEE Trans. Geosci. Remote Sens. **32**, 598-615 (1994).

Deuzè J. L., P. Goloub, M. Herman, A. Marchand, G. Perry, S. Susana, and D. Tanre, “Estimate of the aerosol properties over the ocean with POLDER on ADEOS-1,” J. Geophys. Res. **105**, 15329-15346 (2000).

Deuzè J. L., F. M. Bréon, P. Y. Deschamps, C. Devaux, and M. Herman, “Analysis of the POLDER (POLarization and Directionality of Earth’s Reflectances) airborne instrument observations over land surfaces,” Remote Sens. Environ. **45**, 137-154 (1993).

Diner J. D., C. J. Bruegge, J. V. Martonchik, T. P. Ackerman, R. Davies, S. A. W. Gerstl, H. R. Gordon, P. J. Sellers, J. Clark, J. A. Daniels, E. D. Danielson, V. G. Duval, K. P. Klassen, G. W. Lilienthal, D. I. Nakamoto, R. Pagano, and T. H. Reilly, “MISR: A Multi-angle Imaging SpectroRadiometer for geophysical and climatological research from EOS,” IEEE Trans. Geosci. Remote Sens. **27**, 200-214 (1989).

Dubovik O., “Optimization of numerical inversion in photopolarimetric remote sensing,” in Photopolarimetry in Remote Sensing, G. Videen, Y. Yatskiv, and M. Mishchenko, eds. (Kluwer), 65-106 (2004).

Dubovik O., B. Holben, T. F. Eck, A. Smirnov, Y. J. Kaufman, M. D. King, D. Tanré, and I. Slutsker, “Variability of Absorption and Optical Properties of Key Aerosol Types Observed in Worldwide Locations,” J. Atmos. Sci. **59**, 590-608 (2001).

Dubovik O., A. Smirnov, B. N. Holben, M. D. King, Y. J. Kaufman, T. F. Eck, and I. Slutsker, “Accuracy assessments of aerosol optical properties retrieved from Aerosol Robotic Network (AERONET) Sun and sky radiance measurements,” J. Geophys. Res. **105**, 9791–9806 (2000a).

Dubovik O., and M. D. King, “A flexible inversion algorithm for retrieval of aerosol optical properties from Sun and sky radiance measurements,” J. Geophys. Res. **105**, 20673–20696 (2000b).

Duforet L., R. Frouin, and P. Dubuisson, “Importance and estimation of aerosol vertical structure in satellite ocean-color remote sensing,” Applied Optics **46**, Issue 7, 1107-1119 (2007).

Egan W. G., “Polarization in remote sensing,” in Polarization and Remote Sensing, W. G. Egan, ed., Proc. SPIE **1747**, 2-48 (1992).

Fitch B., and K. L. Couslon, “Polarizing radiometer measurements of skylight at South Pole Station, Antarctica,” in Optical Polarimetry: Instrumentation and Applications, R. M. A. Azzam and D. L. Coffeen, eds., Proc. SPIE **112**, 184-190 (1977).

Forster P., V. Ramaswamy, P. Artaxo, T. Berntsen, R. Betts, D.W. Fahey, J. Haywood, J. Lean, D.C. Lowe, G. Myhre, J. Nganga, R. Prinn, G. Raga, M. Schulz and R. Van Dorland, “Changes in Atmospheric Constituents and in Radiative Forcing,” In: Climate Change 2007: The Physical Science Basis. Contribution of Working Group I to the Fourth Assessment Report of the Intergovernmental Panel on Climate Change [Solomon, S., D. Qin, M. Manning, Z. Chen, M. Marquis, K.B. Averyt, M.Tignor and H.L. Miller (eds.)]. Cambridge University Press, Cambridge, United Kingdom and New York, NY, USA.

Gal J., G. Horvath, V. B. Meyer-Rochow and R. Wehner, “Polarization patterns of the summer sky and its neutral points measured by full-sky imaging polarimetry in Finnish Lapland north of the Arctic Circle,” Proc. R. Soc. A **457**, 1385-99 (2001).

Gerrard A., and J. M. Burch, *Introduction to Matrix Methods in Optics*, Dover Publications, New York (1994).

Hamazaki T, Y. Kaneko, A. Kuze,”Carbon dioxidemonitoring from the GOSAT satellite,” Int. Arch. Photogrammetry Remote Sensing Spat Inf Sci **35,** 225–7 (2004).

Hansen J. , M. Sato, A. Lacis, and R. Ruedy, “The missing climate forcing,” Philos. T. Roy. Soc. **352**, 231-240 (1997).

Haring R. E., R. Pollock, B. M. Sutin, and D. Crisp, “Development status of the Orbiting Carbon Observatory instrument optical design,” Optics & Photonics 2005, SPIE, San Diego, CA, USA, SPIE **5883** (2005).

Hasekamp O. P., J. Landgraf, and R. van Oss, “The need of polarization modeling for ozone profile retrieval from backscattered sunlight,” J. Geophys. Res. **107**, 4692 (2002).

Haywood J., and O. Boucher, “Estimates of the direct and indirect radiative forcing due to tropospheric aerosols: A review,” Rev. Geophys. **38**, 513 (2000).

Haywood J. M., and V. Ramaswamy, “Global sensitivity studies of the direct radiative forcing due to anthropogenic sulfate and black carbon aerosols,” J. Geophys. Res. **103**, 6043-6058 (1998).

Hess M., R. B. A. Koelemeijer, and P. Stammes, “Scattering matrices of imperfect hexagonal ice crystals,” J. Quant. Spectrosc. Radiat. Transfer **60**, 301-308 (1998).

Holben B. N., T. F. Eck, I. Slutsker, D. Tanré, J. P. Buis, A. Setzer, E. F. Vermote, J. A. Reagan, Y. J. Kaufman, T. Nakajima, F. Lavenu, I. Jankowiak, and A. Smirnov, “AERONET-A federated instrument network and data archive for aerosol characterization,” Remote Sens. Environ. **66**, 1-16 (1998).

Houghton J. T., Y. Ding, D. J. Griggs, M. Noguer, P. J. van der Linden, X. Dai, K. Maskell, and C. A. Johnson, eds., “Climate Change 2001: the Scientific Basis” (Cambridge U. Press, 2001).

Houghton J. T., L. G. Meira Filho, B. A. Callander, N. Harris, A. Kattenberg, and K. Maskell, eds., The Science of Climate Change (Cambridge U. Press), 1-572 (1995).

Houweling S., W. Hartmann, I. Aben, H. Schrijver, J. Skidmore, G.J. Roelofs, Evidence”of systematic errors in SCIAMACHY-observed CO2 due to aerosols,” Atmos Chem Phys **5**, 3003–13 (20005).

Hovenier J. W., C. Van der Mee, and H. Domke, *Transfer of Polarized Light in Planetary Atmospheres* (Kluwer, 2004).

Horvath G., B. Bernath, B. Suhai, Barta and R. A. Wehner, “First observation of the fourth neutral polarization point in the atmosphere,” J. Opt. Soc. Am. A 19, 2085-99 (2002).

Johnson B. T., K. P. Shine, and P. M. Forster, “The semi-direct aerosol effect: Impact of absorbing aerosols on marine stratocumulus,” Q. J. Roy. Meteor. Soc. 130, 1407-1422 (2004).

Joseph J. H., W. J. Wiscombe, and J. A. Weinman, “The Delta-Eddington approximation for radiative flux transfer,” J. Atmos. Sci. **33**, 2452-2459 (1976).

Kahn R. A., P. Banerjee, D. McDonald, and D. J. Diner, “Sensitivity of multiangle imaging to aerosol optical depth and to pure-particle size distribution and composition over ocean,” J. Geophys. Res. **103**, 32195-32238 (1998).

Kaufman Y. J., D. Tanre, D., and O. Boucher, “A satellite view of aerosols in the climate system,” Nature **419**, 215-223 (2002).

King M. D., Y. J. Kaufman, D. Tanre, and T. Nakajima, “Remote sensing of tropospheric aerosols from space: past present and future,” Bull. Amer. Meteorol. Soc. **80**, 2229-2259 (1999).

King M. D., Y. J. Kaufman, W. P. Menzel, and D. Tanre, “Remote sensing of cloud, aerosol, and water vapor properties from the Moderate Resolution Imaging Spectrometer (MODIS),” IEEE Trans. Geosci. Remote Sens. **30**, 2-27 (1992).

Knap W. H., L. C.-Labonnote, G. Brogniez, and P. Stammes, ”Modeling total and polarized reflectances of ice clouds: evaluation by means of POLDER and ATSR-2 measurements,” Applied Optics **44**, 4060-4073 (2005).

Koelemeijer R. B. A., J. F. de Haan, and P. Stammes, “A database of spectral surface reflectivity in the range 335–772 nm derived from 5.5 years of GOME observations,” J. Geophys. Res. **108**, 4070 (2003).

Koelemeijer R. B. A., P. Stammes, J. W. Hovenier, and J. F. de Haan, “A fast method for retrieval of cloud parameters using oxygen A band measurements from the global ozone monitoring experiment,” J. Geophys. Res. **106**, 3475-3490 (2001).

Kuang Z. J. S. Margolis, G. C. Toon, D. Crisp, Y. L. Yung, “Spaceborne measurements of atmospheric CO2 by high-resolution NIR spectrometry of reflected sunlight: an introduction study,” Geophys Res. Lett. **29**, 1716 (2002).

Kuze, A., and K. V. Chance, “Analysis of cloud top height and cloud coverage from satellite using the O2A and B bands,” J. Geophys. Res. **99**, 14481-14492 (1994).

Lacis A. A. and M. I. Mishchenko, “Climate forcing, climate sensitivity, and climate response: A radiative modelling perspective on atmospheric aerosols” in Aerosol Forcing of Climate, R. J. Charlson and J. Heintzenberg, eds. (Wiley, 1995).

Lacis A. A., and V. Oinas, “A description of the correlated-k distribution method for modeling nongray gaseous absorption, thermal emission, and multiple scattering in vertically inhomogeneous atmospheres,” J. Geophys. Res. 96, 9027-9064 (1991).

Lee R. L. Jr., “Digital imaging of clear-sky polarization,” Appl. Opt. **37**, 1465-76 (1998).

Ledley T. S., E. T. Sundquist, S. E. Schwartz, D. K. Hall, J. D. Fellows, and T. L. Killeen, “Climate change and greenhouse gases,” Eos Trans. Am. Geophys. Union **80**, 453-458 (1999).

Levelt P. F., E. Hilsenrath, G. W. Leppelmeier, G. H. J. van den Oord, P. K. Bhartia, J. Tamminen, J. F. de Haan and J. P. Veefkind, “Science Objectives of the Ozone Monitoring Instrument,” IEEE Trans. Geo. Rem. Sens. **44**, No. 5, 1199-1208 (2006).

Levy R. C., L. A. Remer, and Y. J. Kaufman, “Effects of neglecting polarization on the MODIS aerosol retrieval over land,” IEEE Trans. Geosci. Remote Sens. **42**, 2576-2583 (2004).

Liou, K. N., An Introduction to Atmospheric Radiation, 2nd ed., Vol. **84** of International Geophysics Series (Academic, 2002).

Lohman U., and J. Feichter, “Global indirect aerosol effects: a review,” Atmos. Chem. Phys. **5**, 715-737 (2005).

Lohman, U., and G. Lesins, “Stronger constraints on the anthropogenic indirect aerosol effect,” Science **298**, 1012-1016 (2002).

Lohman U., and J. Feichter, “Can the direct and semi-direct aerosol effect compete with the indirect effect on a global scale," Geophys Res Lett **28,** 159-161 (2001).

Mao J., and S. R. Kawa, “Sensitivity studies for space-based measurement of atmospheric total column carbon dioxide by reflected sunlight,” Applied Optics **43**, no 4, (2004).

Mishchenko M. I., B. Cairns, G. Kopp, C. F. Schueler, B. A. Fafaul, J. E. Hansen, R. J. Hooker, T. Itchkawich, H. B. Maring, and L. D. Travis, “Precise and accurate monitoring of terrestrial aerosols and total solar irradiance: introducing the Glory Mission,” BAMS (Bulletin of the American Meteorological Society) **88**, No 5, 677-691 (2007).

Mishchenko M. I., B. Cairns, J. E. Hansen, L. D. Travis, R. Burg, Y. J. Kaufman, J. V. Martins, and E. P. Shettle, “Monitoring of aerosol forcing of climate from space: analysis of measurement requirements,” J. Quant. Spectros. Rad. Trans. **88**, 149-161 (2004).

Mishchenko M. I., I. V. Geogdzhayev, L. Liu, J. A. Ogren, A. A. Lacis, W. B. Rossow, J. W. Hovenier, H. Volten, and O. Muñoz, “Aerosol retrievals from AVHRR radiances: Effects of particle nonsphericity and absorption and an updated long-term global climatology of aerosol properties,” J. Quant. Spectrosc. Radiat. Transfer **79-80**, 953-972 (2003).

Mishchenko M. I., and L. D. Travis, “Satellite retrieval of aerosol properties over the ocean using measurements of reflected sunlight: Effect of instrumental errors and aerosol absorption,” J. Geophys. Res. **102**, 13543-13553 (1997).

Mishchenko M. I., A. A. Lacis, B. E. Carlson, and L. D. Travis, “Nonsphericity of dustlike tropospheric aerosols: implications for aerosol remote sensing and climate modeling,” Geophys. Res. Lett. **22**, 1077-1080 (1995).

Mukai S., I. Sano, and T. Takashima, “Investigation of atmospheric aerosols based on polarization measurements and scattering simulations,” Opt. Rev. **3**, 487- 491, 1996.

Natraj V., R. J. D. Spurr, H. Bosch, Y. Jiang, and Y. L. Yung, “Evaluation of errors from neglecting polarization in the forward modelling of O_2A band measurements from space, with relevance to CO_2 column retrieval from polarization-sensitive instruments,” J. Quant. Spectros. Rad. Trans. **103**, 245-259 (2007).

O’Brien D. M., and P. J. Rayner: “Global observations of the carbon budget, 2, CO_2 column from differential absorption of reflected sunlight in the 1.61 μm band of CO_2,” J. Geophys. Res.**107**, 4354 (2002).

O’Brien D. M., R. M. Mitchell, S. A. English, and G. A. Costa, “Airborne measurements of air mass from O_2A band absorption spectra ,” J. Atmos. Ocean Technol. **15**, 1272-1286 (1998).

O'Brien D. M., and R. M. Mitchell, "Error estimates for retrieval of cloud-top pressure using absorption in the A band of oxygen," J. Appl. Meteorol. **31**, 1179-1192 (1992).

Penner J. E., et al., "Aerosols, their direct and indirect effects" in Climate Change 2001: The Scientific Basis: Contribution of Working Group I to the Third Assessment Report of the Intergovernmental Panel on Climate Change, edited by J. T. Houghton et al., chap. 5, 291-336, Cambridge Univ. Press, New York (2001).

Preusker R., U. Boetger, and J. Fischer, "Spectral and bidirectional measurements of the Stokes vector in the O_2A band and their interpretation," Atmospheric Sensing and Modelling II, Proceedings SPIE **2582**, 13-20 (1995).

Ramanathan V., P. J. Crutzen, J. T. Kiehl and D. Rosenfeld, "Aerosols, Climate, and The Hydrological Cycle," Science **294**, 2119-2124 (2001a).

Ramanathan V., et al., "Indian Ocean experiment: An integrated analysis of the climate forcing and effects of the great Indo-Asian haze," J. Geophys. Res. **106**, 28371–28398 (2001b).

Ramaswamy V., et al., "Radiative forcing of climate change," in Climate Change 2001: The Scientific Basis, J. T. Houghton et al., Eds., Cambridge University Press, 349-416.

Rao C. R. N., E. P. McClain, and L. L. Stowe, "Remote sensing of aerosols over the oceans using AVHRR data theory, practice, and applications," Int. J. Remote Sens. **10**, 743-749 (1989).

Rast M., and J. L. Bezy, "ESA Medium Resolution Imaging Spectrometer MERIS a review of the instrument and its mission," International Journal of Remote Sensing **20**, no 9, 1681-1702 (1999).

Rayleigh Lord J. W. S., "On the light from the sky, its polarization and colour," Phil. Mag. **61**, 107-20 and 274-9 (1871).

Rosenfeld D., and G. Feingold, "Explanation of discrepancies among satellite observations of the aerosol indirect effects," Geophys. Res. Lett. **30**, 1776 (2003).

Rothman L. S., A. Barbe, D. Chris Benner, L. R. Brown, C. Camy-Peyret, M. R. Carleer, K. Chance, C. Clerbaux, V. Dana, V. M. Devi , A. Fayt, J.-M. Flaud, R. R. Gamache, A. Goldman, D. Jacquemart, K.W. Jucks, W. J. Lafferty, J.-Y. Mandin, S. T. Massie, V. Nemtchinov, D. A. Newnham, A. Perrin, C.P. Rinsland, J. Schroeder, K. M. Smith, M. A. H. Smith, K. Tang, R.A. Toth, J. Vander Auwera, P. Varanasi, K. Yoshino, "The HITRAN molecular spectroscopic database: edition of 2000 including updates through 2001," J. Quant. Spectrosc. Radiat. Transfer **82,** 5-44 (2003).

Ruhtz T., E. Boesche, and J. Fischer, "Development of a new sensor module for hyperspectral polarimetric measurements," in Polarization Analysis and Measurement IV, D. H. Goldstein, D. B. Chenault, W. G. Egan, and M. J. Duggin, eds., Proc. SPIE **4481**, 242-246 (2002).

Sassen K, M. K. Griffin, and G. C. Dodd, "Optical scattering and microphysical properties of subvisible cirrus clouds, and climatic implications," J. Appl. Meteor. **28**, 91-98 (1989).

Seinfeld J. H., and S. N. Pandis, *Atmospheric Chemistry and Physics: From Air Pollution to Climate Change*, J. Wiley, New York (1998).

Sekera Z., "Light scattering in the atmosphere and the polarization of sky light," J. Opt. Soc. Am. **47**, 484-90 (1957).

Schollaert S. E., J. A. Yoder, J. E. O'Reilly, and D. L. Westphal, "Influence of dust and sulfate aerosols on ocean color spectra and chlorophyll a concentrations derived from SeaWiFS off the U.S. east coast," Journal of Geophysical Research **108,** 1-14 (2003).

Schulz F. M., K. Stamnes, and J. J. Stamnes, "Modeling the radiative transfer properties of media containing particles of moderately and highly elongated shape," Geophys. Res. Lett. **25**, 4481-4484 (1998).

Schutgens N. A. J., and P. Stammes, "Parameterization of Earth's polarization spectrum in the ultra-violet," J. Quant. Spectrosc. Radiat. Transfer **75**, 239-255 (2002).

Shurcliff W. A., *Polarized Light* (Harvard U. Press, 1962).

Stam D., J. F. De Haan, J. W. Hovenier, and P. Stammes, " A fast method for simulating observations of polarized light emerging from the atmosphere applied to the O_2A band," J. Quant. Spectrosc. Radiat. Transfer **64**, 131-149 (2000a).

Stam D., J. F. De Haan, J. W. Hovenier, and I. Aben, "Detecting radiances in the O_2A band using polarization sensitive satellite instruments, with application to GOME," J. Geophys. Res. **105**, 22379-22392 (2000b).

Stam D., J. F. De Haan, J. W. Hovenier, and P. Stammes, "The degree of linear polarization of light emerging from the cloudless atmosphere in the O_2A band," J. Geophys. Res. **104**, 16843-16858 (1999).

Stammes P., "Spectral radiance modelling in the UV-Visible range," in: "IRS 2000: Current problems in Atmospheric Radiation", Eds. W.L. Smith and Y.M. Timofeyev, Deepak Publ., Hampton, VA, 385-388 (2001).

Stammes P., and J. S. Henzing, "Multispectral aerosol optical thickness at De Bilt, 1997–1999," J. Aerosol Sci. **31**, 283-284, special issue EAC 2000 (2000).

Stammes P., F. Kuik, and J. F. De Haan, "Atmospheric polarization in the oxygen A and B bands," Proceedings of Progress in Electromagnetic Research Symposium (PIERS), 1994, 2255-2259, B. Arbesser-Rastburg et al. (eds.), Kluwer Academic Publishers, Dordrecht, The Netherlands, 1994.

Stammes P., J. F. De Haan, and J. W. Hovenier, "The polarized internal radiation field of a planetary atmosphere" Astron. & Astrophys. **225**, 239-259 (1989).

Stokes G. C., "On the composition and resolution of streams of polarized light from different sources," Trans. Cambridge Philos. Soc. **9**, 399-416 (1852).

Takashima T., K. Masuda, S. Mukai, and I. Sano, "Detection of atmospheric aerosol over Lunar Lake, Nevada, using ground-based skylight polarization measurements," Adv. Space Res. **23**, 1525-1528 (1999).

Tanre D., M. Herman, and Y. J. Kaufman, "Information on aerosol size distribution contained in solar reflected spectral radiances." J. Geophys. Res. **101**, 19 043-19 060 (1996).

Thieuleux F., C. Moulin, F. M. Breon, F. Maignan, J. Poitou, and D. Tanre, “Remote sensing of aerosols over the ocean using MSG/SEVIRI imagery,” Annales Geophysicae 23, 1–8 (2005).

Tilstra L. G., and P. Stammes, “Earth reflectance and polarization intercomparison between SCIAMACHY onboard Envisat and POLDER onboard ADEOS-2,” J. Geophys. Res. 2007 **112**, 11304 (2007).

Torres O., R. Decae, J. P. Veefkind, and G. de Leeuw, “OMI aerosol retrieval algorithm,” in OMI Algorithm Theoretical Basis Document, Volume III, Clouds, Aerosols, and Surface UV Irradiance, P. Stammes, ed., NASA Goddard Space Flight Center, 1 August 2002, http://eospso.gsfc.nasa.gov/eos_homepage/for_scientists/atbd/.

Twomey S. A., M. Piepgrass, and T. L. Wolfe, “An assessment of the impact of pollution on global cloud albedo,” Tellus Ser. B **36**, 356-366 (1984).

Twomey S. A., “The influence of pollution on the shortwave albedo of clouds,” J. Atmos. Sci. **34**, 1149-1152 (1977).

Vanbauce C., J.C. Buriez, I.F. Paro, I.B. Bonne, G. Se`ze, P. Couvert, ”Apparent pressure derived from ADEOS-POLDER observations in the oxygen A-band over ocean,” Geophys. Res. Lett. **25**, 3159–62 (1998).

van de Hulst H. C., *Light Scattering by Small Particles* (Dover, 1981).

van de Hulst H.C., “Scattering in a Planetary Atmosphere,” Astrophysical Journal **107**, 220-46 (1948).

van Diedenhoven B., O. P. Hasekamp, and I. Aben, “Surface pressure retrieval from SCIAMACHY measurements in the O_2A band: validation of the measurements and sensitivity on aerosols,” Atmos. Chem. Phys. Discuss. **5**, 1469-1499 (2005).

Vermeulen A., C. Devaux, and M. Herman, “Retrieval of the scattering and microphysical properties of aerosols from ground-based optical measurements including polarization. I. Method,” Applied Optics **39**, 6207-6220 (2000).

Wylie D. P., and W. P. Menzel, “Eight years of global high cloud statistics using HIRS,” J. Climate **12** , 170-184 (1999).

Zhao F. S., Z. B. Gong, H. L. Hu, M. Tanaka, and T. Hayasaka, “Simultaneous determination of the aerosol complex index of refraction and size distribution from scattering measurements of polarized light,” Applied Optics **36**, 7992-8001 (1997).

Acknowledgements

Closing, I would like to thank my thesis supervisor Prof. Dr. Jürgen Fischer who offered me the opportunity to work on this topic and for providing support whenever it was needed.

Special thanks are due to Dr. Piet Stammes, my main thesis advisor. I couldn't have asked for a better thesis advisor. You were not only an enormous store of knowledge in the field of remote sensing, but you also took your time to share it, to meticulously revise each article, taking your time for long and fruitful discussions, and to suggest new approaches whenever I thought I got stuck. All things considered you help me with words and deeds. Thanks a lot!

I am very grateful to Ass. Prof. Dr. Ralf Bennartz for taking on the second expert report regarding my thesis. Furthermore I really enjoyed the research stay at his department at the University of Wisconsin and the lively discussions over the past few months.

Many thanks go to all present and former colleagues at the Institute for Space Sciences in Berlin, and at the Royal Netherlands Meteorological Institute (KNMI) who contributed to the excellent working climate, to fruitful discussions. Wouter Knap I wish to thank for the outstanding collaboration over the years. He was always very supporting, helpful and it was fun working together.

I also would like to thank a few friends for keeping the spirits high. Wouter Knap, Rob Roebeling and Martin de Graaf, thank you lot for the time-outs and the fun at the KNMI. My friends Heimann Hindi, Tim Hoger, Maximilian Reuter, Arne Steinhof and David van der Kemp I can hardly thank enough. I am looking forward seeing you soon again (I mean some trips are really overdue!). Lorenz Moroni and Gianluca Marino, what would I have done without you guys. It is great to have found such good friends as you two. Luca, you are one of a kind. Well, that counts for you as well Jerome. Hugo Fernandes, idiot, you are a weird Portuguese, but a real good friend. Birgit Romberg, I hope that we manage to meet up again soon. Thank you for being such a good friend over the years. German Delgado, it was great fun having you here at the KNMI. We are looking forward to come over to Barcelona. Thanks my friend. Thanks a lot to my climbing friends Aart van Apeldoorn, Maike Brans and Wojtek Zbijewski for never letting go of the rope, even though there was some considerable weight at the other end. I really really enjoyed it. Lucas Ellison, I want to thank for the great discussions and for having a night on the town every now and then. They all contributed to finalize this work, one way or the other. Thanks to all of them!

Special thanks go out to Kristina Ellison for tons of moral support and for keeping me grounded all the time. Dankje van harte Kris voor je geduldige support en voor de geweldige tijd die ik met jou heb! Dankzij jou voel ik mij hier echt thuis. Na, en natuurlijk ook bedankt voor de Nederlandse taal die je mij stukje bij beetje hebt geleerd. Alida Ellison-Wassenaar, ik wil je bedanken voor de geweldige weekends in Coevorden en voor de gezonde prak. Mijn moeder zal je danken.

Zu guter Letzt möchte ich mich ganz besonders bei meinen Eltern Heinz und Renate Bösche bedanken für die stetige Unterstützung in all den Jahren. Ich bin Euch im wahrsten Sinne des Wortes etwas schuldig ;-)

Curriculum Vitae

Der Lebenslauf ist in der Online-Version
aus Gründen des Datenschutzes nicht enthalten